SEVERE CONVECTIVE WIND ENVIRONMENTS IN GEORGIA

by

CHRISTOPHER M. FUHRMANN

(Under the Direction of Thomas L. Mote)

ABSTRACT

Severe winds pose a tremendous threat to people and property and are the most frequently reported form of severe weather in the United States. This study examines three aspects of severe convective windstorms in Georgia during the warm season. Severe thunderstorm wind reports and radar data from the WSR-88D network are used to determine the convective organization and evolution of severe windstorms. The synoptic-to-mesoscale environments associated with these events are evaluated using surface weather maps, re-analysis data, and radiosonde observations. Lastly, the characteristics of cloud-to-ground (CG) lightning are observed during the evolution of a subset of severe windstorms. Results of this study indicate that the majority of severe windstorms in Georgia are non-linear, are influenced by land-atmosphere interactions, and develop under relatively quiescent synoptic conditions. Severe windstorms exhibit fewer positive CG flashes than non-severe thunderstorms, suggesting that the diabatic effects of evaporation and sublimation may enhance the negatively-charged cloud center.

INDEX WORDS: Severe wind, convective system, Georgia, climatology, lightning

SEVERE CONVECTIVE WIND ENVIRONMENTS IN GEORGIA

by

CHRISTOPHER M. FUHRMANN

A.B., The University of North Carolina at Chapel Hill, 2004

A Thesis Submitted to the Graduate Faculty of The University of Georgia in Partial Fulfillment of the Requirements for the Degree

MASTER OF SCIENCE

ATHENS, GEORGIA

2006

SEVERE CONVECTIVE WIND ENVIRONMENTS IN GEORGIA

by

CHRISTOPHER M. FUHRMANN

Major Professor:	Thomas L. Mote
Committee:	Andrew J. Grundstein John A. Knox J. Anthony Stallins

Electronic Version Approved:

Maureen Grasso
Dean of the Graduate School
The University of Georgia
May 2006

ACKNOWLEDGEMENTS

I would like to thank the following people for their valuable and unique contributions to this project: Dr. Thomas Mote, for supporting and guiding this research; Drs. Andrew Grundstein, John Knox, and Tony Stallins, for their thorough evaluations of this thesis; Dr. Thomas Mote, for his assistance with the lightning and radar overlays; Dr. Andrew Grundstein, for his assistance with FORTRAN; Drs. Tony Stallins and Mace Bentley, for generously sharing their lightning dataset (part of NSF grant BCS-0241062); Dr. Walker Ashley, for his assistance with the base reflectivity and velocity data and for sharing his derecho dataset; Mr. Ron Holle, who clarified various issues with the NLDN data; and those individuals at the 5th Southeast Severe Storms Symposium, for their spirited conversations and helpful suggestions on earlier versions of this work. I would also like to thank Dr. Thomas Mote and the Graduate Faculty of the UGA Geography Department for providing financial support during my time at the University.

TABLE OF CONTENTS

Page

LIST OF TABLES

Page

LIST OF FIGURES

Page

CHAPTER 1

INTRODUCTION

The tremendous hazard posed by severe, straight-line winds is well documented. These winds have resulted in forest blow-downs, agricultural damage, structural damage, property loss, injury, loss of life, and have been causally linked to a number of aircraft accidents (Fujita and Caracena 1977; Fujita 1981; Bentley et al. 2002; Ashley and Mote 2005). The most damaging of these winds, known as derechos, originate from organized, convectively-generated storm systems and occur over broad temporal (days) and spatial (hundreds of km) scales (Johns and Hirt 1987). Derechos have resulted in over 3,000 km^2 of forest blow-down and nearly $0.5 billion in insured property loss over the U.S. since 1986 (Ashley and Mote 2005). Severe winds also occur over small temporal (min.) and spatial (<1 km) scales and are commonly referred to as microbursts. These winds frequently originate from more isolated modes of convection and may pose operational challenges to pilots due to sudden changes in wind speed and direction during take-off and landing (Fujita 1985). Derechos and microbursts represent the largest and smallest scales of convective wind damage, respectively. Within this spectrum of wind damage there are other types of convectively-driven winds, such as macrobursts, rear-flank downdrafts, and gust fronts (Wakimoto 2001).

The patterns of severe winds across the U.S. have been described through a few climatological studies which used archived severe thunderstorm data from the Storm

Prediction Center (SPC, formerly the National Severe Storms Forecast Center) and from publications produced by the National Climatic Data Center (NCDC), such as *Climatological Data* and *Storm Data* (Pautz 1969; Kelly et al. 1985; Weiss et al. 2002). These studies illustrate regional differences in the patterns of severe winds, defined by the National Weather Service (NWS) as surface winds exceeding 26 m s^{-1} (50 kt.) or producing damage identified through surveys. A number of observational and modeling studies have demonstrated that severe winds can occur under a variety of meteorological environments, adding to the challenge of forecasting these potentially dangerous events. As a response, Wakimoto (2001) suggests that site-specific nowcasts of convection, beginning with thunderstorm initiation, may improve the predictability of severe winds. Klimowski et al. (2003) provide some initial insight into the convective nature of severe windstorms. They described the modes of convection responsible for severe winds across the Northern High Plains (NHP) from May to September using data from the Weather Surveillance Radar-1988 Doppler (WSR-88D) network. They determined that approximately 80% of the severe wind reports across this region from 1996 to 1999 were associated with organized convection (e.g. squall lines, bow echoes, supercells). Interestingly, these results disproved the initial theory of Kelly et al. (1985), which held that most warm-season severe winds in this region may be tied to microbursts occurring in disorganized, or non-linear, convective cells.

Presently, there is no information on the modes of convection responsible for severe winds in the Southeast U.S. This lack of information is odd because a recent study by Doswell et al. (2005) demonstrates that the Southeast is one of the regions where the probability of experiencing severe wind on any given day is highest (Figure 1.1). This

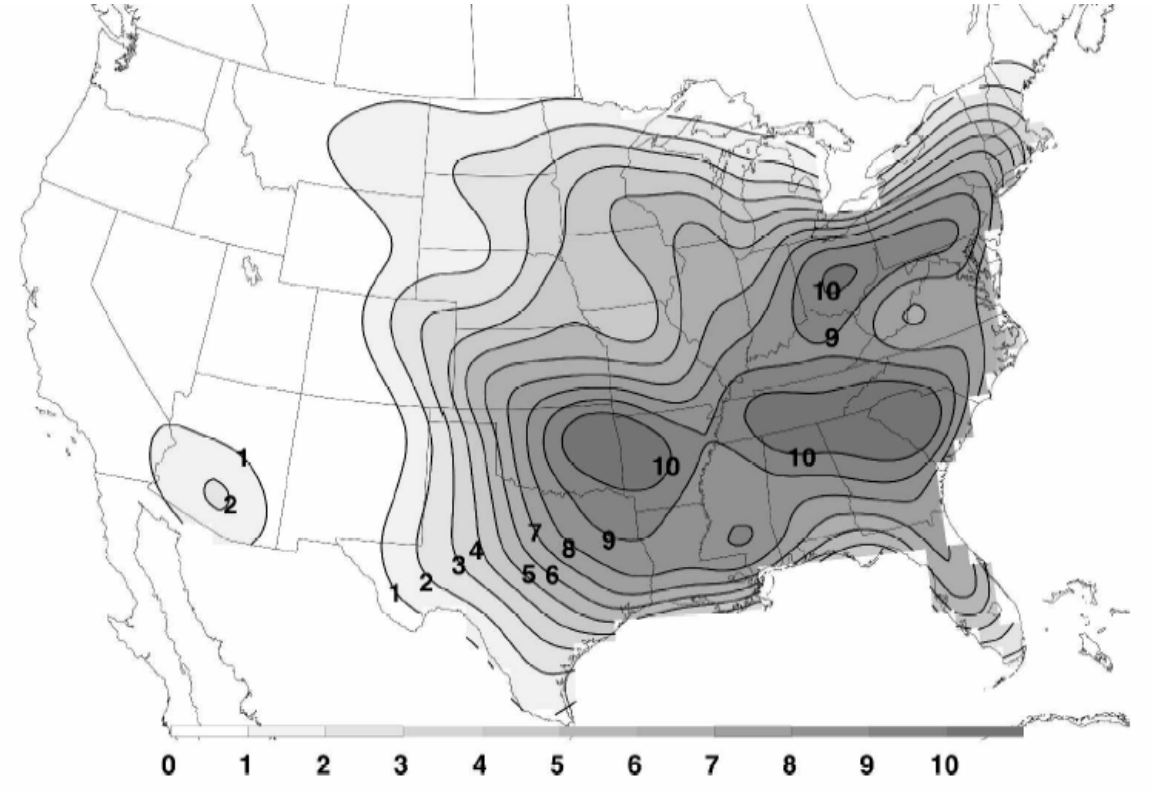

Figure 1.1. Percent probability of a severe wind day across the U.S. based on data archived at the SPC from 1995-1999 (Doswell et al. 2005).

pattern suggests that the meteorological ingredients necessary for severe winds, as well as the environments supportive of their development, are commonly found across the Southeast. Senn (2003) speculates that outbreaks of severe winds across this region are driven mainly by isolated, convective cells because most of these outbreaks occur under relatively benign synoptic conditions. Such a hypothesis seems appropriate given the infrequent nature of organized, convectively-generated storm systems across the Southeast (e.g. mesoscale convective systems (MCS); Anderson and Arritt 2001), particularly when compared to the Midwest. Further, although the Southeast has been identified as a seasonal corridor for derecho activity (Bentley and Mote 2000; Bentley

and Sparks 2003; Ashley et al. 2005), it is not clear what fraction of severe winds across the Southeast is due to derechos. This study will determine the convective organization and evolution of severe windstorms over Georgia using data from the WSR-88D network. It is hypothesized that about an equal number of these windstorms are associated with either organized (e.g. MCS) or unorganized (e.g. microburst) convective modes.

A recent survey by Wakimoto (2001) on severe convective winds illustrates that the atmospheric conditions favorable for these events are numerous. As mentioned earlier, there exists a broad spectrum of severe wind damage with the longer-lived, widespread events producing the most extensive damage. These events fall under the umbrella of MCS and include squall lines (Houze et al. 1990) and bow echoes (Fujita 1978). Such organized, linear convective systems commonly form along the leading edge of a cold front in the warm sector of a mid-latitude cyclone, while a diffluent pattern is often observed in the mid and upper levels of the troposphere (Holton 2004). In other situations, organized convective systems may form downstream of an amplified, warm-core anticyclone (Johns 1984). These northwest flow events are common across the Upper Midwest and may re-generate along shortwave troughs across the South (Bentley and Sparks 2003; Ashley et al. 2005). Organized systems can exhibit convective lines as long as 300 km and can persist for 18 h or more (Pryzbylinski 1995; Ashley 2005). Less organized modes of convection are also capable of producing severe winds through evaporative cooling, melting, and precipitation loading (Fujita 1978). Aside from their transient nature, these singular to multi-cellular thunderstorms often develop in the absence of strong synoptic-scale support, such as under a sub-tropical ridge. In these

environments, the role of mesoscale features and circulations, such as the Piedmont front (Businger et al. 1991) and the outflow boundaries of decaying thunderstorms (Koch and Ray 1997), likely become more important in the formation of strong convective storms. This study will examine the importance of synoptic-to-mesoscale patterns and processes in the development of severe wind-producing storms over Georgia that span a range of convective organization. It is hypothesized that these events do not occur under a single set of meteorological conditions and instead are influenced by processes acting across multiple scales and in conjunction with the local topography.

Forecasting convection, particularly in association with severe weather (Johns and Doswell 1992), may be aided by examining the patterns and characteristics of cloud-to-ground (CG) lightning. The separation of electrical charge necessary to produce CG lightning is contingent upon the existence and interactions of ice particles, graupel, and super-cooled water at the cloud scale (MacGorman and Rust 1998). These interactions occur within the mixed-phase region of the storm cloud and are most active when vigorous updrafts are present (Williams 1995). The mixed-phase region is characterized by a sub-freezing layer, bounded by the -10°C and -20°C isotherms, and develops in response to the vertical displacement of convective available potential energy (CAPE) (Saunders 1995). Thus, while radar data may describe the horizontal and vertical extent of convective processes (e.g. conditional instability, hydrometeor volume and motion), CG lightning data may be able to express the outcome of these processes over the lifecycle of a convective event (Elson and Margraf 1996). Further, the high temporal (1-s) and spatial (0.5 km) resolution of CG lightning data allow for a more detailed evaluation of the convective development of thunderstorms than radar or satellite data

(Orville et al. 1983; Biagi et al. 2004). This is particularly useful in determining the small-scale patterns of convection which may alert forecasters to the development of severe thunderstorms. This study will identify the characteristics and evolution of CG lightning associated with severe wind-producing convective systems across Georgia. By comparing these trends in CG lightning activity to those observed over non-severe convective systems, it is possible to ascertain potential signals in the development of severe winds, particularly those that originate from less organized convective modes. It is hypothesized that CG lightning data, when combined with radar and other diagnostic tools, may provide additional feedback to forecasters when faced with a developing severe weather condition. The resulting patterns in CG lightning are also discussed in the context of cloud-scale charge structures and the mechanisms responsible for lightning production in severe wind-producing and non-severe thunderstorms.

The central goal of this research is to improve the conceptual models of warm-season severe convective wind environments across a part of the Southeast U.S., such as those presented by Kelly et al. (1985) and Senn (2003), by addressing some persistent issues. First, the range of convective modes associated with severe winds is unknown across the region. To address this issue, both national composite radar summaries and base reflectivity scans from individual radar sites in the WSR-88D network are examined to determine the predominant and persistent convective modes associated with severe winds using a set of radar-based criteria developed by previous studies (Fujita 1978, Moller et al. 1994; Klimowski et al. 2003). Secondly, the synoptic-to-mesoscale patterns and processes which conspire to produce severe winds across the Southeast are not known. This issue is addressed using re-analysis data, surface weather maps, and

sounding data to determine the environments favorable for severe winds and whether they are distinguishable from ordinary (i.e. non-severe) convective environments. Lastly, the potential applicability of CG lightning data in nowcasting severe local storms continues to be elusive. Maps of CG lightning activity at various stages of thunderstorm development are produced and examined to determine if the evolutionary pattern in CG lightning density and polarity during a severe wind-producing thunderstorm varies significantly from the patterns observed in non-severe thunderstorms. The results of this research will help forecasters in the Southeast identify the environmental characteristics of severe wind-producing convective systems, thus enabling them to more accurately detect where and when these events will occur.

CHAPTER 2

BACKGROUND

This chapter provides a review of the downdraft types and meteorological environments associated with severe, convectively-generated surface winds. A general description of the downdraft and its properties are followed by a discussion of the downdraft types, their physical origin, and the parent convective systems commonly associated with severe winds. The spatial and temporal patterns of severe winds across the U.S. are also examined as well as the synoptic-scale environments favorable for their development. This chapter concludes with an analysis of published case studies which describe distinctive signatures in the CG lightning properties associated with severe winds.

2.1 The Downdraft

The lifecycle of a typical thunderstorm can be divided into three general stages (Byers and Braham 1949; Wakimoto 2001). The first stage (initiation) occurs when sufficient potential instability allows surface-based air parcels to rise through the troposphere (i.e. parcel theory, as described in Holton 2004). The second stage occurs when these rising parcels are able to expand, cool, and condense, forming clouds. This stage is enhanced by the updraft and may incite deep, moist convection given a sufficiently deep mid-tropospheric moist layer, a steep lapse rate, and enough lift for the

parcel to reach the level of free convection (Johns and Doswell 1992). The final stage involves the convective downdraft, enhanced by evaporative cooling, and the resulting gust front, which cools and dries the boundary layer as it undercuts the warmer ambient air near the surface (Doswell 1982; Wakimoto 1982). If the downdraft is strong enough, it can produce severe damage to crops, trees, and man-made structures as well as pose a significant threat to aircraft during landing and take-off (Fujita 1981; Fujita and Wakimoto 1981; Fujita 1985).

When the downdraft from a thunderstorm produces strong winds over a horizontal area of 1 to 10 km, it may be referred to as a downburst (Knupp and Cotton 1985). The downburst may be further divided into "microburst" and "macroburst" depending on the spatial and temporal extent of the outflow. Microbursts (macrobursts) typically have an outflow boundary of less than (greater than) 4 km with peak gusts lasting between 2 and 5 min. (5 and 20 min.) (Fujita 1981). Microbursts are commonly associated with dangerous wind shear conditions during aircraft landing and take-off, while macrobursts have been shown to produce wind damage comparable to an F3 tornado (i.e. winds between 70 and 93 m s^{-1} with uprooting of heavy trees and walls and roofs of buildings torn away) (Fujita 1981).

The most comprehensive descriptions of microburst and macroburst frequency, as well as their meteorological environments, stem from a number of field studies. These include the Northern Illinois Meteorological Research on Downburst project (NIMROD) (Fujita 1978, 1985), the Joint Airport Weather Studies project (JAWS) (McCarthy et al. 1982, Wakimoto 1985), the FAA/Lincoln Laboratory Operational Weather Studies project (FLOWS) (Wolfson et al. 1985), and the Microburst and Severe Thunderstorm

project (MIST) (Dodge et al. 1986; Atkins and Wakimoto 1991). Some results may appear biased toward the time scales and geographic constraints specific to each study, such as a nocturnal microburst maximum across parts of the eastern U.S. during JAWS (Wakimoto 1985). A few results appear to be consistent across the studies. For example, the small temporal scale of the microburst is evident in nearly all studies, and the percentage of thunderstorms observed with some horizontal wind shear is typically between 60 and 80%. Further, there exists an exponential decrease in the frequency of microbursts as the peak outflow wind speed increases. During the JAWS project, only 12 out of 186 microbursts studied had wind speeds exceeding the severe threshold of 26 m s^1 (50 kt.) (Fujita 1985).

The most damaging thunderstorm winds occur primarily within large convective systems that produce clusters of microbursts and downbursts over a fairly extensive area (Fujita and Wakimoto 1981). One class of these events was first defined in 1888 by Gustavis Hinrichs as derechos. Nearly 100 years later, Johns and Hirt (1987) provided an initial treatment of the characteristics and environmental conditions of derechos, covering 70 warm season derecho events between 1980 and 1983. Their study also developed an initial set of criteria for defining a derecho, which may be divided into five characteristics: 1) the major axis length of the concentrated area of severe wind reports, 2) the temporal restriction between successive reports, 3) the occurrence of "extreme" wind reports, 4) the origin of the convective system (i.e. MCS) which spawns the severe wind reports, and 5) the spatial and temporal continuity of the severe wind reports associated with the convective system (Table 2.1). A recent study by Ashley and

Table 2.1. Criteria used to identify derechos from previous studies (Ashley 2005).

Criterion	Johns and Hirt (1987)	Bentley and Mote (1998) and Bentley and Sparks (2003)	Evans and Doswell (2001)	Coniglio and Stensrud (2004)
Minimum Length	There must be a concentrated area of convectively induced wind damage and/or gusts greater than 26 m s^{-1} that has a major axis length of at least 400 km	There must be a concentrated area of convectively induced wind damage and/or gusts greater than 26 m s^{-1} that has a major axis length of at least 400 km	There must be a concentrated area of convectively induced wind damage and/or gusts greater than 26 m s^{-1} that has a major axis length of at least 400 km and a minor axis width of at least 74 km	There must be a concentrated area of convectively induced wind damage and/or gusts greater than 26 m s^{-1} that has a major axis length of at least 400 km
Chronological Progression	The wind reports must have chronological progression	The wind reports must have chronological progression	The wind reports must have chronological progression	The wind reports must have chronological progression
Temporal Restriction	No more than 3 h can elapse between successive wind reports	No more than 2 h can elapse between successive wind reports	Exhibits either a near-continuous damage path with no more than a 2 h or 167 km gap between successive concentrations of severe wind reports	No more than 2.5 h can elapse between successive wind reports
"Extreme" Wind Gust Criteria	There must be at least 3 reports of either F1 damage or wind gusts greater than 33 m s^{-1} separated by at least 64 km	Not used	Not used	Low end: not used; moderate: same as in Johns and Hirt (1987); high end: there must be at least three reports greater than 38 m s^{-1} or comparable damage, at least two of which must occur during the MCS stage of the event
Origin of Wind Swath	Multiple swaths of wind damage (including gusts) must be a part of the same MCS as indicated by the available radar data	Multiple swaths of damage must be part of the same MCS as seen by temporally mapping the wind reports of each event	Convective system must exhibit a linear signature on archive radar charts	Multiple swaths of wind damage (including gusts) must be a part of the same MCS as indicated by the available radar data
MCS Continuity	The associated MCS must have temporal and spatial continuity	The associated MCS must have temporal and spatial continuity with no more than 2° of latitude and longitude separating successive wind reports	The associated MCS must not be associated with tropical storms or hurricanes	The associated MCS must have spatial and temporal continuity and each report must be within 200 km of the other reports within a wind gust swath

Mote (2005) indicates that derechos produce as much damage as many of the tornadoes and hurricanes which affect the U.S.

The strongest downdrafts that reach the surface are typically associated with cumulonimbus convection from a MCS (Knupp and Cotton 1985) and have been divided into convective and mesoscale downdrafts according to their spatial scale (Zipser 1969). Convective downdrafts tend to originate from the convective region of an MCS and include forward flank and rear flank downdrafts, microbursts, and gust fronts. Mesoscale downdrafts, which tend to occur over wider areas and longer time periods (e.g. derecho), often originate from the stratiform region of a MCS, typically a squall line or bow echo.

2.2 Convective Downdrafts

Observational studies of supercell thunderstorms have identified two common convective downdraft types: forward flank and rear flank downdrafts (Lemon and Doswell 1979; Lemon 1976). The forward flank downdraft originates from within the main convective region of the supercell. As seen on radar, this region is typically found near the center of the echo where precipitation is the most intense (Lemon and Doswell 1979). Although this type of downdraft is not known to produce damaging winds, the leading edge of its outflow boundary has been shown to play a role in the development of the low-level mesocyclone, a defining feature of the supercell thunderstorm and favorable location for tornadogenesis (Klemp 1987).

The rear flank downdraft, which originates along the outflow boundary nearest the center of the updraft (i.e. mesocyclone), has been shown to produce wind speeds capable of microburst damage (Lemon 1976). This is supported by studies which report

fan-shaped patterns of wind damage near tornado tracks (Orf and Anderson 1999). Numerical studies, most notably Wicker and Wilhemson (1995), have indicated that the strongest wind speeds associated with the rear flank downdraft originate from an embedded outflow defined as the occlusion downdraft. Although difficult to identify observationally from damage surveys, the occlusion downdraft has been identified in modeling studies and vertical radar velocity cross-section analysis as a more dynamic feature than the rear flank downdraft (Wicker and Wilhemson 1995). The former is typically driven by low-level rotation near a meso-low while the latter is typically driven by precipitation loading and evaporative cooling (Wakimoto 2001).

Perhaps the most widely studied convective downdraft type is the microburst (Wakimoto 2001). This downdraft is characterized by strong surface divergence at its center, with the strongest winds occurring at the tails (or periphery when viewed from above) of the outflow in a feature defined by Proctor (1988) as an "overturning rotor" (Figure 2.1). Spatially, microbursts occur over areas less than 4 km wide while typically lasting no longer than 5 min. These limits help discriminate microbursts from larger downbursts, which often occur under different environmental conditions and impart different damage patterns (Fujita 1985).

As mentioned earlier, microbursts have been blamed for a number of commercial aircraft accidents (Fujita and Caracena 1977; Fujita 1985). The dramatic changes in wind speed and direction over very short time and space scales create a number of operational dilemmas for pilots, particularly when changing the degree of pitch of the aircraft's nose to compensate for rapid changes in headwind and tailwind conditions as it encounters the microburst (Job 1996).

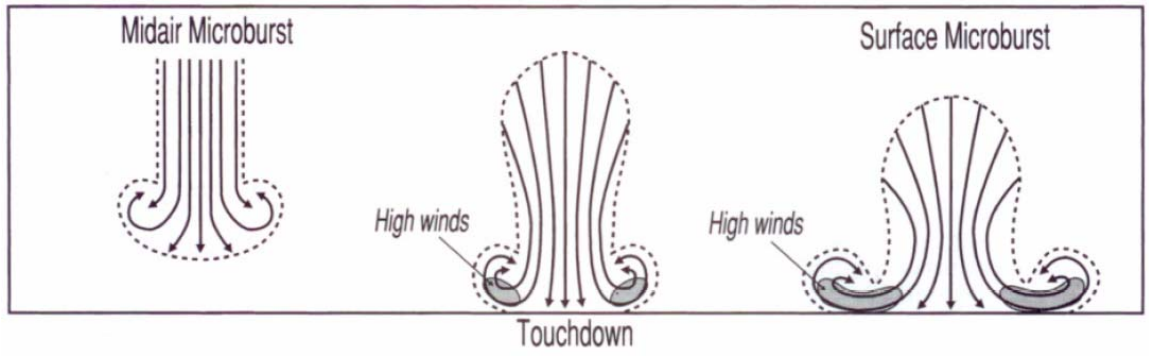

Figure 2.1. Conceptual model of a microburst and the resultant outflow patterns beginning with the midair microburst (Wakimoto 2001). The outflow pattern associated with the strongest winds (shaded region) represents the "overturning rotor" described by Proctor (1988).

There is some debate as to the dynamic origin of the microburst. Some studies point to small-scale structures in the upper-troposphere, such as misocyclones, and the associated rotation (Rinehart et al. 1995). In other words, the magnitude of the outflow is dictated by the degree of rotation in the storm cloud. Other studies identify the outflow magnitude as a function of hydrometeor interactions, phase changes and the sub-cloud lapse rate. Following the latter hypothesis, Fujita (1985) and Wakimoto (1985) further define a microburst as either "dry" or "wet" depending on the intensity of the base reflectivity factor and the amount of precipitation over the microburst area. Dry (wet) microbursts are characterized by a reflectivity factor lower (greater) than 35 dBZ and less than (greater than) 0.25 mm of precipitation. In both cases, the presence of frozen condensate (e.g. snowflakes, grapuel) is important in initiating the outflow (Proctor 1989). Dry microbursts are driven primarily through sublimation of these frozen particles through a deep sub-cloud adiabatic layer while wet microbursts are driven by high rainwater mixing ratios (from the melting of frozen hydrometeors) under more

stable atmospheric conditions (Fujita and Wakimoto 1981). A recent case study by the NWS forecast office in Raleigh, NC, examined a large swath of damaging microburst winds across much of North Carolina (Locklear et al. 2004). They found that the deep adiabatic layer favorable for dry microbursts was the product of strong upper-level dynamics and cold air advection from a vigorous upstream trough (i.e. northwest flow aloft) (Figure 2.2).

The outflow boundary from thunderstorm downdraft air plays an important role in both the initiation and dissipation of new and nearby thunderstorms (Purdom and Marcus 1982). In some instances, the cool, dry outflow may undercut the warmer, ambient near the surface, creating a positively buoyant air parcel, while in other instances this outflow may choke-off the inflow from a nearby thunderstorm (Wakimoto 1982). This outflow boundary is defined as a gust front and is marked by the transition between the over-riding warm air and the under-cutting cool air (Mueller and Carbone 1987). Operationally, the gust front may be visible on radar in advance of a strong MCS with reflectivity factors between 5 and 20 dBZ. Such a radar signature may signal potentially damaging wind gusts, as was the case with a strong squall line in northwest Kansas shown in Figure 2.3. From an observational perspective, the strongest gust fronts, and consequently the ones most capable of producing widespread wind damage, may be identified by the presence of a shelf cloud, which forms along the base of the thunderstorm and extends horizontally along the vertical cap of the mesofront (Wakimoto 1982).

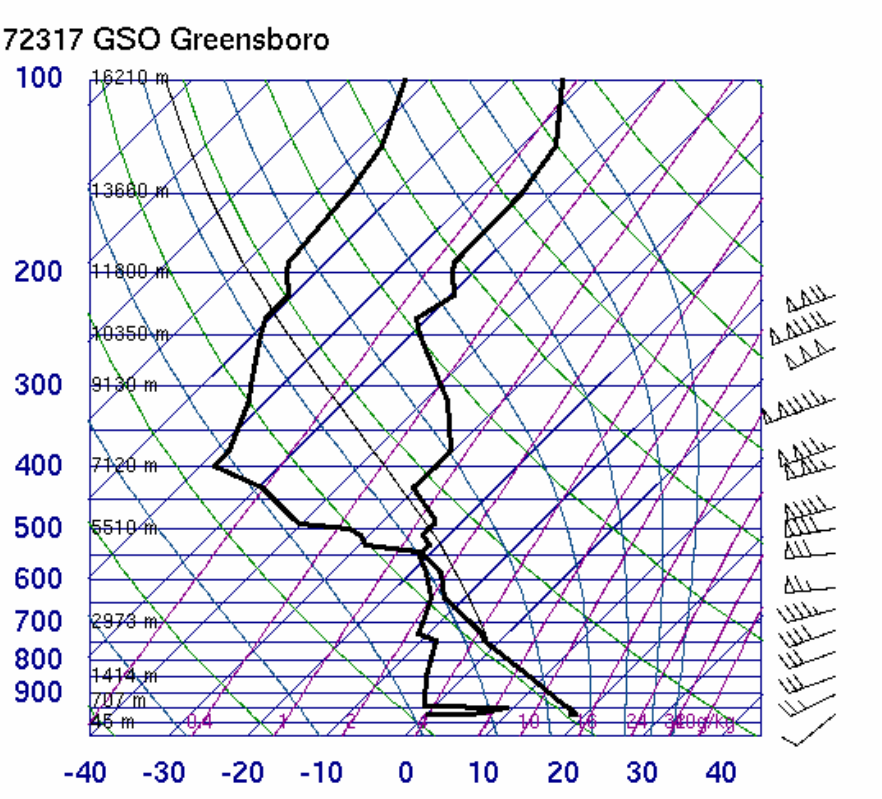

Figure 2.2. Greensboro, NC (KGSO) sounding from 00 UTC 08 March 2004 during the time of severe wind gusts across the central half of the state. The dry, sub-cloud adiabatic layer, as indicated by the inverted "V" profile (Johns and Doswell 1992) on the Skew-T diagram, is exceptionally deep in this case (extending from the surface to 650 hPa) and is an excellent indicator of dry downburst conditions.

2.3 Mesoscale Downdrafts

The most common type of mesoscale downdraft is the derecho (Wakimoto 2001). This downdraft event is unique in that it occurs over extensively broad time (days) and space (hundreds of km) scales and is composed of numerous severe wind reports. The resulting pattern of damaging winds may pose a significant threat to property and life (Fujita and Wakimoto 1981; Ashley and Mote 2005). A derecho is typically produced by an MCS characterized by bow-shaped segments of cells between 60 and 100 km in length, otherwise known as a bow echo (Fujita 1978). This feature was first identified as

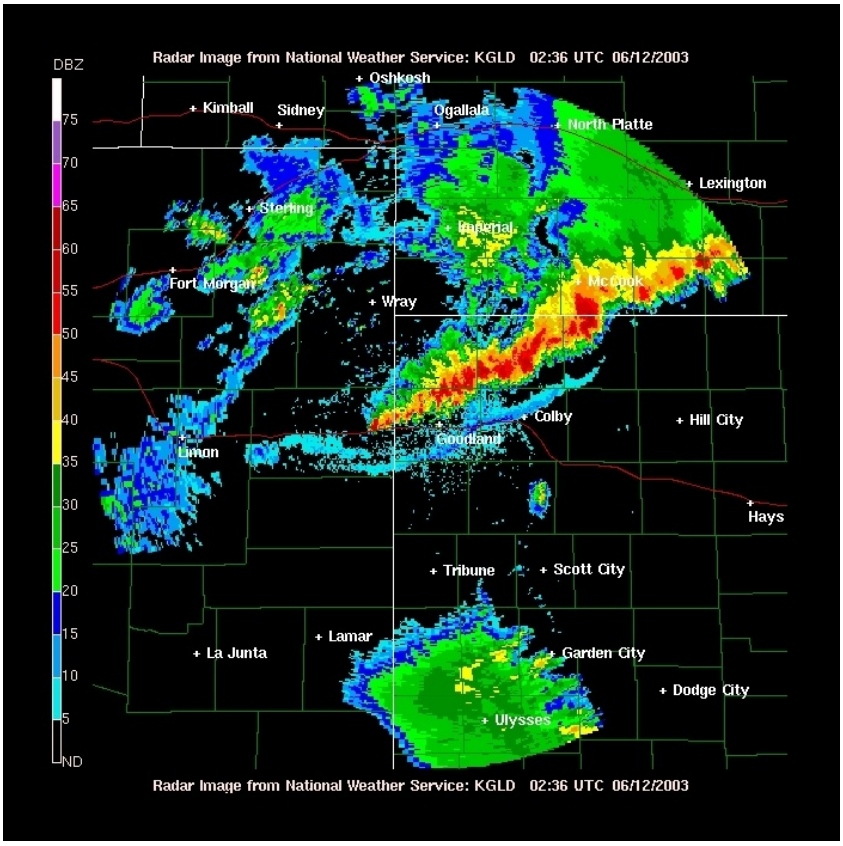

Figure 2.3. WSR-88D base reflectivity image from Goodland, KS of a strong squall line with its gust front (reflectivity factor <20 dBZ) leading the main convective line (reflectivity factor >40 dBZ). Image available online from the NOAA Photo Library at http://www.photolib.noaa.gov/historic/nws/wea01259.htm.

a line echo wave pattern (LEWP) by Nolan (1959) where certain regions of the convective line appeared to accelerate. A study by Hamilton (1970) later confirmed that these regions of storm acceleration were often associated with damaging surface winds. More recent studies have identified the bow echo as being the most likely convective source for derecho activity (Houze et al. 1990; Przybylinski 1995).

The evolutionary characteristics of the bow echo are usually visible on radar (Figure 2.4). The system may begin as a single convective echo either isolated or part of

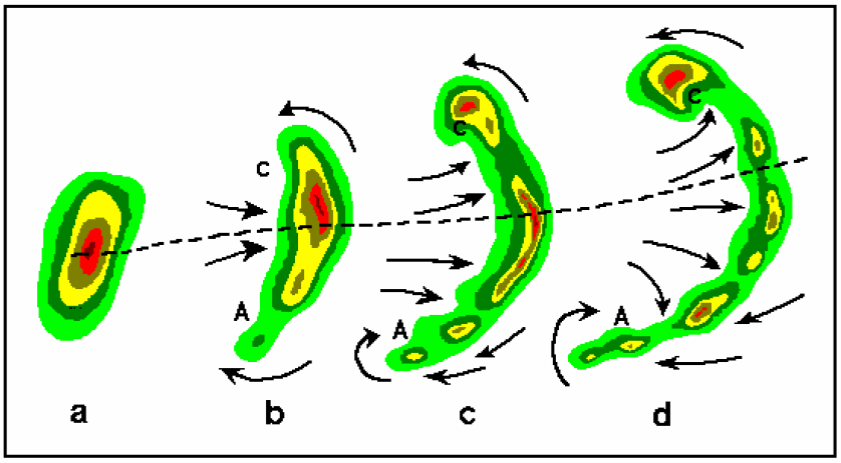

Figure 2.4. Gross schematic of the evolution of a bow echo as seen on radar beginning with (a) thunderstorm radar echo, (b) convective line, (c) bow echo, and (d) comma echo. Anticyclonic rotation (A) and cyclonic rotation (C) are noted during the mature phases of the storm. Dashed line indicates the axis of greatest potential for downburst damage. Arrows indicate storm-relative wind direction. Image available online from the NWS Forecast Office, Norman, OK, at http://www.srh.noaa.gov/oun/severewx/.

a more extensive system, such as a squall line. As the system develops, a strong rear inflow jet near the apex of the convective line accelerates this region of the system (Weisman 2001). This inflow jet may be accompanied by inflow notches along the trailing edge of the radar echo. Fujita (1978) postulated that the rear inflow jet was the source of the damaging surface winds observed ahead of the apex of the bow. A more recent study by Przybylinski (1995) identified four radar signatures associated with derechos, each accompanied by reflectivity notches indicative of a rear inflow. At the mature stage, the bow echo may develop cyclonic and anticyclonic circulations at the tails of the system. On radar, these features may be identified as “commas” or “rotating heads”. Numerical simulations by Weisman (1993) and Weisman and Davis (1998)

determined that these counter-rotating circulations (or vortices) play an important role in tilting the storm's updraft-downdraft couplet to initiate damaging surface winds.

Although derechos were initially identified over 100 years ago, the first formal criteria for defining these events were not developed until the work of Johns and Hirt (1987). Their study termed a derecho a "family of downburst clusters" (Fujita and Wakimoto 1981) associated with an extra-tropical MCS meeting specific criteria determined from severe thunderstorm archives in *Storm Data* and at the SPC. Since the initial study by Johns and Hirt (1987), the criteria for defining a derecho have been amended by Bentley and Mote (1998), Evans and Doswell (2001), and Coniglio and Stensrud (2004) (see Table 2.1). The most comprehensive database of derechos in the U.S. to date was developed by Ashley and Mote (2005). They updated the database from Coniglio and Stensrud (2004) to include the years 2002 and 2003 while adding events that did not meet the length criteria set forth by Johns and Hirt (1987). Ashley and Mote (2005) further scrutinized available radar data to identify multiple severe wind swaths as part of a coherent MCS. The climatology of derechos has been difficult to describe, owing primarily to the different time periods examined while also likely affected by the removal of the 33+ m s^{-1} gust requirement and the tightening of the spatial and temporal boundaries of the wind reports (Coniglio and Stensrud 2004).

The number of studies relating outbreaks of severe weather in the Southeast to a prevailing synoptic regime is heavily biased towards tornadic outbreaks (Senn 2003). A limited number of studies have investigated the influence of synoptic-scale features in the production of severe windstorms (particularly derechos) in this region. Bentley and Mote (2000) analyzed 14 cool season derechos between 1986 and 1995 in the eastern U.S. and

found a prevailing synoptic environment similar to that of cool season tornadic outbreaks. This environment was characterized by marginal instability and strong synoptic forcing (i.e. a highly amplified trough at 500 hPa).

Bentley and Sparks (2003) identified regional characteristics of derechos associated with annual and seasonal shifts in the favorable synoptic environments. For instance, the warm season derecho frequency maximum in the central and northern Plains may be tied to a persistent warm-core anticyclone at 500 hPa with a strong geopotential height gradient on the northern and western edges of the ridge (Bentley and Sparks 2003). Additionally, the tendency for derecho corridors to activate during or shortly after the demise of previously activated corridors may be tied to the prevailing low to mid-tropospheric flow (i.e. shifts and changes in the intensity of the subtropical high in relation to an approaching 500 hPa ridge) (Bentley and Sparks 2003). Distinctive patterns in the mid-tropospheric flow associated with derecho-producing convective systems have also been identified by Coniglio et al. (2004). Using a cluster analysis technique, they found three predominant flow regimes: up-stream, trough, and ridge. Interestingly, nearly one third of the derechos studied included features from more than one of these regimes.

Ashley (2005) recently examined the large-scale atmospheric features which conspired to produce the most active period of derecho activity on record in the U.S. Over a 47-day period in the early summer of 1998, 29 derechos were identified, six of which affected the Southeast U.S. He found an anomalously strong sub-tropical ridge at 500 hPa, indicative of strong sub-tropical convection, over much of the U.S., with anomalously strong mid- and upper-level winds along the periphery of the ridge. This

ridge helped to feed low-level moisture necessary for deep convection, while easterly winds aloft helped to produce a capping inversion, which allowed for a tremendous release of stored convective energy when juxtaposed with upper-level dynamic forcings (i.e. jet streaks, vorticity maximums) and instability (i.e. anomalously high warm-season lapse rates). The location of the sub-tropical ridge and the persistence of the associated large-scale atmospheric features over favorable derecho corridors (e.g. Northern Plains) may have been partially initiated by the strong positive phase of the El Nino-Southern Oscillation, although more directed studies are needed to assess any correlation between teleconnection patterns and derecho activity (Ashley 2005).

The only comprehensive synoptic climatology to date of severe wind outbreaks (without regard to the parent convective systems and derecho criteria) in the Southeast is the one by Senn (2003). An outbreak was defined by the occurrence of three or more like reports with no more than a 6-h lapse between reports. This study found some distinguishing signals in the synoptic environment associated with severe wind outbreaks compared to hail and tornadic outbreaks: (1) stronger surface divergence, (2) weaker divergence at 200 hPa, (3) a lower lapse rate from 850-500 hPa, and (4) a more westerly low-level circulation with a pronounced northwesterly flow at 500 hPa. Senn (2003) further suggests that severe wind events in the Southeast are driven more by isolated, convective cells than widespread, dynamic lift and that, overall, severe wind events show a synoptic pattern which more closely resembles tornadic events.

2.4 Climatology of Severe Wind Reports

The most comprehensive examination of the spatial and temporal patterns of severe and damaging wind reports across the U.S. is provided by Kelly et al. (1985). Their work updated an initial account of non-tornadic severe thunderstorms by Pautz (1969), who examined 13 years of data from 1955 to 1967. The dataset compiled by Kelly et al. (1985) includes more than 75,000 reports of severe and damaging wind and hail for the period 1955-1983. No attempt was made to segregate the wind reports according to their downdraft characteristics (e.g. microburst) or parent convective system (e.g. bow echo).

Severe thunderstorm wind gusts occur primarily during the heart of the warm season (June and July). This is in contrast to hail and tornado climatologies, which indicate a spring season frequency maximum across much of the U.S. (Kelly et al. 1978; Kelly et al. 1985). Annually, only 2% of severe wind reports occur during the winter months (December-February). When segregated according to gust speed, an interesting distribution emerges among the wind reports. Roughly 70% had "unknown" gust speeds, 23% had "strong" gust speeds (26-33.5 m s^{-1}), while the remaining 7% were deemed "violent" (>33.5 m s^{-1}). When examined in normalized solar time[1], 55% of severe wind reports occur between noon and sunset with a peak in the late afternoon. The severe wind report climatology shows a minimum in activity around sunrise. Further, the frequency of gusts meeting the violent criteria was maximized before sunrise and minimized when instability is typically greatest. As a result, Kelly et al. (1985) suggest

[1] Normalized solar time (NST) sets the sunrise time to 12 UTC and the sunset time to 00 UTC and divides the hours of daylight and night between 12 NST hours of sunlight and 12 NST hours of darkness. This technique allows for analysis of relationships between climatological parameters and the diurnal cycle (Kelly et al. 1985).

that forecast algorithms based on atmospheric negative buoyancy (see Doswell et al. 1982) may not be practical for the most violent of wind gusts.

Severe wind reports occur most frequently across the Great Plains through to the western slopes of the Appalachian Mountains (Figure 2.5). A small area of high frequency may also be discerned through the Piedmont and upstate of Georgia and over the Megalopolis in the Northeast. When only the violent winds are considered, the frequency maximum shrinks to just the Midwest, extending from the Front Range east of the Rocky Mountains to the Mississippi River. The frequency maximum that begins along the Front Range may be related to the diurnal patterns of convection, as indicated by CG lightning frequencies (Zajac and Rutledge 2001; Klimowski et al. 2003). The maximum extending east of the Mississippi River may be partially related to the increased number of trees in the eastern U.S., as nearly one half of severe wind reports in the historical archives are damage-based (Schaefer and Brooks 2000). There are a number of shortcomings to the various databases used to study severe wind events; nevertheless, the work of Kelly et al. (1985) and others provide a necessary framework for understanding the patterns of severe wind gusts and the environments within which they originate.

Senn (2003) provides the only climatology to date which focuses exclusively on severe weather outbreaks across the Southeast U.S. Over a 51 year period (1950-2000), the average annual frequency of wind outbreaks was greater (10.7 per year) than both hail outbreaks (2.8 per year) and tornadic outbreaks (4.6 per year). Similar to Kelly et al. (1985), severe wind outbreaks exhibited a maximum frequency during the summer months; however, a diurnal peak was noted at 1600 LST when instability is typically

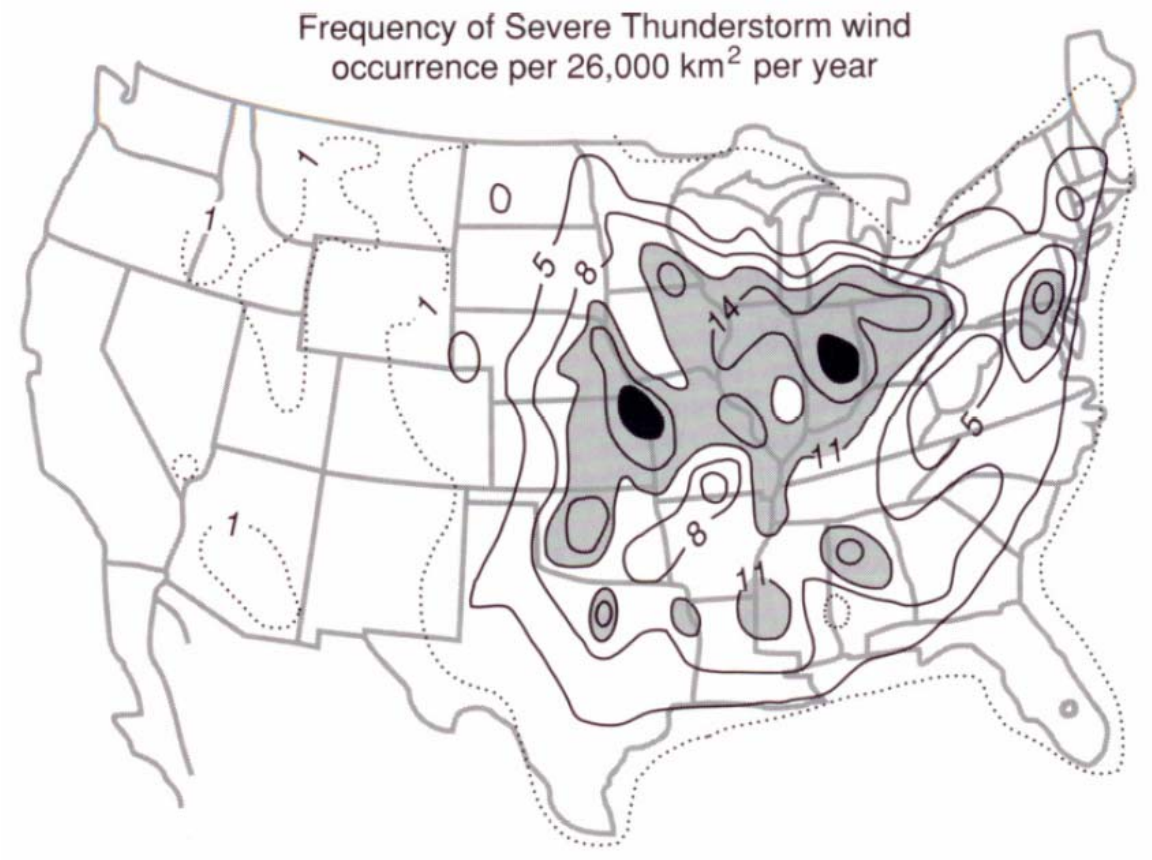

Figure 2.5. Frequency of severe thunderstorm wind occurrence per 26,000 km^2 per year based on data from 1955-1983. Dark-shaded values begin at 11 reports (Kelly et al. 1985).

maximized. A fourth outbreak type – hybrid – was defined if there were at least three reports of severe wind and hail. Annually, hybrid outbreaks were more common (7.1 per year) than tornadic and hail outbreaks and exhibited a longer mean duration. Such a result complements observational studies of supercell thunderstorms where severe winds and large hail swaths are often observed in the same storm (Moller et al. 1994), although Senn (2003) speculates that hybrid outbreaks in the Southeast may be part of more widespread and enduring storms.

Annual trends in the frequency of severe and damaging winds are strongly influenced by changes in reporting techniques (Weiss and Vescio 1998; Weiss et al. 2002). These reporting techniques will be discussed in Chapter 3. From 1970 to 1999, the number of severe wind reports increased by more than 400% (Figure 2.6). The largest increase occurred in the 1990s at a rate of 400 reports per year. An interesting trend in the time series in Figure 2.6 shows a sharp increase in the frequency of "gust reports" with a nearly simultaneous decrease in the frequency of "damage reports". Such a discontinuity may be attributed to the practice of arbitrarily assigning wind speed values to all damaging thunderstorm wind events (Schaefer and Brooks 2000). The most commonly assigned wind speed values occur at 5 and 10 kt. intervals (e.g. 60, 65, 70 kt.), while a large number of reports are assigned the minimum speed value (50 kt.) (Figure 2.7).

The directional characteristics of potentially damaging wind gusts have recently been examined in the Southeast U.S. using maximum hourly wind gust observations at automated surface observing stations from 1995 to 2003 (Martin and Konrad, forthcoming). The highest gust category in their study was 13.4-17.9 m s^{-1} (30-40 mph), which falls below the severe thunderstorm criteria used by the NWS. Throughout much of the region, the predominant gust direction had a westerly component (either from the southwest or northwest). These gusts were generally tied to the passage of strong mid-latitude cyclones during the late winter and early spring and tropical cyclones during the fall. The frequencies of high wind gusts were minimized during the summer months with only 8% of all wind gusts associated with thunderstorms (Martin and Konrad, forthcoming). It is likely that the sparse network of observation stations is not adequate

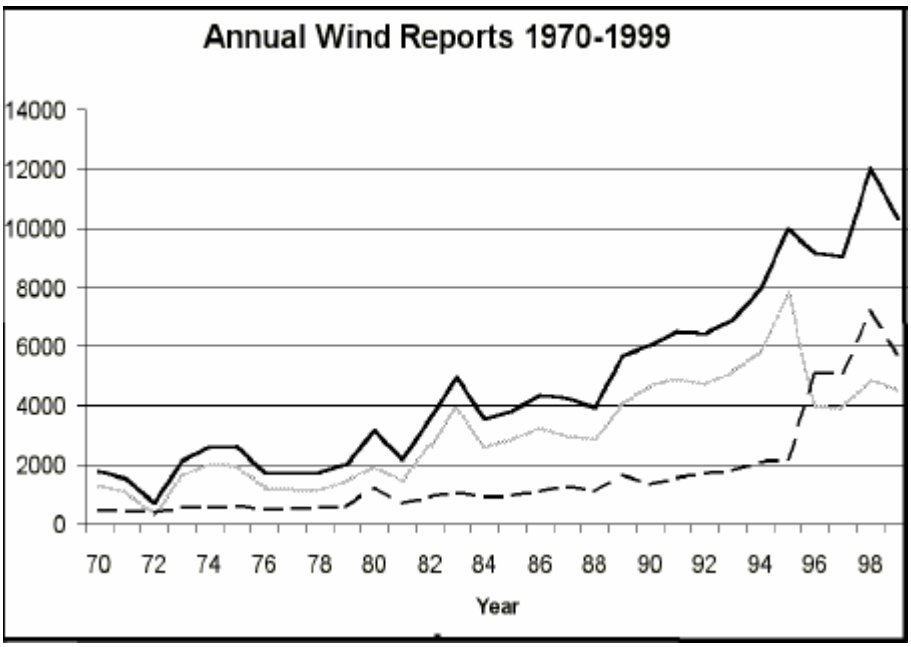

Figure 2.6. Annual number of severe convective wind reports from 1970-1999. Total reports indicated by solid black line, gust reports indicated by the dashed line, and damage reports indicated by the solid gray line (Weiss et al. 2002).

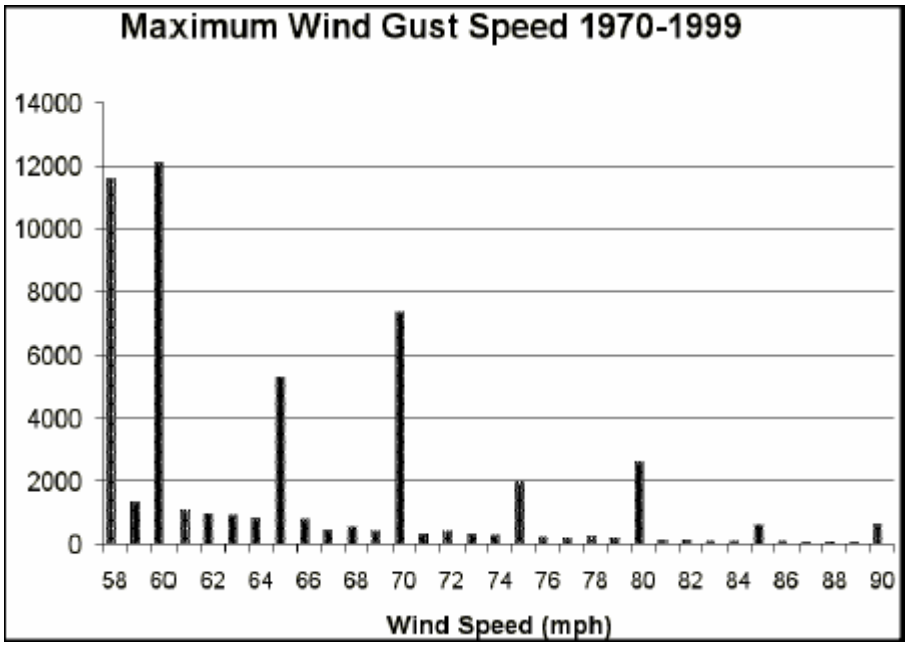

Figure 2.7. Frequency of severe wind gusts from 1970-1999 by gust speed (Weiss et al. 2002).

enough to cover all modes of severe wind gusts, particularly those that occur over the smallest spatial scales (e.g. microbursts). Taken together with the results from Kelly et al. (1985), Weiss et al. (2002), and Senn (2003), such discontinuities in the observation, measurement, and reporting of severe wind-producing thunderstorms makes rendering an accurate and robust climatology a difficult task.

2.5 Cloud-to-Ground Lightning and Severe Wind

While the convective and microphysical environments associated with severe wind-producing storms have been observed and modeled (see Wakimoto 2001), comparatively little attention has been given to the character of their CG lightning activity. The patterns, frequencies, and characteristics of CG lightning associated with severe storms has garnered significant attention in the past decade or so as advancements in lightning detection systems have resulted in spatial and temporal resolutions which allow for analysis on the storm scale (Orville et al. 1983; Cummins et al. 1998; Orville and Huffines 2001). The resulting patterns of CG lightning may provide useful nowcasting signatures of severe weather in local storms if the patterns can be demonstrated consistently from one storm to the next (Branick and Doswell 1992).

A few case studies have illustrated both peaks and lulls in CG lightning associated with thunderstorm downbursts. Kane (1991) examined the properties of CG lightning associated with a damaging downburst-producing storm in central Massachusetts on 3 June 1989. Wind gust reports exceeding 36 m s^{-1}, along with reports of large hail, were found to follow the peak in the 5-min. CG lightning flash rate. The percentage of positive CG (+CG) lightning flashes increased during the lifetime of the storm, from

0.6% during peak CG lightning activity to 49.2% around the time of the downburst. It is suggested that the descending mass of ice through the downdraft may generate a net positive charge beneath the main negative charge in the cloud (i.e. an inverted vertical dipole or tripole structure, Williams 2001), promoting more +CG lightning flashes (Kane 1991).

Elson (1993) studied the CG lightning patterns associated with 14 severe thunderstorms that raced across Indiana on 2 June 1990. Collectively, there were 16 reports of severe wind, 31 reports of tornado touch-downs, and 5 reports of large hail. His analysis found a strong tendency for severe winds to occur during or shortly after a period of high CG lightning activity (>300 strikes per hour per storm). Moreover, Elson (1993) found that severe wind reports, compared to reports of tornadoes and large hail, showed the strongest relationship to the CG lightning flash rate within the parent storm. Further, the centroid of high CG lightning activity in these storms occurred between 11 and 34 km to the west (i.e. upstream) of the severe wind reports. Similar to the results of Goodman et al. (1988) and Williams et al. (1989), it is suggested that a decrease in the CG lightning flash rate during a period of storm collapse may signal a potentially damaging downdraft (Elson 1993).

Price and Murphy (2002) studied the CG lightning characteristics associated with the Boundary Waters derecho in Minnesota, which occurred on 4 July 1999. They found that while the total CG lightning flash rate dropped during the most intense phase of the derecho, the percentage of +CG lightning reached as high as 97%. The suppression in the total CG lightning flash rate was further substantiated by van den Broeke et al. (2005), who analyzed two cool season derecho-producing convective lines. Using the

CG lightning nowcast parameter developed by Bright et al. (2005), they found that the production of CG lightning in these storms was sensitive to the occurrence and vertical distribution of instability in the mixed-phase region of the storm cloud. When little or no instability was found in the mixed-phase region, little or no CG lightning occurred along the convective line, although severe weather was still observed.

Altino et al. (forthcoming) recently studied a severe, microburst-producing thunderstorm that occurred over the Huntsville, AL area in August of 2002. They found that the total CG lightning flash rate exhibited a peak-lull-peak pattern beginning approximately 20 min. before the microburst occurred (Figure 2.8). The frequency maximum in the total CG lightning flash rate peaked at the time of the microburst, then dissipated and became erratic as the storm collapsed. It is suggested that the liquid water content and vertical motions within the storm contributed to the enhancement in CG lightning activity (Altino et al., forthcoming). The rapid descent of graupel and small hail through the melting layer, which can result in enhanced production of CG lightning, has also been shown to signal a strong downburst (Carey and Rutledge 1996).

Even among a number of case studies suggesting distinctive signals in the CG lightning characteristics associated with severe winds, few studies have attempted to examine these relationships over broader temporal scales (e.g. >10 yr.) or incorporate larger sample sizes. Carey et al. (2003) suggest that the results of such an analysis would be inconclusive given that the environmental causes for severe winds are so numerous. Instead, future studies of CG lightning and severe weather should segregate the severe wind reports into unique categories (e.g. bow echoes, microbursts) for comparison with

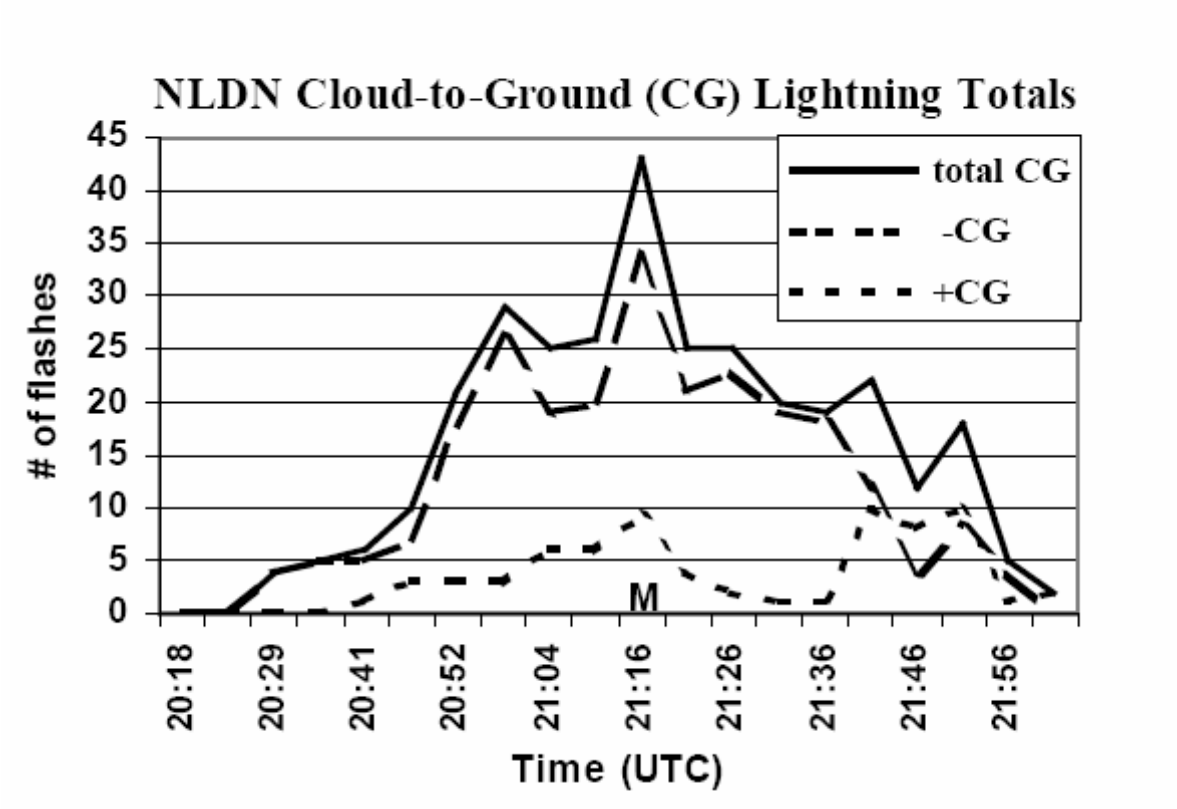

Figure 2.8. CG lightning flash rates associated with a microburst producing storm over Huntsville, AL. The "M" denotes the time of the microburst (Altino et al., forthcoming).

large hail and tornado reports as well as with non-severe thunderstorms (Carey et al. 2003).

2.6 Summary

It is clear that a large volume of research exists on the frequency, distribution, and meteorological environments associated with severe winds. Yet, these events are still inherently difficult to forecast. Unfortunately, much of what we know about these events stems from case studies with limited geographic scope. The convective organization of

severe windstorms in the Southeast is unknown, even though these events occur rather frequently across the region (Senn 2003; Doswell et al. 2005). This is particularly the case when compared to hailstorms and tornadic thunderstorms. Further, the synoptic-to-mesoscale environments associated with severe winds in the Southeast are not documented. As a result, there is much uncertainty as to what atmospheric environments, topographic boundaries, and land-atmosphere interactions conspire to produce thunderstorms capable of severe winds, particularly in the absence of strong dynamics.

In addition, the use of CG lightning data to determine the convective development and severity of thunderstorms has shown some promise in operational forecasting. Since most of the relationships between CG lightning and thunderstorm severity have been derived from case studies, their potential applicability to current forecasting techniques should be considered embryonic. As Wakimoto (2001) suggests, the ability to diagnose the convective development of severe wind events may greatly improve their predictability. This research will determine the convective modes, synoptic-to-mesoscale environments, and CG lightning characteristics that typify a warm season, severe windstorm event across Georgia. The results of this work will provide a frame of reference from which forecasters can improve their situational awareness and verify existing numerical models when confronted with conflicting or ambiguous output.

CHAPTER 3

DATA AND METHODS

The purpose of this research is to provide a description of the convective modes, meteorological environments, and CG lightning patterns associated with warm season, severe windstorms across Georgia. It is hypothesized that severe winds in this area develop from both organized (e.g. linear) and unorganized convective systems and that the synoptic-to-mesoscale environments which facilitate these event are multi-faceted. Further, it is hypothesized that the patterns and characteristics of CG lightning, when combined with analysis of radar scans, may be used to differentiate between ordinary thunderstorms and those capable of producing severe wind.

Individual reports of severe thunderstorm wind were initially grouped according to whether they occurred in a pattern suggesting they may have originated from the same convective system. These groupings were confirmed using available national composite radar summaries. Upon confirmation, short-range base reflectivity scans were examined to determine the predominant and persistent convective mode associated with each of the identified windstorm events. Analysis of the synoptic and mesoscale environments associated with each windstorm event was performed using surface weather maps, re-analysis data, and radiosonde observations. The patterns and density of CG lightning associated with a subset of severe wind-producing thunderstorms and non-severe thunderstorms were evaluated by mapping the distribution of CG flashes at 5-min.

intervals during the lifecycle of these events. The map-times indicating potential CG lightning signatures are presented and discussed in the context of thunderstorm development and the cloud-scale charging structures facilitating the production of lightning.

3.1 Severe Wind Report Data

Individual reports of severe thunderstorm wind occurring in Georgia during the warm season months (April-September) of 2000-2003 were extracted from the SPC historical database and plotted using the SeverePlot software (Hart and Janish 1999). The accuracy and precision of severe wind reports have been questioned repeatedly in the meteorological literature. This stems from the manner in which these reports are made and recorded. An individual generally must observe the event, correctly identify and classify the event, and report the event to the appropriate authorities to be placed in the historical records (Doswell and Burgess 1988).

A number of factors influence the reporting of severe weather (Kelly et al. 1985; Weiss and Vescio 1998; Weiss et al. 2002). The observation of a severe weather event may be obscured by the local topography, intervening clouds, and darkness. Misidentification of a severe weather event may occur due to improper training or deficient scientific understanding. Common mistakes in the identification of severe weather include incorrectly measuring or estimating wind gust speed or hail size and reporting thunderstorm downdraft damage as a tornado. Variations in population density may result in a biased distribution of severe weather reports.

As previously mentioned, a dramatic increase in the reporting of severe weather is apparent over the past 30 years. Weiss et al. (2002) discuss some of the likely factors influencing this trend. These include the implementation of a national warning verification system, the development of trained spotter networks, the deployment of the Next Generation Radar (NEXRAD) network, population increases and urban sprawl, and an overall increase in weather awareness among the populace through media and government agencies. Results from Weiss and Vescio (1998) and Weiss et al. (2002) show regional biases in the effect these factors have on severe weather reporting practices. For instance, specific wind gust assignments (e.g. 50 kt.) are favored in particular regions (e.g. coincident with NWS county warning areas), mainly throughout the Midwest and Ohio River Valley (Weiss et al. 2002). Additionally, the increase in severe weather reports, particularly since the 1990s, has favored reports of lower magnitude (e.g. F0 tornado reports, 50 kt. wind gusts). Severe wind events are considered the most subjective in terms of reporting criteria. For example, many reports are not assigned a magnitude, or peak gust value[2]. Further, there is some ambiguity in the information being reported. For instance, are the reports merely "best guess" of wind speed or are they interpreted from damage surveys? Are the wind speed values estimated (e.g. subjectively assigned 50 kt.) or measured (e.g. wind gust calculated with an anemometer)? (Weiss and Vescio 1998). A field study of wind damage from intense Midwest bow echoes by Trapp et al. (2005) conclude that "there is no alternative to the *Storm Data* reports if a reasonable sample size is required, but both underestimates and overestimates should be expected."

[2] Changes in severe weather event reporting policy now require wind damage reports to be accompanied by a wind gust report, which likely resulted in large spikes in the frequency of 50 kt. reports in the mid-1990s (Weiss et al. 2002).

3.2 Radar Data

National composite radar summaries from the UCAR image archive[3] were examined to confirm the initial grouping of individual severe wind reports into patterns suggesting they originated from the same convective system. Composite reflectivity summaries display the maximum echo intensity from any elevation angle at any range from individual radar sites in the WSR-88D network. National composite reflectivity images are displayed at 15-min. intervals with a resolution of 2 km. The composites are displayed with 16 reflectivity factors, color-coded in 5-dBZ increments. Parker and Johnson (2000) determined that the spatial and temporal resolution of the national composite reflectivity summaries is adequate for identification of convective systems with meso-beta (20-200 km) and meso-gamma (2-20 km) organization (Orlanksi 1975).

Following confirmation of the initial grouping of severe wind reports, short-range (230 km) base reflectivity and base velocity scans from selected radar sites in the WSR-88D network were examined to more accurately determine the reflectivity signatures associated with severe wind-producing convective systems. Base reflectivity and velocity scans have a temporal resolution of between 5 and 7 min., a spatial resolution of 1 km, and an elevation angle of 0.5°. The distribution of radar sites used in this study is shown in Figure 3.1, while the temporal coverage of these sites is given in Table 3.1. Base reflectivity and velocity data were uploaded from NCDC[4] with the resulting images displayed using the Java NEXRAD Viewer and Data Exporter[5].

[3] http://locust.mmm.ucar.edu/case-selection/
[4] http://hurricane.ncdc.noaa.gov/pls/plhas/HAS.FileAppSelect?datasetname=7000
[5] http:// www.ncdc.noaa.gov/oa/radar/jnx/

Figure 3.1. Locations of local radar sites from the WSR-88D network used in this study.

Table 3.1. Local radar sites from the WSR-88D network identified in Figure 3.1. "Complete" indicates that base reflectivity and storm-relative velocity data were available for the period of record used in this study (April 2000-September 2003).

Radar Sites	ID	Latitude °N	Longitude °W	Record
Peachtree City, GA	KFFC	33.367	84.579	Complete
Robins AFB, GA	KJGX	32.679	83.364	1/1/2001-present
Moody AFB, GA	KVAX	30.894	83.006	5/1/2001-present
Jacksonville, FL	KJAX	30.488	81.723	Complete
Tallahassee, FL	KTLH	30.402	84.342	Complete
Fort Rucker, AL	KEOX	31.464	85.480	5/1/2001-present
Birmingham, AL	KBMX	33.176	86.783	Complete
Huntsville, AL	KHTX	34.935	86.088	Complete
Greer, SC	KGSP	34.887	82.233	Complete
Columbia, SC	KCAE	33.953	81.123	Complete
Charleston, SC	KCLX	32.659	81.055	Complete

3.3 Radiosonde Data

Radiosonde data from Peachtree City, GA, (KFFC) and Jacksonville, FL, (KJAX) were used in this study to calculate convective parameters commonly associated with severe thunderstorm winds. Sounding data were obtained from the Forecast Systems Laboratory (FSL)[6]. Similar to Klimowski et al. (2003), only data from the 00 UTC soundings were used, as few events occurred during the early morning soundings (12 UTC). It is important to note that this study does not use a proximity sounding approach (see Evans and Doswell 2001). The surface-based parcel was used to calculate relevant thermodynamic parameters, while the virtual temperature correction (Doswell and Rasmussen 1994) was not utilized.

Since a number of errors may occur in the recording of upper-air observations, quality-control checks of the data were performed following the suggestions of Klimowski et al. (2003). A sounding was omitted if it recorded a surface wind speed of >25 m s^{-1} or if the 110 hPa level was not reached. Additionally, all meteorological variables were checked for credibility. If the variables calculated at a given level were intolerable, that level was omitted from the sounding (e.g. a wind direction value of 365°). Approximately 12% of the soundings recorded during the period of record were discarded due to these constraints.

3.4 Cloud-to-Ground Lightning Data

The CG lightning dataset used in this study covers the entire state of Georgia for the period 1992-2003. The production of CG lightning across the U.S. is monitored and recorded by Vaisala-Global Atmospherics, which operates the National Lightning

[6] http://raob.fsl.noaa.gov/

Detection Network (NLDN). The NLDN is comprised of 106 ground-based sensors spread across the U.S. These sensors record the location (in latitude and longitude coordinates), date, time, and peak current of each CG flash. A central processor calculates the polarity and multiplicity of each CG flash (Cummins et al. 1998). The most recent upgrade of the NLDN occurred in 2002 (Biagi et al. 2004), resulting in a detection efficiency of over 90% across the Southeast, a locational accuracy of 0.5 km, and a temporal accuracy of 1 s. It has been demonstrated that positive flashes with a peak current <10 kA are actually strong intra-cloud discharges and should be removed from analysis (Wacker and Orville 1999; Biagi et al. 2004). This routine eliminated 8% of the flashes recorded in the NLDN dataset.

3.5 Research Methodology

The initial step in this research was to identify all warm season, severe wind-producing convective systems across the state of Georgia for the period 2000-2003. The study period was limited to these four years since the national radar composite summaries prior to 2000 were mostly limited to one image per day and thus were inadequate to capture the evolutionary features of the convective systems. The analysis was limited to the state of Georgia due to boundary limitations of the CG lightning dataset. Thus, an under-sampling of events for the Southeast region as a whole is inherent, although it is suggested that many of the results from this study may be applied to other parts of the Southeast.

Individual severe thunderstorm wind reports recorded in Georgia were extracted from the SPC archive and plotted using the SeverePlot software (Figure 3.2). The reports

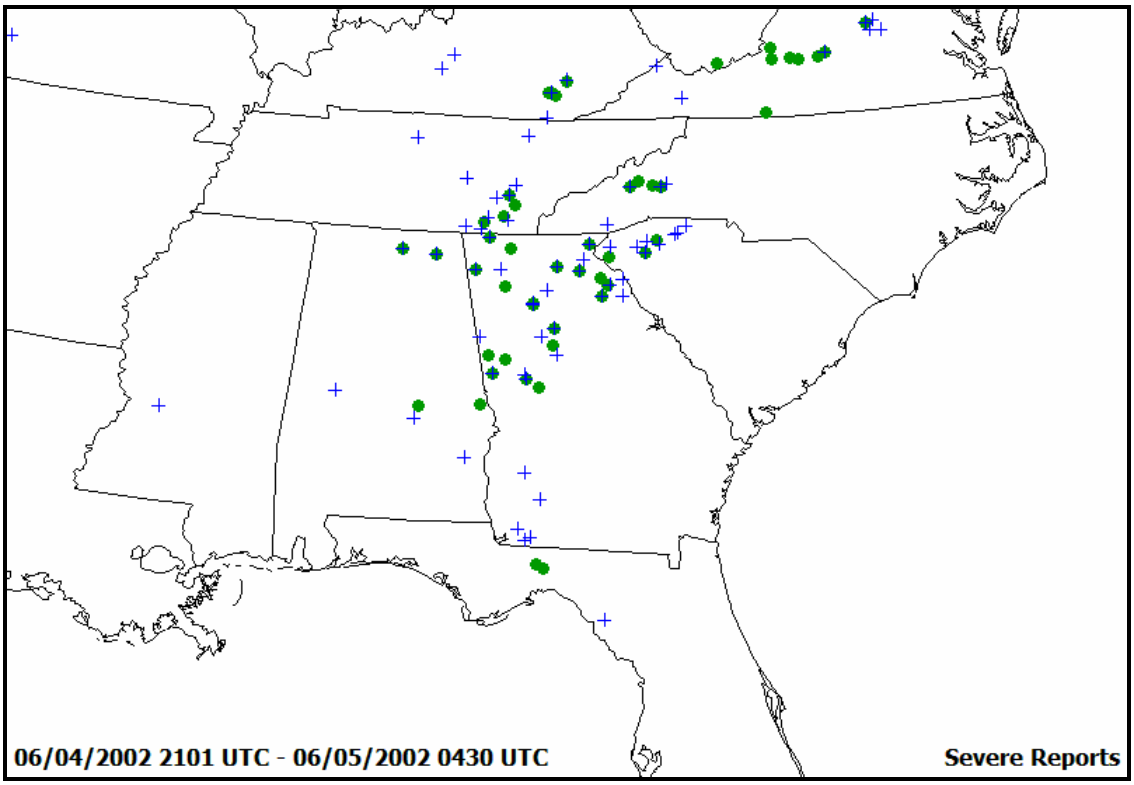

Figure 3.2. Map of severe wind (blue crosses) and large hail (green circles) reports using the SeverePlot software. This event was classified as a severe wind-producing squall line (26 severe wind reports in GA) using the national composite summaries and base reflectivity scans from KFFC.

were sorted according to their spatial and temporal continuity. In other words, each group of reports must have occurred in a pattern that suggested they may have originated from the same convective system. After sorting the severe wind reports, an examination of the national composite radar summaries was conducted to confirm the initial grouping of reports. Only non-tornadic windstorms were examined in this study. These methods yielded 211 windstorm events (Appendix A).

Once these windstorm events were confirmed, both the national composite radar summaries and the short-range base reflectivity scans were examined more closely to

determine the convective mode associated with each of the events. The convective mode was defined as the predominant structure of the convective system as it was producing severe winds in Georgia. This is similar to the criteria used by Parker and Johnson (2000) in that *only the persistent, predominant organizational mode was considered, not the instantaneous structure*.

Radar-observed criteria adopted from Klimowski et al. (2003) were used to classify the convective mode of each of the 211 non-tornadic, severe windstorm events. Six categories were used in this classification: squall line, bow echo, supercell, irregular, single report, and indeterminate. In each case, two or more severe wind reports were required, otherwise the event was classified as a single report. If the radar data were insufficient for identifying a predominant convective mode, or unavailable, the event was classified as indeterminate. Convective (stratiform) regions were defined as radar pixels with a reflectivity factor >40 (20-40) dBZ (Geerts 1998; Parker and Johnson 2000). A detailed description of the reflectivity signatures and characteristics of each convective mode is presented below.

- **Squall lines** should exhibit a reflectivity length-to-width ratio of 5:1, exhibit convective cells along a line >50 km, and persist for >30 min. Squall lines may contain either a contiguous or nearly contiguous chain of convective cells, even if a moderate amount of stratiform precipitation is absent (Houze et al. 1990; Parker and Johnson 2000). Linear systems with moderately curved arcs, if not meeting the other requirements for bow echo structure, may be classified as squall lines. Squall lines with stratiform precipitation may be further divided into one of three archetypes after Parker and Johnson (2000): trailing stratiform, leading stratiform, and parallel stratiform. It is possible for the convective line to separate from its stratiform region by a distance of 50 km. The intensity of convection (i.e. the maximum reflectivity factor) or storm severity (i.e. the frequency or maximum gust speed of the wind reports) are not examined.

- **Bow echoes** are defined by a bow or crescent-shaped radar echo with a tight reflectivity gradient on the convex (leading) edge and the characteristic rotating heads (Fujita 1978). The bow must demonstrate linear organization and exhibit an increasing radius with time or a persistent arc. The bow shaped radar echo may be singular (i.e. isolated) or embedded within a larger convective system, such as a squall line. The presence of rear inflow notches or jets was not required for the system to be classified as a bow echo.

- **Supercells** are defined by the presence of a mesocyclone for tens of min. and extending through at least one-third of the storm's depth (Moller et al. 1994). If the presence of a mesocyclone is ambiguous from the base reflectivity animation, base velocity data were examined from a nearby radar site. A supercell can remain either as a single, continuous cell, or take on characteristics of the "multicell-supercell hybrid" defined by Nelson (1987). While most supercells demonstrate deviate motion (i.e. move to the right of the mean winds), some may be classified as left-moving (Bunkers et al. 2000). No distinction is made between high-precipitation and low-precipitation supercells.

- **Irregular** convective storms are generally characterized by scattered strong cells with irregularly (i.e. non-linear) shaped convective regions and little or no organizational pattern.

Additionally, the national composite summaries and the base reflectivity images were used to determine the beginning and end times and locations of each convective system, their evolutionary characteristics (e.g. cell mergers), and any distinctive radar-observed features (e.g. parallel stratiform precipitation). The derecho criteria developed by Ashley et al. (2005) were used in this study to determine if any of the convective systems were associated with these long-lived, widespread windstorms (Table 3.2). One of the goals of this thesis was to determine whether the meteorological environments associated with severe wind are distinguishable from non-severe convection. An independent sample of non-severe thunderstorm (i.e. convective) days was created using daily counts of CG lightning. If at least five CG flashes were reported in Georgia over a

Table 3.2. Criteria used to identify derechos in this study (Ashley et al. 2005).

Minimum length	There must be a concentrated area of convectively induced wind gusts greater than 26 m s^{-1} that has a major axis length of 400 km or more (unless a land constraint necessitates using a shorter distance)
Chronological progression	The wind reports must have chronological progression, either as a singular swath (progressive) or as a series of swaths (serial), and nonrandom pattern of occurrence by temporally mapping the wind reports of each event
Temporal and spatial resolution	No more than 2.5-h can elapse between successive wind reports with no more than 2° of latitude and longitude separating successive wind reports
Origin of wind swath	Multiple swaths of damage must be part of the same MCS as indicated by examining available radar data
MCS continuity	The associated MCS, as indicated by available surface pressure and wind fields or radar data, must have temporal and spatial continuity

24 h period beginning at 12 UTC and no severe weather was reported, the environment was classified as non-severe.

To determine the influence of synoptic-scale surface features (e.g. frontal boundaries) on convective processes associated with severe winds and non-severe convective environments, daily surface weather maps from the Unisys Weather Image and Map archive[7] were examined. Similar to Dixon and Mote (2003) and Bentley and Stallins (2005), if a synoptic-scale frontal boundary was within 500 km of the study area, the environment was characterized as strongly forced. These strongly-forced environments were further divided according to the air mass sector (warm, cold, or cool) within which they originated. To further characterize the large-scale environment

[7] http://weather.unisys.com/archive/sfc_map/

associated with severe windstorms, composite maps of five synoptic fields and their anomalies (i.e. departures from the climatological mean) were studied. The mid-tropospheric flow and shear patterns were assessed from 500 hPa geopotential height and vector wind composites. The low to mid-tropospheric moisture profile was assessed from composites of 925 hPa and 700 hPa specific humidity, while the large-scale stability profile was assessed from composites of the lifted index. Data from the NCEP/NCAR re-analysis project (Kalnay et al. 1996) were used to produce the composite maps.

The mesoscale environments associated with severe windstorms were evaluated from thermodynamic profiles of instability, moisture, shear, and convective energy. Nine sounding parameters were selected based on the findings of previous severe windstorm projects and the well-established connection between severe thunderstorm winds and deep, moist convection (see Johns and Doswell 1992). These parameters were calculated from radiosonde observations taken at 00 UTC over Peachtree City, GA, (KFFC) and Jacksonville, FL, (KJAX) and include: K-index, convective available potential energy (CAPE), total column precipitable water, convective inhibition, Bulk-Richardson number, lifted index, mean mixed-layer mixing ratio, equivalent potential temperature (Θ_e), and the lifting condensation level. Detailed descriptions of thermodynamic parameters are provided in Appendix B. Box plots were created to illustrate the distribution of individual sounding profiles, while a Student's t-test was conducted to assess the statistical significance of the differences in the mean values of each sounding parameter between severe wind environments and non-severe convective environments.

In this study, six severe wind-producing thunderstorms and five non-severe thunderstorms were chosen to study the CG lightning patterns associated with these

events. Individual CG flashes were mapped at 5-min. intervals beginning with the first recorded flash associated with each event. To identify the locational relationships between CG lightning production, storm structure, and severe wind, the CG flashes in each 5-min. interval were plotted atop the local base reflectivity scan which most closely corresponded to the end time of the CG flash interval. For example, the CG flashes recorded from 2150 UTC to 2155 UTC were plotted atop the radar scan at 2254 UTC. This was done to account for variations in the motion vector of each convective system (see Parker et al. 2001), thus depicting storm-relative CG flash locations. Both the CG lightning data and local base reflectivity data were analyzed using the Java NEXRAD Viewer and Data Exporter. After analyzing the 11 cases, one severe wind case and one non-severe case that best demonstrated the CG lightning behavior of that group were selected for discussion.

3.6 Summary

This study used severe thunderstorm wind reports archived by the SPC, available radar data from NCAR and NCDC, surface weather maps from the Unisys Weather Map and Image Archive, synoptic field data from the NCEP/NCAR re-analysis project, radiosonde observations archived by the FSL, and CG lightning data from the NLDN to evaluate the characteristics of warm season severe windstorms across Georgia. Specifically, the convective organization and evolution of these events were identified, followed by an analysis of the synoptic-scale and mesoscale environments which favor their development. Finally, the temporal and spatial patterns of CG lightning were observed across a subset of severe wind-producing thunderstorms and non-severe

thunderstorms. The results of this study are presented in the next chapter. By summarizing these characteristics, forecasters may better anticipate the development of thunderstorms capable of severe and damaging wind.

CHAPTER 4

RESULTS AND DISCUSSION

This thesis examines three aspects of warm season (April-September) severe windstorms in Georgia. First, the convective organization and evolution of severe windstorms are determined through examination of national and local radar images. Second, the synoptic-to-mesoscale environments associated with these events are evaluated using surface weather maps, re-analysis data, and thermodynamic profiles of deep, moist convection. Lastly, the characteristics and evolution of CG lightning associated with severe wind-producing thunderstorms are presented. By comparing these results to those from an independent sample of non-severe convective events, the distinguishing aspects of severe windstorm environments are revealed. The results of this research may aid in interpretation of numerical forecast models and the situational awareness of forecasters when faced with developing severe weather conditions.

4.1 Convective Modes of Severe Windstorms

4.1.1 Overview of Severe Windstorm Characteristics

During the warm season months of 2000-2003, 1,354 severe wind reports were recorded in Georgia and archived in the SPC severe weather database. Of these reports, 554 (46%) were associated with squall lines, 8 (1%) were associated with supercells, and

Table 4.1. Summary of severe wind-producing convective system characteristics in Georgia during the warm season months of 2000-2003.

	Squall-lines	Super-cells	Irregular	Single Report	Indeterminate
Total Events	37	2	94	63	15
Frequency of wind reports (% of total)	550 (46.1)	8 (0.7)	532 (44.6)	63 (5.3)	39 (3.3)
Frequency of wind reports per event	14.9	4.0	5.7	1.0	2.6
Frequency of events with large hail (%)	31 (83.8)	2 (100)	66 (70.2)	13 (20.6)	6 (40.0)
Frequency of derecho events (%)	9 (24.3)	---	---	---	---
Average duration (wind reports)	4.7-h	3.5-h	3.1-h	1.0-h	1.9-h
Average duration (convective system)	6.8-h	3.2-h	---	---	---

532 (45%) were associated with irregular storm systems (Table 4.1). There were 63 single reports (5%), of which 24 were associated with convective systems occurring outside the study area. The balance of these single reports was likely associated with isolated microbursts, heat bursts, or was non-convective. The remaining 39 severe wind reports (3%) were associated with indeterminate storm systems. Interestingly, there were no *persistent* non-tornadic bow echoes observed during the study period, although four

squall lines under northwest steering flow did originate from decaying bow echoes over the central Plains.

There were 133 convective storm systems where at least two severe wind reports occurred in a pattern suggesting spatial and temporal coherence. Thirty-seven (28%) of these systems were classified as squall lines, 2 (1%) were classified as supercells, and 94 (71%) were classified as irregular. Examples of these convective types are presented in Figures 4.1-4.3. Of the 37 squall lines, 34 (92%) exhibited trailing stratiform precipitation, 1 exhibited parallel stratiform precipitation, 1 exhibited leading stratiform precipitation, and 1 did not exhibit stratiform precipitation. The convective region of severe wind-producing squall lines was generally between 50 and 80 km in length (81% of squall lines), although a few events exhibited convective regions extending beyond 100 km (8% of squall lines). The spatial extent of stratiform precipitation varied significantly; squall lines under northwest steering flow exhibited stratiform regions between 8,000 and 60,000 km², while 69% of the events under southwest steering flow exhibited stratiform regions greater than 50,000 km².

Although squall lines exhibited far more severe wind reports per event (14.9) than other convective types, likely due to the increased spatial coverage of these systems, the majority (71%) of severe wind-producing convective types were associated with less organized modes of convection. This is in stark contrast to severe wind-producing events over the Northern High Plains (NHP), where over 80% of the severe wind-producing convective types were comprised of squall lines, bow echoes, and supercells (Klimowski et al. 2003).

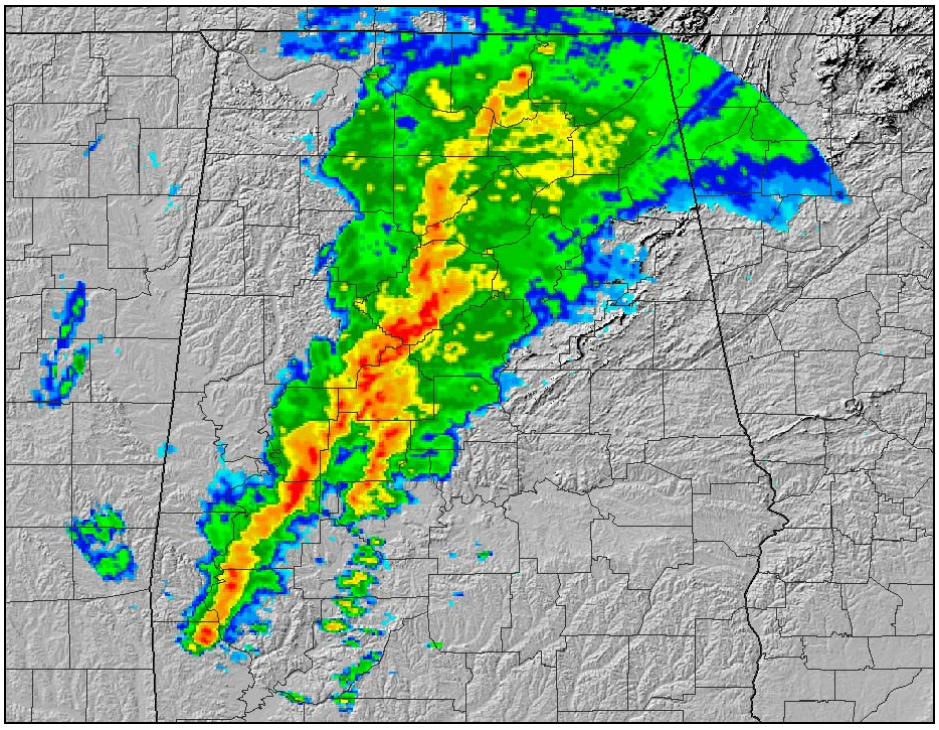

(a)

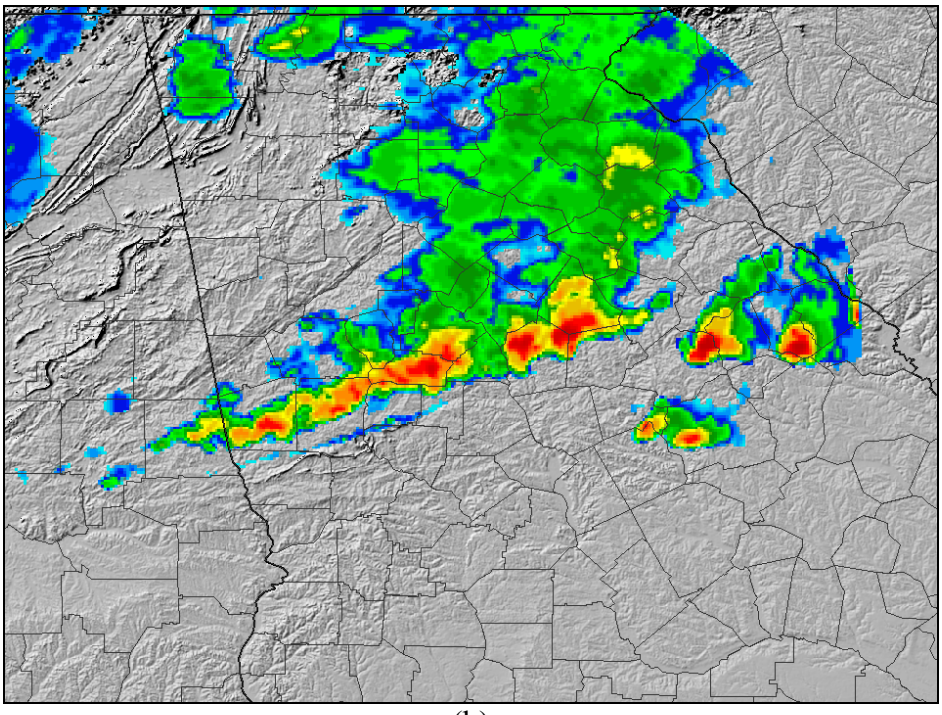

(b)

Figure 4.1. Examples of severe wind-producing squall lines using base reflectivity scans from individual radar sites in the WSR-88D network. (a) 1801 UTC 03 April 2000 (KBMX), (b) 2203 UTC 03 May 2002 (KFFC), (c) 2308 UTC 04 June 2002 (KHTX), (d) 2349 UTC 02 May 2003 (KHTX).

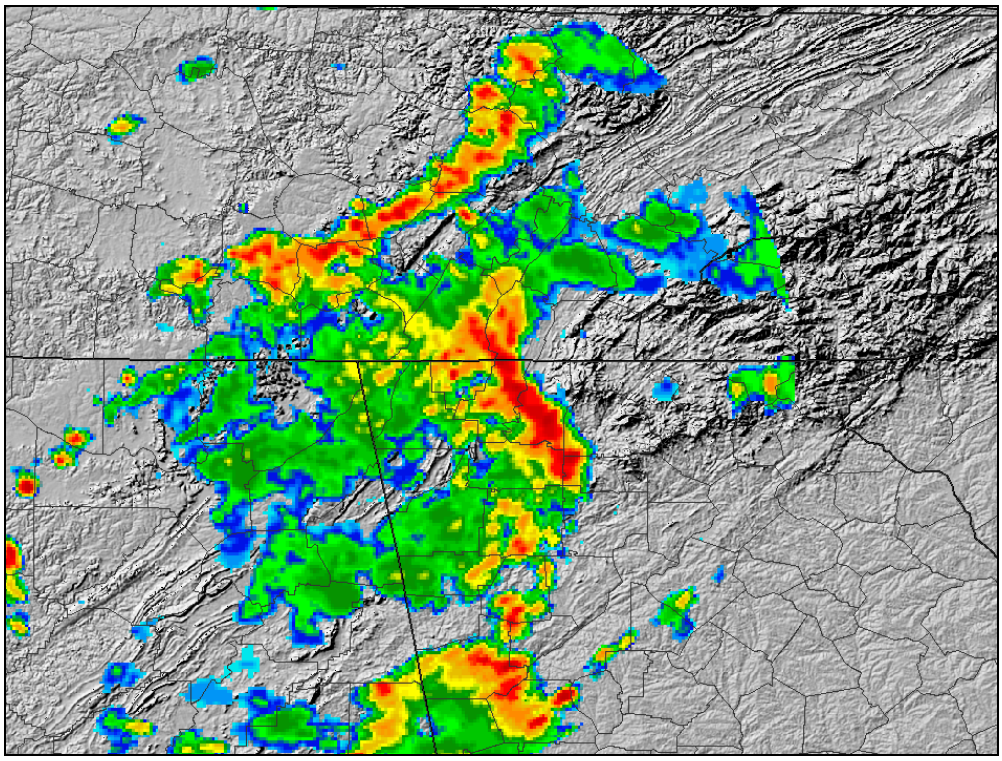

(c)

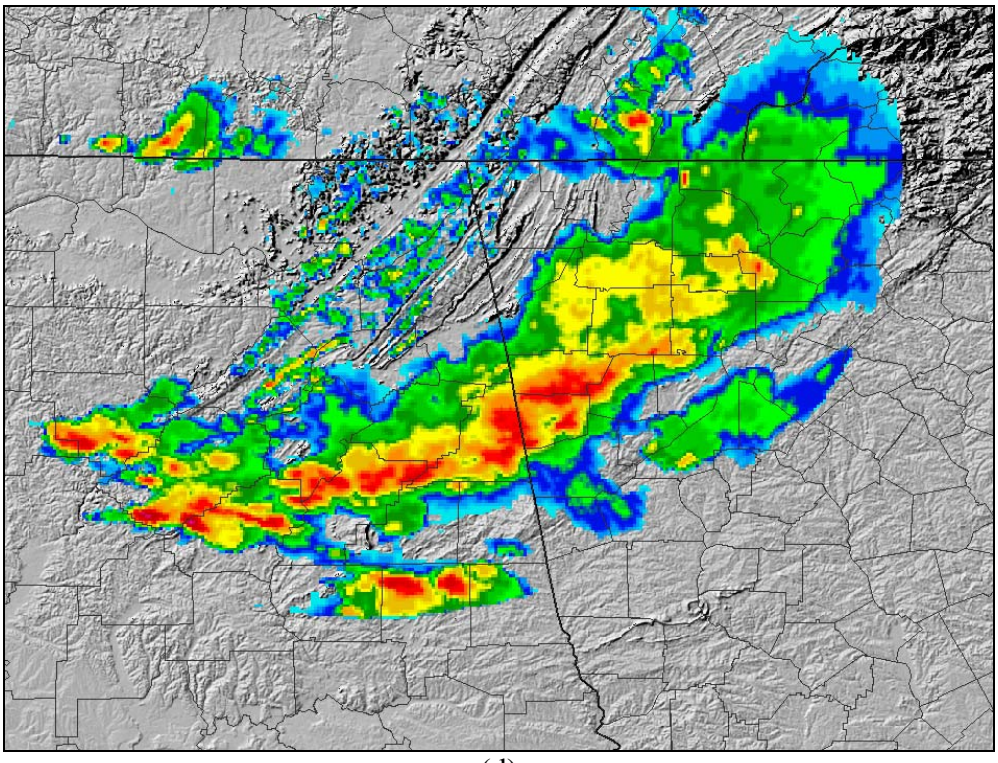

(d)

Figure 4.1. (continued)

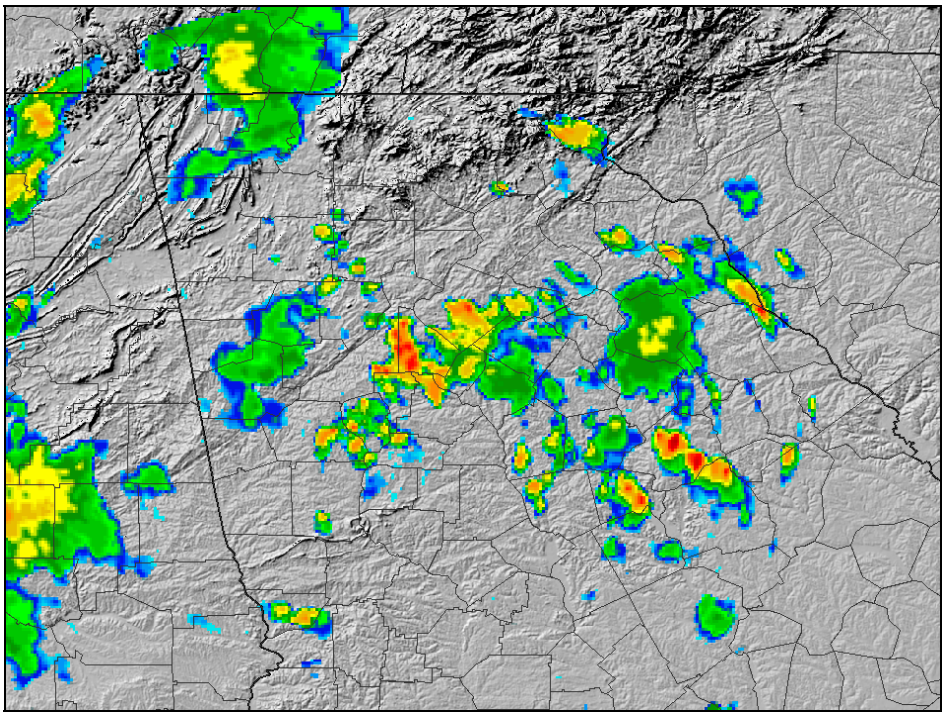

(a)

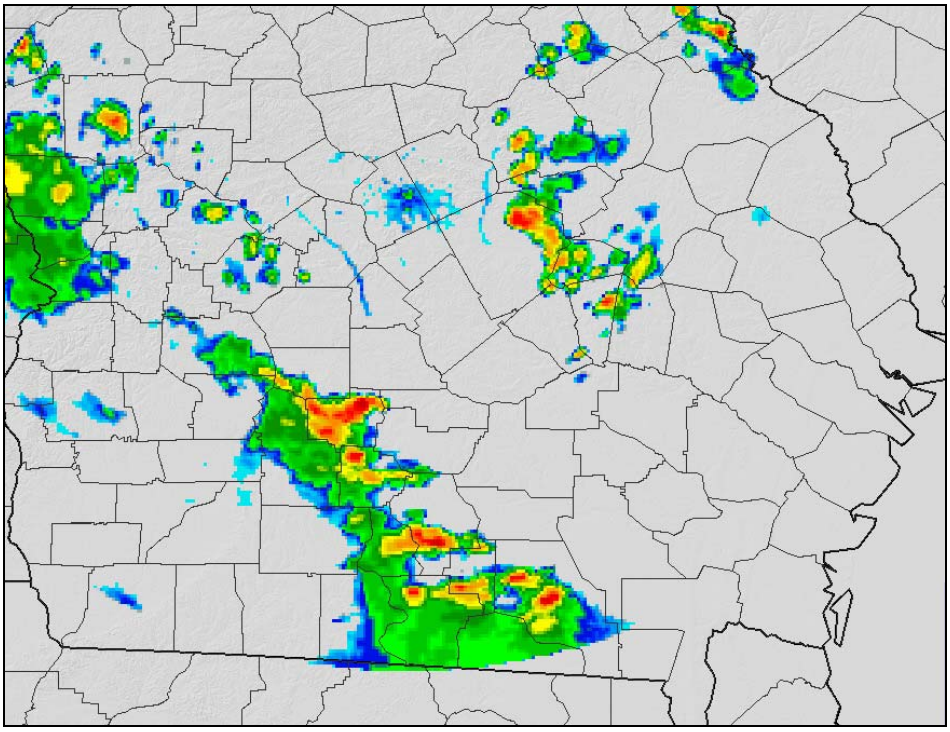

(b)

Figure 4.2. Same as Figure 4.1, but for severe wind-producing irregular storms. (a) 2330 UTC 30 July 2000 (KFFC), (b) 2348 UTC 30 May 2002 (KJGX), (c) 2215 UTC 02 July 2002 (KFFC), (d) 2302 UTC 12 June 2003 (KJGX).

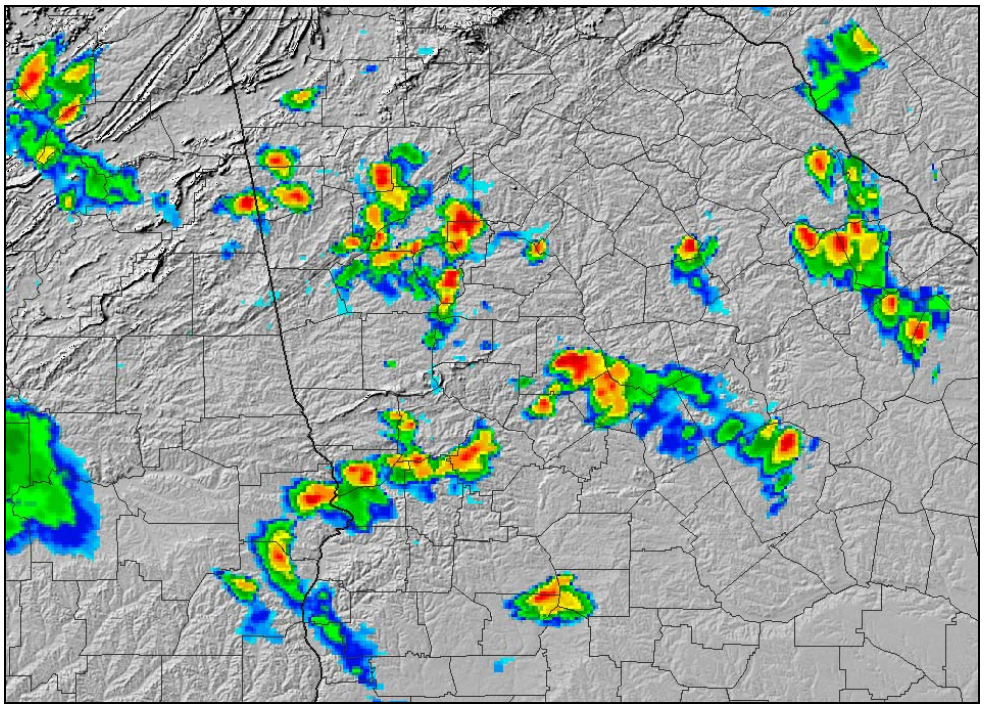

(c)

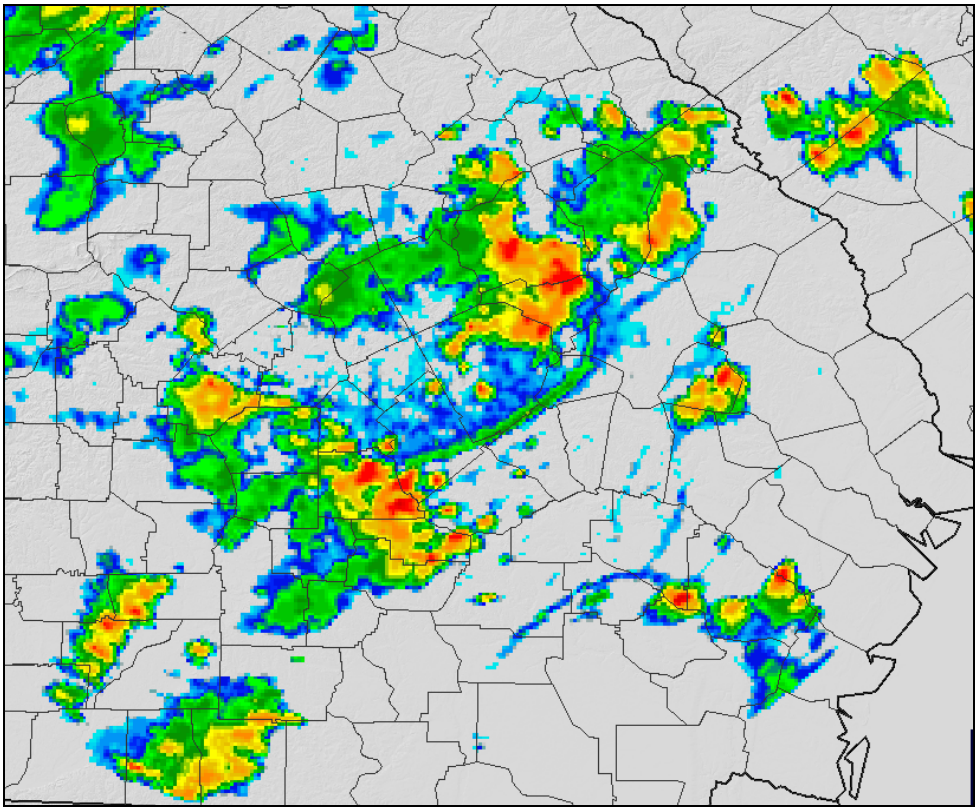

(d)

Figure 4.2. (continued)

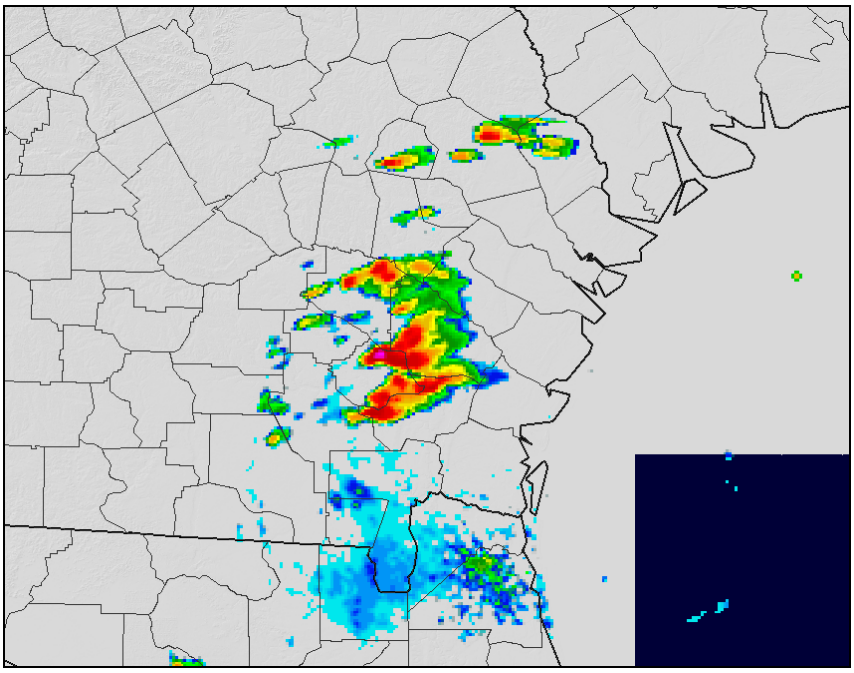

(a)

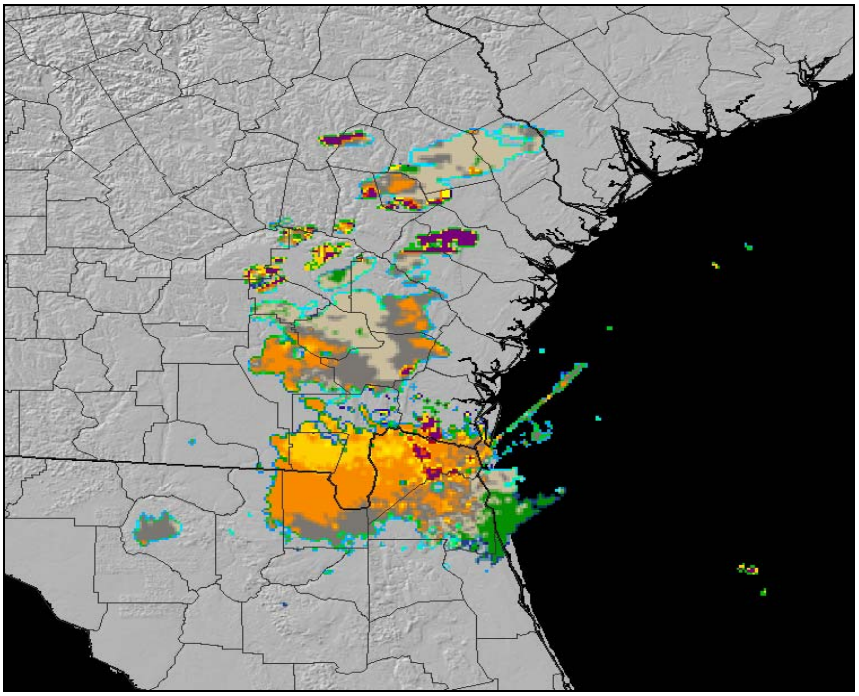

(b)

Figure 4.3. Non-tornadic severe wind-producing supercells for 2255 UTC 10 May 2002 (KJAX) (a) base reflectivity scan and (b) base velocity scan, 2250 UTC 25 April 2003 (KFFC) (c) base reflectivity scan and (d) base velocity scan. Base velocities (kt.) and their corresponding color scheme are orange (positive) for outbound velocities and gray (negative) for inbound velocities.

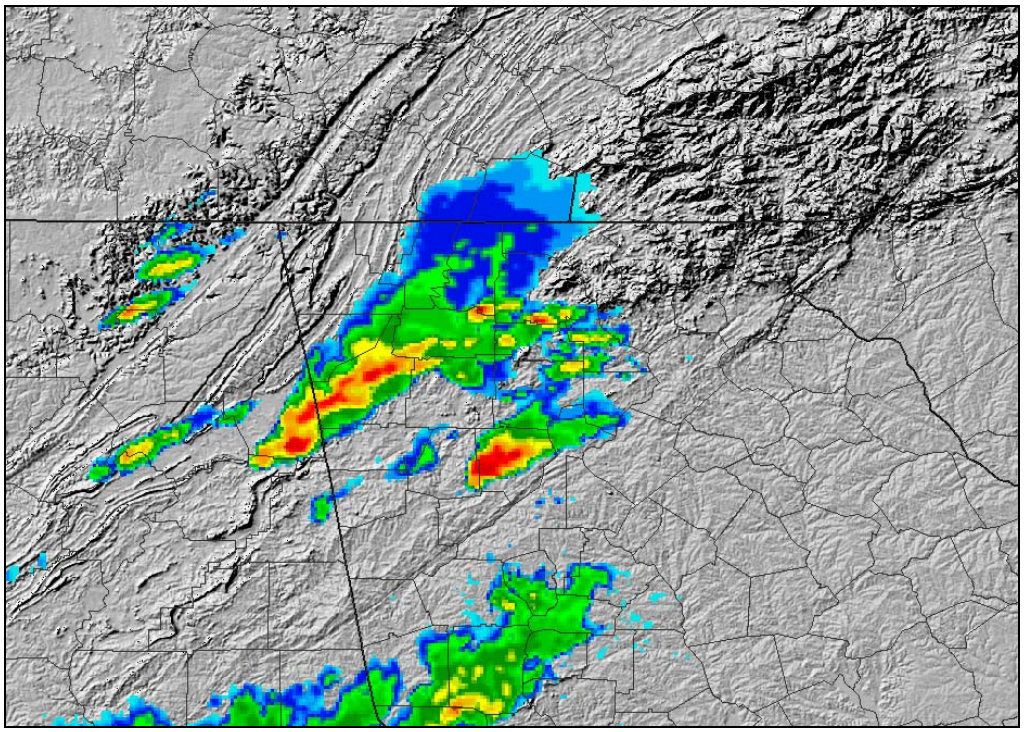

(c)

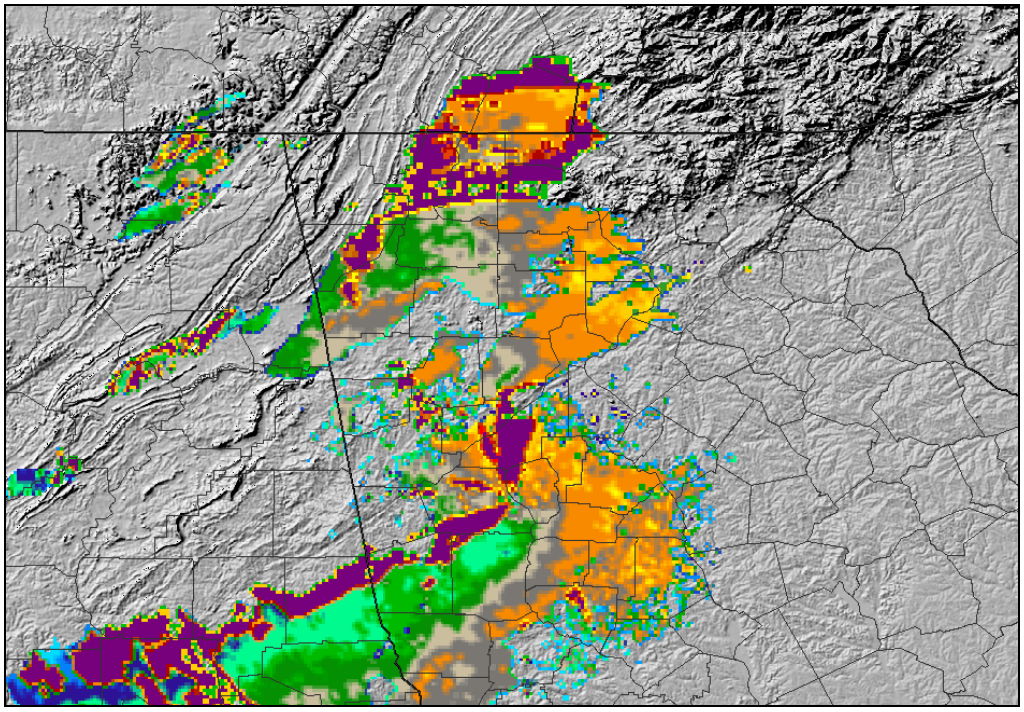

(d)

Figure 4.3. (continued)

The average duration of severe wind-producing squall lines over Georgia (6.8-h) was somewhat shorter than the mean MCS lifespan given by Geerts (1998) for the Southeast (9-h), yet was twice as long as the mean squall line duration identified over the NHP (Klimowski et al. 2003). Supercell duration over Georgia (3.2-h) was comparable to that experienced over the NHP (3.9-h), although the incidence of severe wind reports associated with non-tornadic supercells over Georgia lasted longer than the supercell storm structure itself (Table 4.1). Similar to prior studies of linear MCS and supercells, the majority of these events in Georgia were associated with large hail (Browning 1977; Moller et al. 1994; Klimowski et al. 2003). Of the 37 squall lines identified in this study, 9 (24%) were associated with derecho activity in Georgia. These events accounted for 49% of all severe wind reports associated with squall lines and 20% of all severe wind reports across the study period. Six of the 9 derechos originated in the central and southern Plains, with Georgia being a terminus region for most these events.

4.1.2 Spatial Patterns

The spatial distribution of severe wind reports in Georgia is primarily linked to population density and land-sea interactions (Figure 4.4). The former is demonstrated by the clustering of reports around the Atlanta metropolitan area (highlighted in yellow) and in northeast Georgia. The latter is demonstrated by the clustering of single reports and those associated with irregular storms along the outer coastal plain. The Georgia coastal plain was also the location for one of the severe wind-producing supercells. Brown (2002) found the coastal plain of the Carolinas, which is of similar surface topography and relief to the coastal plain of Georgia, to be a hot zone of supercell development. It is

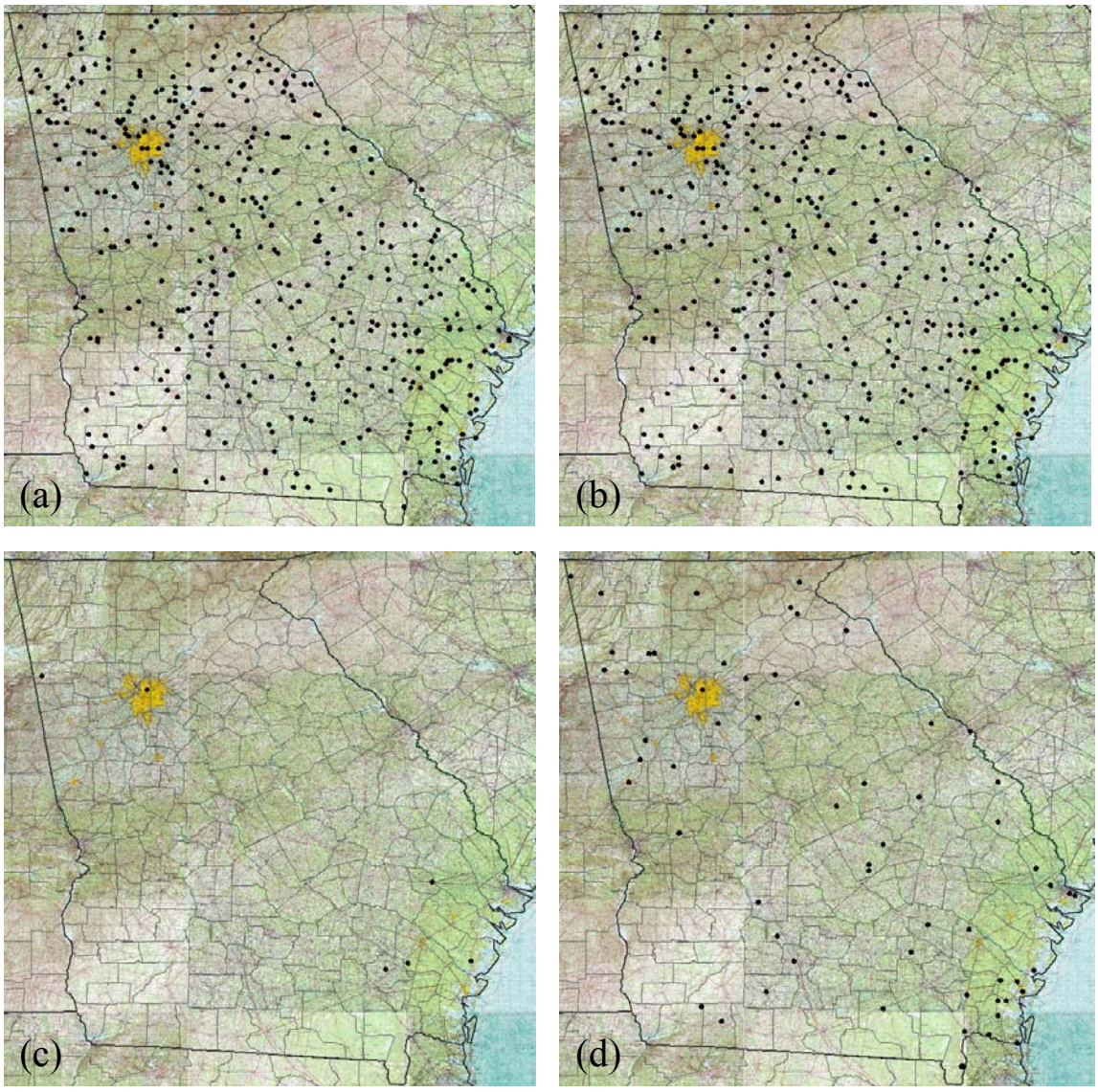

Figure 4.4. Spatial distribution of warm season severe wind reports across Georgia for the period 2000-2003 associated with (a) squall lines, (b) irregular storms, (c) supercells, and (d) single events.

likely that complex land-sea breeze interactions within the coastal plain are capable of producing relatively isolated convective storms, as well as organized supercells, with severe wind gusts. Brown (2002) also speculated that the sea breeze circulation may be acting as a focusing mechanism for moisture convergence, promoting local

destabilization of the lower-troposphere. Further, the development of irregular, multi-cellular thunderstorms over a broad area devoid of significant land-cover features may generate mesoscale cold-pools, with the resulting pressure gradient triggering severe surface winds (Kuchera and Parker, forthcoming).

The overall distribution of severe wind reports in Georgia is nearly identical to the patterns of convection identified by Bentley and Stallins (2005) using CG lightning data. This is not surprising given that many of the warm season severe wind events in the central and eastern U.S. are convectively-driven (Johns and Hirt 1987) and often follow the diurnal patterns of convection (Kelly et al. 1985). The clustering pattern around Atlanta, however, is more likely due to population density than initiated convection, as storms which commence along the urban-rural convergence zone are likely too shallow to produce severe weather (Bornstein and Lin 2000; Dixon and Mote 2003).

There does not appear to be a strong topographic influence on the distribution of severe wind reports in Georgia. Previous studies have demonstrated that the fall line, a topographic boundary characterized by an abrupt rise in elevation of approximately 200 m and demarcating the land-cover boundaries between the Sandhills and coastal plain to the southeast and the Piedmont to the northwest, may initiate convection due to low-level convergence (i.e. Piedmont front, Businger et al. 1991). It is unclear from Figure 4.4 whether this topographic feature is responsible for the deep convection associated with severe windstorms. Since many severe wind reports are damage-based, their distribution across the southern half of Georgia, which comprises agriculturally-intensive farmlands, may be a function of where crop damage from severe winds is more likely to be reported. For instance, a severe thunderstorm wind over a peanut farm is less likely to cause

damage than a severe thunderstorm wind over a corn field. Additionally, since irregular convective systems typically remain quasi-stationary, their point of initiation is closely collocated with the location of the associated wind report(s). This provides further evidence that the fall line boundary may not be a primary trigger for severe wind-producing convection. The relative minimum in severe wind reports in the immediate northeast corner of the state is likely associated with the "Appalachian Effect" described by Livingston et al. (1996) whereby a prevailing northwesterly wind causes downsloping conditions with adiabatic warming and drying, which may suppress convective activity.

4.1.3 Temporal Patterns

Convectively-generated severe wind reports across Georgia were most common during the warm season months of May, June, and July (Figure 4.5). These months comprised nearly 80% of all warm season severe wind reports, with July exhibiting the most reports. This 3-month frequency maximum is shifted earlier in the warm season compared to the NHP (Klimowski et al. 2003). This is likely due to the passage of mid-latitude synoptic systems and a drier, more stable atmosphere (e.g. northwest flow) during the spring season. Indeed, when examined by storm type (Figure 4.6), 37% of all squall lines and both non-tornadic supercells occurred in April and May, comprising over 40% of all severe wind reports for the period of record. Interestingly, the monthly frequency maximum for squall lines occurred in July. Irregular storms were most common during the summer months of June to August when instability and moisture are maximized in the absence of strong synoptic-scale support.

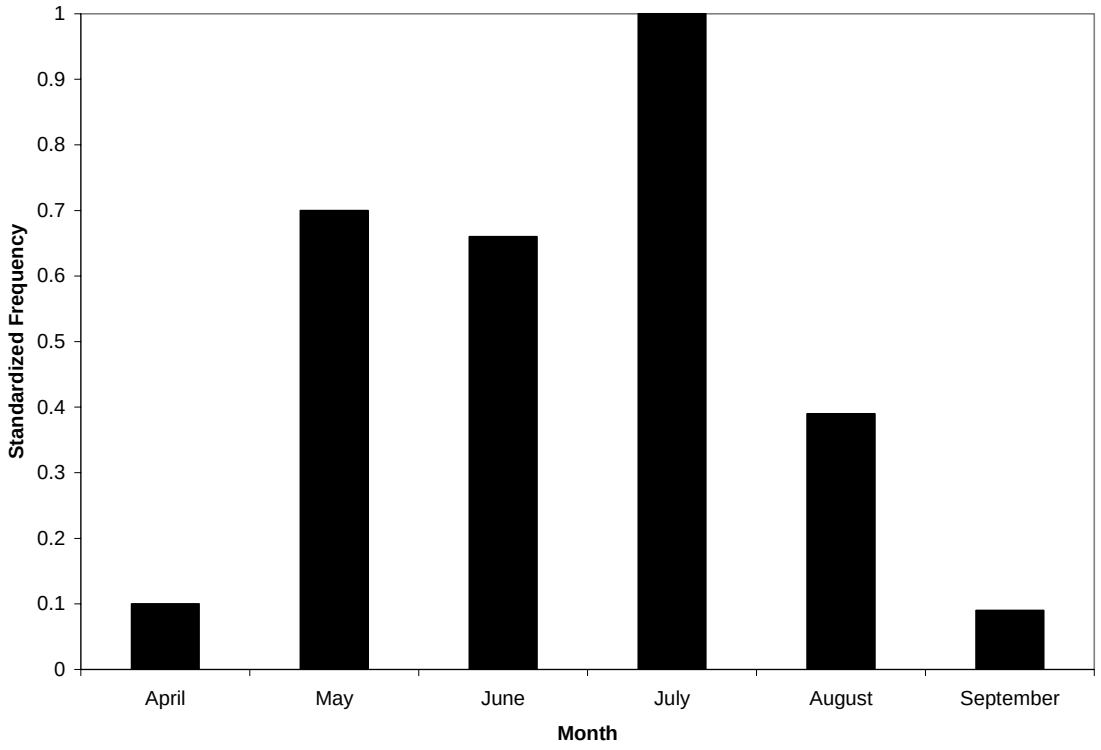

Figure 4.5. Standardized frequency of warm season severe wind reports by month across Georgia from 2000-2003. Frequencies are standardized to the greatest monthly value (464 reports in July).

When examined by hour of day (Figure 4.7), the distribution of severe wind reports suggests strong diurnal dependence, with a late-afternoon frequency maximum at 1700 EDT. The amplitude of the diurnal frequency distribution is similar to that exhibited for the NHP, indicating that severe wind reports in both regions are strongly influenced by the diurnal heating cycle (Klimowski et al. 2003). Severe wind reports before 1200 EDT were rare, and there was a marked decrease in activity after 2000 EDT. These results complement those of Kelly et al. (1985) and Senn (2003) for the Southeast.

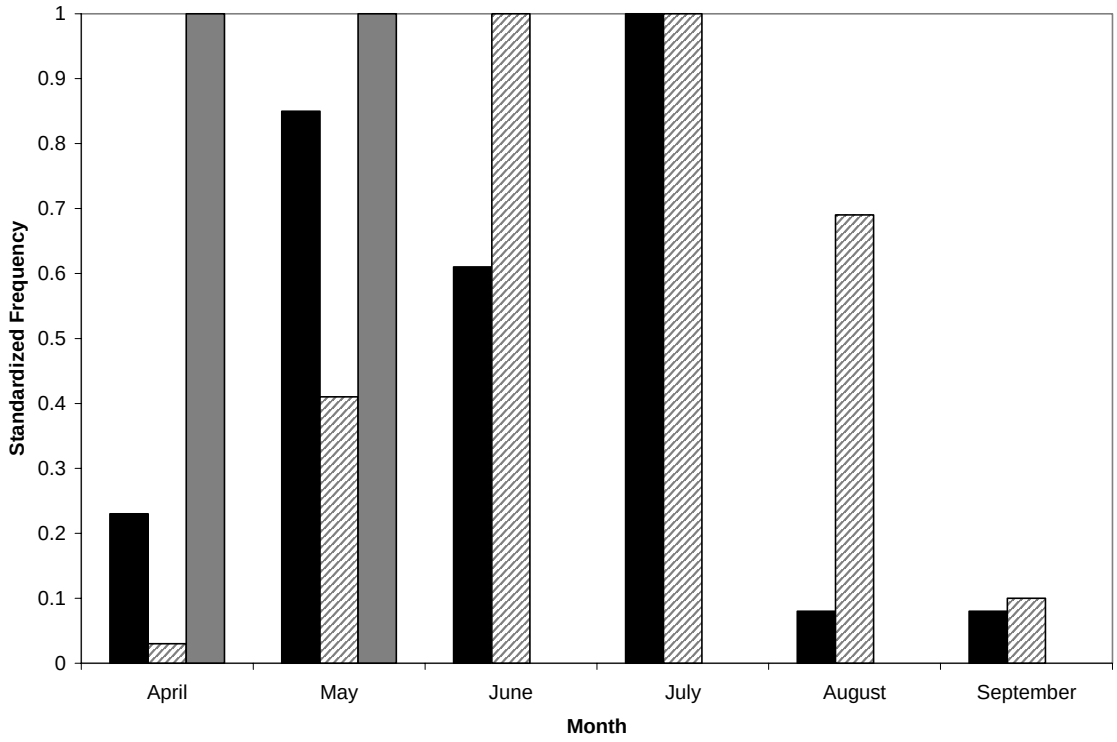

Figure 4.6. Standardized frequency of warm season severe wind-producing squall lines (solid bars), supercells (gray bars), and irregular storms (hatched bars) by month across Georgia from 2000-2003. Frequencies are standardized to the greatest monthly value (13 squall lines in July, 1 supercell in April and May, 29 irregular storms in June and July).

Compared to the NHP, the diurnal frequency maximum occurs 2-h earlier in Georgia (1700 EDT compared to 1900 CDT; Klimowski et al. 2003).

To determine the evolutionary pattern of severe winds associated with organized convective systems, the start and end times of each squall line were plotted relative to the start and end times of the associated severe storm reports. Organized severe wind-producing convective systems commonly form in the early to mid-afternoon and dissipate, or lose their signature reflectivity pattern, in the early evening hours (Figure 4.8). Some systems that develop later in the day may not dissipate until after midnight.

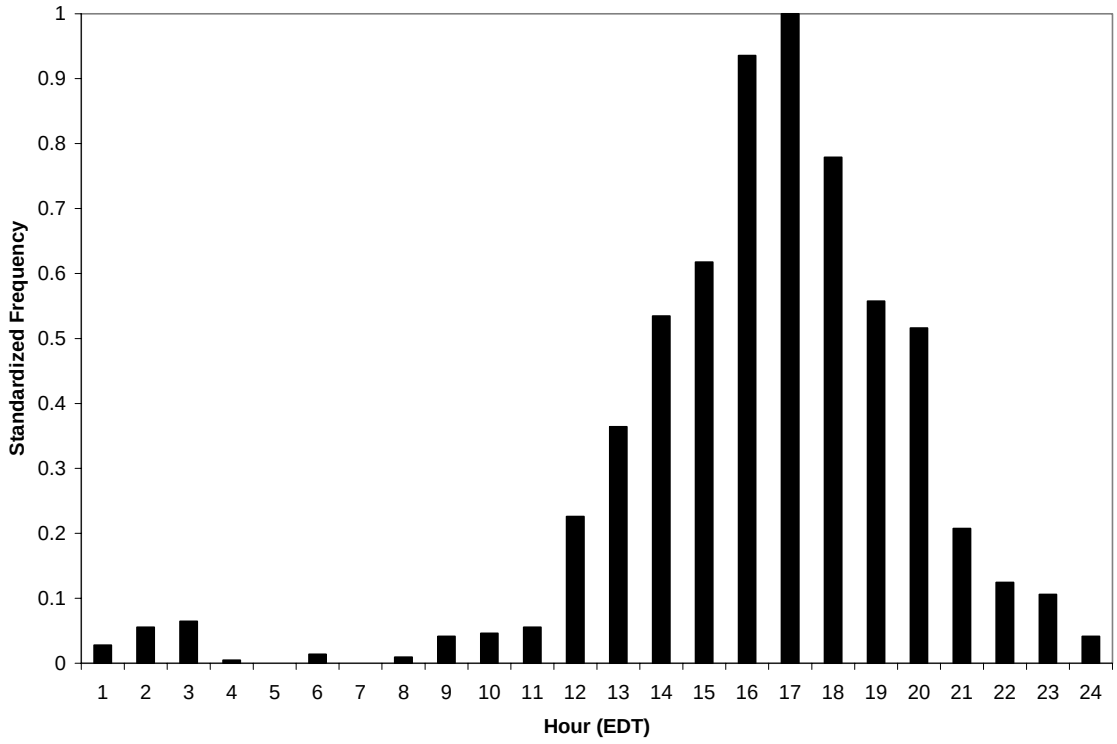

Figure 4.7. Standardized frequency of warm season severe wind reports by hour of day (Eastern Daylight Time) across Georgia from 2000-2003. Frequencies are standardized to the greatest hourly value (217 reports at 1700 EDT).

A secondary peak in squall line initiation occurred in the mid to late morning hours. Four (11%) of these storms began as larger systems (e.g. bow echoes) in the central Plains and retained their linear structure along shortwave troughs embedded in the steering flow (Ashley et al. 2005). The distribution of start times of severe wind reports illustrates that there may be a period of up to 3-h between the initial time of the convective system's reflectivity signature and the onset of severe winds (Figure 4.9). There is less of a discrepancy between the end times of the convective systems and severe wind reports, suggesting more rapid convective decay following the terminus of severe winds. Similar

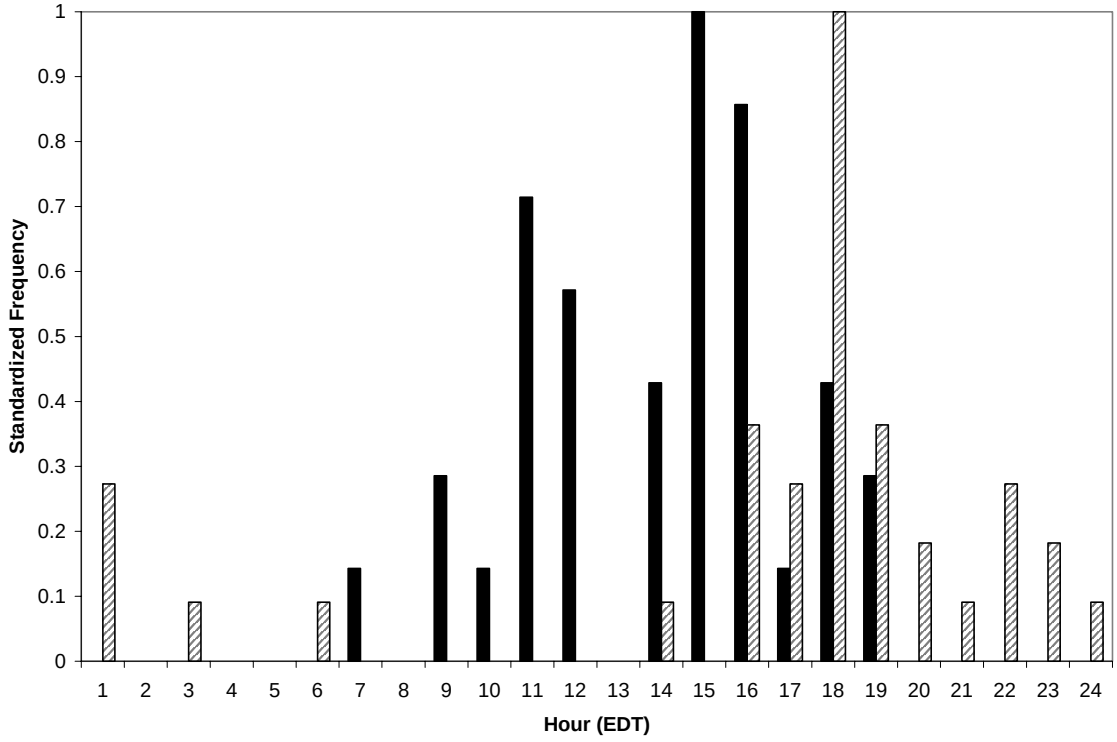

Figure 4.8. Standardized frequency of the start (solid bars) and end (hatched bars) times, by hour of day, of warm season severe wind-producing squall lines across Georgia from 2000-2003. Frequencies are standardized to the greatest hourly value (7 squall lines initiated at 1500 UTC, 11 squall lines dissipated at 1800 UTC).

to the spatial pattern of severe wind reports described earlier, there is good agreement between the diurnal patterns of severe wind activity and the diurnal patterns of convection as indicated by CG lightning (Bentley and Stallins 2005) and thunderstorm observation (Changnon 2001).

4.1.4 Steering Flow Regimes

The evolutionary tracks of severe wind-producing squall lines, defined by the location and movement of the center of the storm's convective line, are shown in Figure

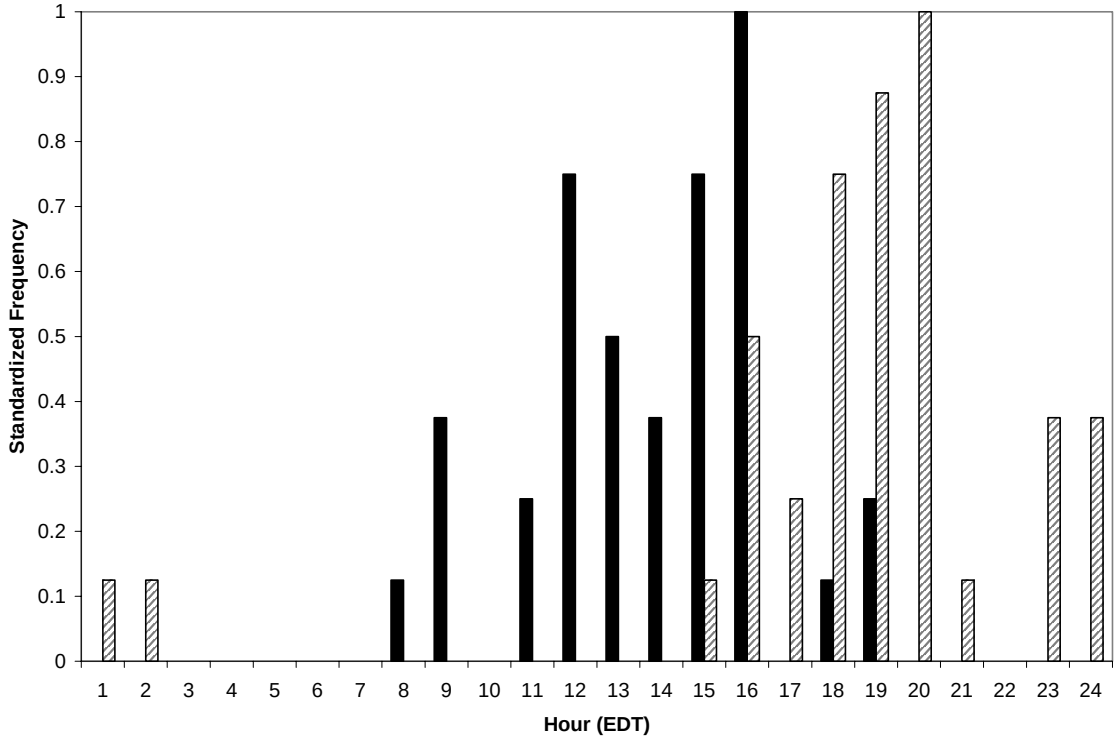

Figure 4.9. Same as Figure 4.9, but for severe wind reports associated with squall lines. Frequencies are standardized to the greatest hourly value (8 initial reports at 1600 EDT, 8 terminating reports at 2000 EDT).

4.10 and are segregated according to the prevailing steering wind direction. The beginning and ending point of each storm track was defined by the location of the first and last convective reflectivity factor (>40 dBZ), respectively, as indicated on the national radar composite summaries. Smith et al. (2005) demonstrate that the direction of the large-scale environmental flow influences both humidity and stability, and therefore, the amount of convection. The steering wind was estimated through calculation of the mean wind in the 850-200 hPa layer of the troposphere. Newton and Fankhauser (1975) found that this wind provides an approximate measure of the direction of movement of

thunderstorm cells. NCEP/NCAR re-analysis data (Kalnay et al. 1996) were used to identify the wind components at each layer.

Of the 37 severe wind-producing squall lines identified over Georgia, 22 (60%) were associated with a northwesterly steering flow (Figure 4.10a). The environmental conditions associated with northwest flow, namely a steep lapse rate and drier mid-troposphere, are generally conducive to severe wind-producing convective systems if ample low-level moisture is available (Johns 1984). Thirty-one (84%) of these events originated east of the Mississippi River in a band extending from southeast Alabama to the border of Tennessee and Missouri. This coincides with the location of the mid-tropospheric flow vector. Ashley et al. (2005) found that quasi-stationary surface boundaries oriented parallel to this vector may help initiate organized convection and derecho activity through the central Plains and Deep South. The few northwest flow squall lines with points of origin along the western rim of the Ozarks were initiated from supercells and/or bow echoes which formed in the central Plains. Analysis of the synoptic environment and national composite radar animation suggests that these squall lines initiated from deep cold-pools generated by the decaying outflow of the central Plains supercells and bow echoes. With a synoptic-scale environment supportive of deep convection, new convective lines were able to form and propagate through the Deep South.

Thirteen (35%) of the 37 severe wind-producing squall lines were associated with southwest steering flow (Figure 4.10b). The majority of these events initiated in southern Alabama and more generally along the northern Gulf Coast. Squall lines under southwest steering flow were shorter-lived than their northwest flow counterparts, exhibited shorter

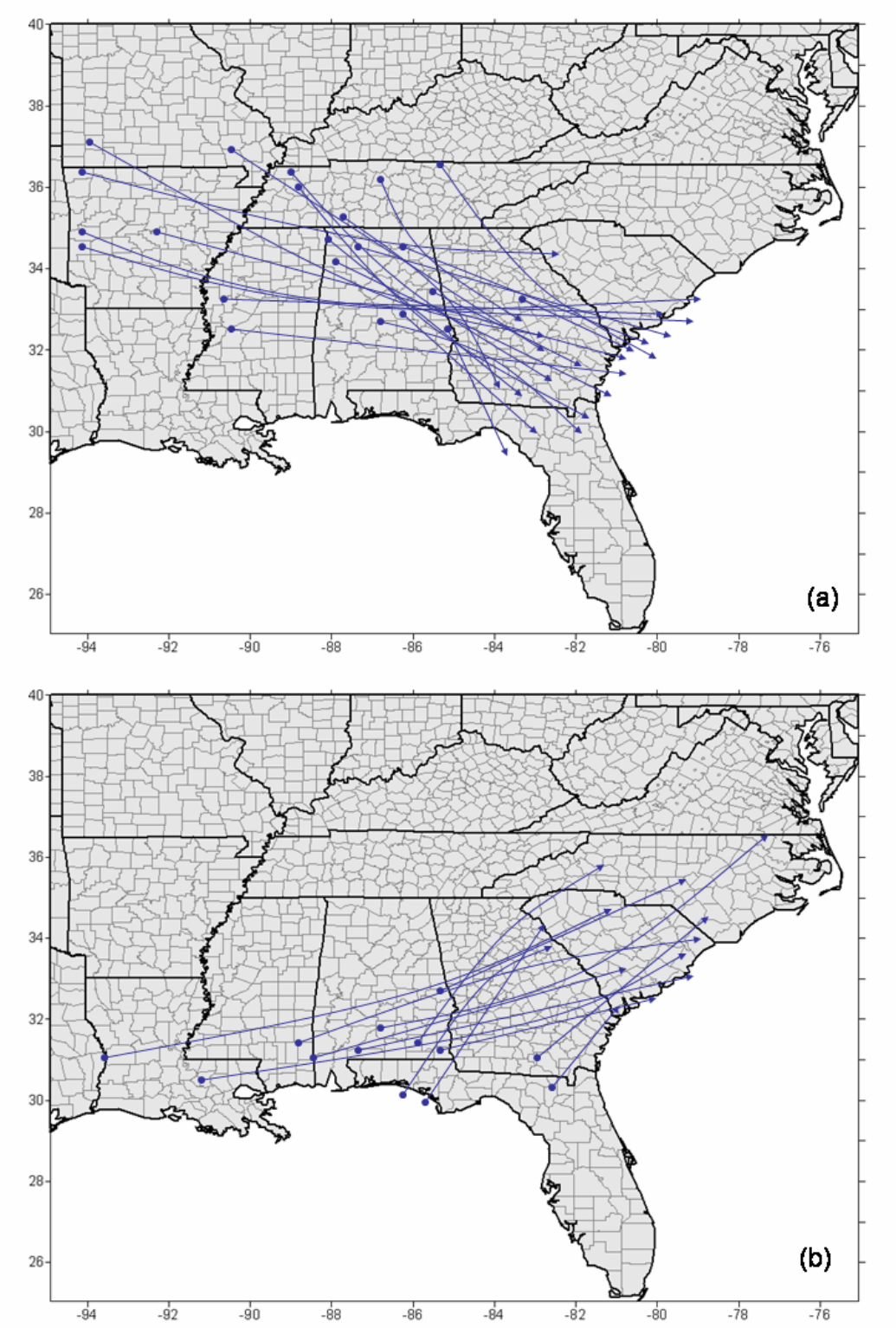

Figure 4.10. Storm tracks of severe wind-producing squall lines under (a) northwest steering flow and (b) southwest steering flow impacting Georgia during the warm season months of 2000-2003.

convective lines, and more areally-extensive stratiform regions of precipitation. Another distinguishing characteristic of southwest flow squall lines was their points of dissipation. While northwest flow squall lines typically terminated somewhere in southeast Georgia or just off-shore, southwest flow squall lines extended into the Carolinas.

4.2 Synoptic and Mesoscale Environments

4.2.1 Synoptic Environment

A recent study by Smith et al. (2005) demonstrates that the spatial patterns of convection are strongly influenced by the prevailing synoptic flow. As such, it is instructive to determine the degree of synoptic-scale surface forcing associated with convective processes to better determine if and when the convection will organize into systems capable of producing strong and potentially damaging outflows. Table 4.2 provides a summary of the percentage of severe wind-producing convective systems and non-severe convective days under weak and strong synoptic-scale surface forcing.

Nearly two-thirds of all severe wind-producing squall lines occurred under strong synoptic forcing with over half occurring in the warm sector of a mid-latitude cyclone. An example of this type of event is demonstrated in Figure 4.11a. Cool sector severe wind events were rather uncommon, as these regions are characterized by stable air below the warm frontal boundary (e.g. elevated convection; Evans and Doswell 2001). Conversely, more than half of the 94 irregular storm systems identified across Georgia occurred in the absence of a synoptic-scale frontal boundary, as demonstrated by the example in Figure 4.11b. These patterns may further support the assertion of Brown

Table 4.2. Percentage of severe wind-producing squall lines, supercells, irregular storms, and non-severe convective days under weak and strong synoptic-scale surface forcing. Percentages of events under strong forcing are subdivided according to their location relative to the cyclone center and frontal boundaries (warm sector, cold sector, or cool sector).

		Strong Forcing		
	Weak Forcing	Warm Sector	Cold Sector	Cool Sector
Squall-lines	38.5	52.3	7.7	1.5
Supercells	0	100	0	0
Irregular	55.8	35.2	4.8	4.2
Non-Severe	51.7	31.1	13.8	3.4

(2002) that mesoscale circulations driven by topographic, density, and thermal differences focus moisture and promote destabilization in more localized areas. Further, it has been suggested that, while mid-latitude cyclones are efficient at destabilizing the lower troposphere, they are rather inefficient at forcing air parcels to rise to the level of free convection. This supports the theory that synoptic-scale systems provide environments favorable for processes operating on smaller scales (Doswell and Bosart 2002).

Since ground-relative wind shear is a key ingredient for severe winds (Kuchera and Parker, forthcoming) the low to mid-tropospheric flow pattern is examined for each convective type (Figure 4.12). All severe wind-producing systems over Georgia occurred ahead of a migratory trough at 500 hPa. This is in contrast to widespread convectively generated windstorms over the central and northern Plains, which tend to form on the periphery of a warm-core anticyclone (ridge) centered over the central U.S. (Bentley and

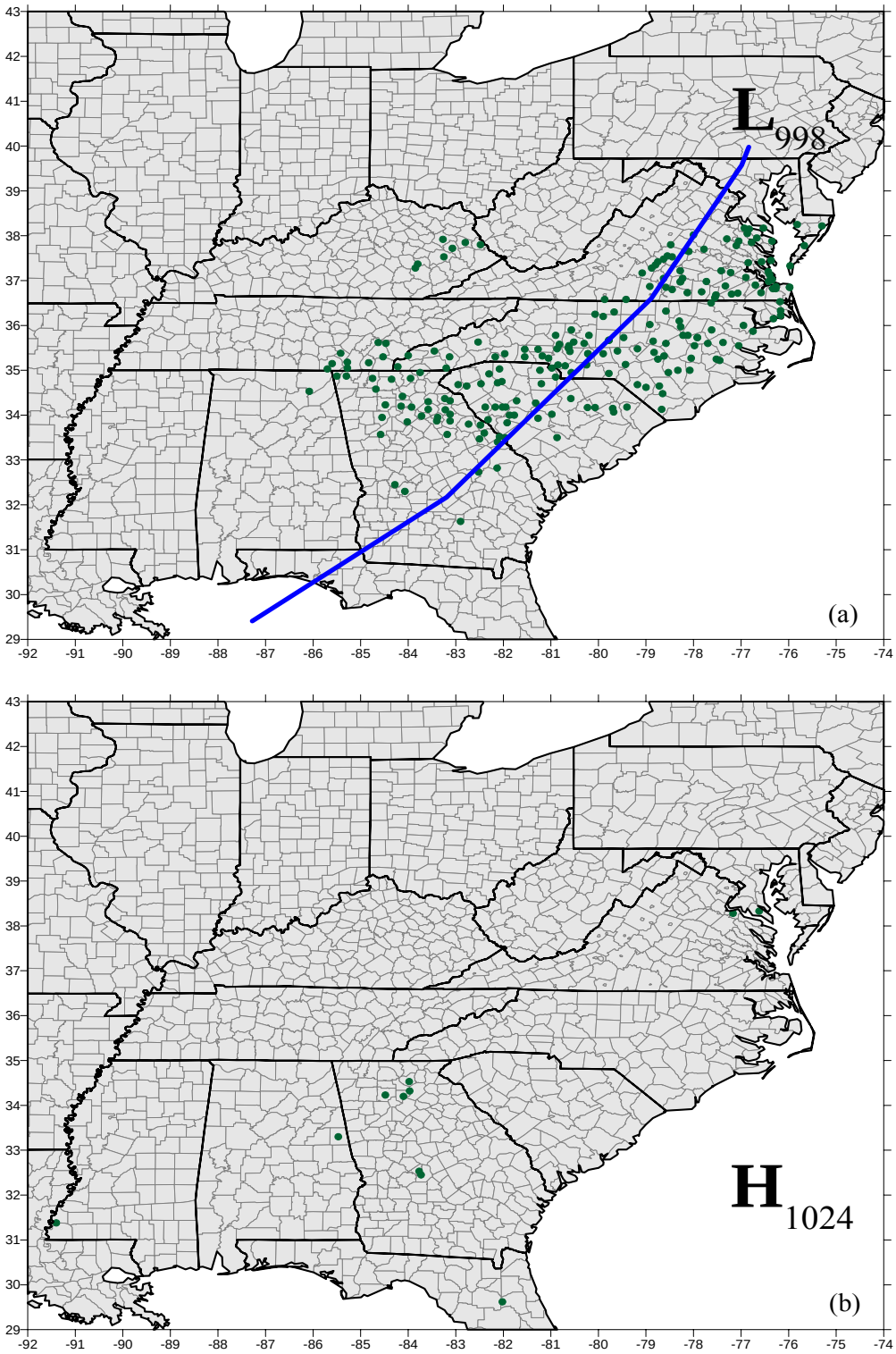

Figure 4.11. Examples of (a) strong (14 May 2002) and (b) weak (12 June 2003) synoptic-scale surface forcing. Severe wind reports are represented by green circles. Surface features are based on the corresponding daily surface weather maps constructed at 00 UTC. The solid blue line in (a) represents the location of the cold front.

Sparks 2003). The position and amplitude of this trough varies by convective storm type. In the squall line composite, the trough axis is centered over the Mississippi River Valley, whereas in the supercell composite the trough axis shifts to the west and digs further south. The irregular storm composite also shows some trough digging through the Ohio River Valley and Deep South.

Analysis of the 500 hPa wind vector reveals that severe wind-producing squall lines and supercells occur in a region of strong winds (13-20 m s^{-1}) that extends from the central Plains to the Northeast (Figure 4.13). In contrast, the irregular storm composite shows the core of strongest winds displaced to the northern half of the U.S. Even though the strongest winds are located north of the region, the 500 hPa flow associated with irregular storms is still somewhat faster (1-3 m s^{-1}) than the climatological mean. Furthermore, the lower-tropospheric shear profile indicates anomalously strong ground-relative winds over Georgia during these events (Figure 4.14). Coupled with the high-amplitude mid-tropospheric wave pattern and stronger winds aloft, this large-scale setting is conducive to fast moving storm systems. When organized systems are able to develop in these conditions, they produce fast-moving gust fronts which promote rapid lifting along their leading edge (Mueller and Carbone 1987). In the absence of a large-scale lifting mechanism, storms which form in this environment may develop a horizontally tilted, updraft-downdraft couplet, which can lead to evaporative cooling and the downward momentum capable of producing severe winds (Fujita 1985).

In addition to strong ground-relative winds in the lower troposphere, the profiles of moisture and instability are crucial ingredients in promoting an environment supportive of deep convection. Even though severe wind-producing convective systems

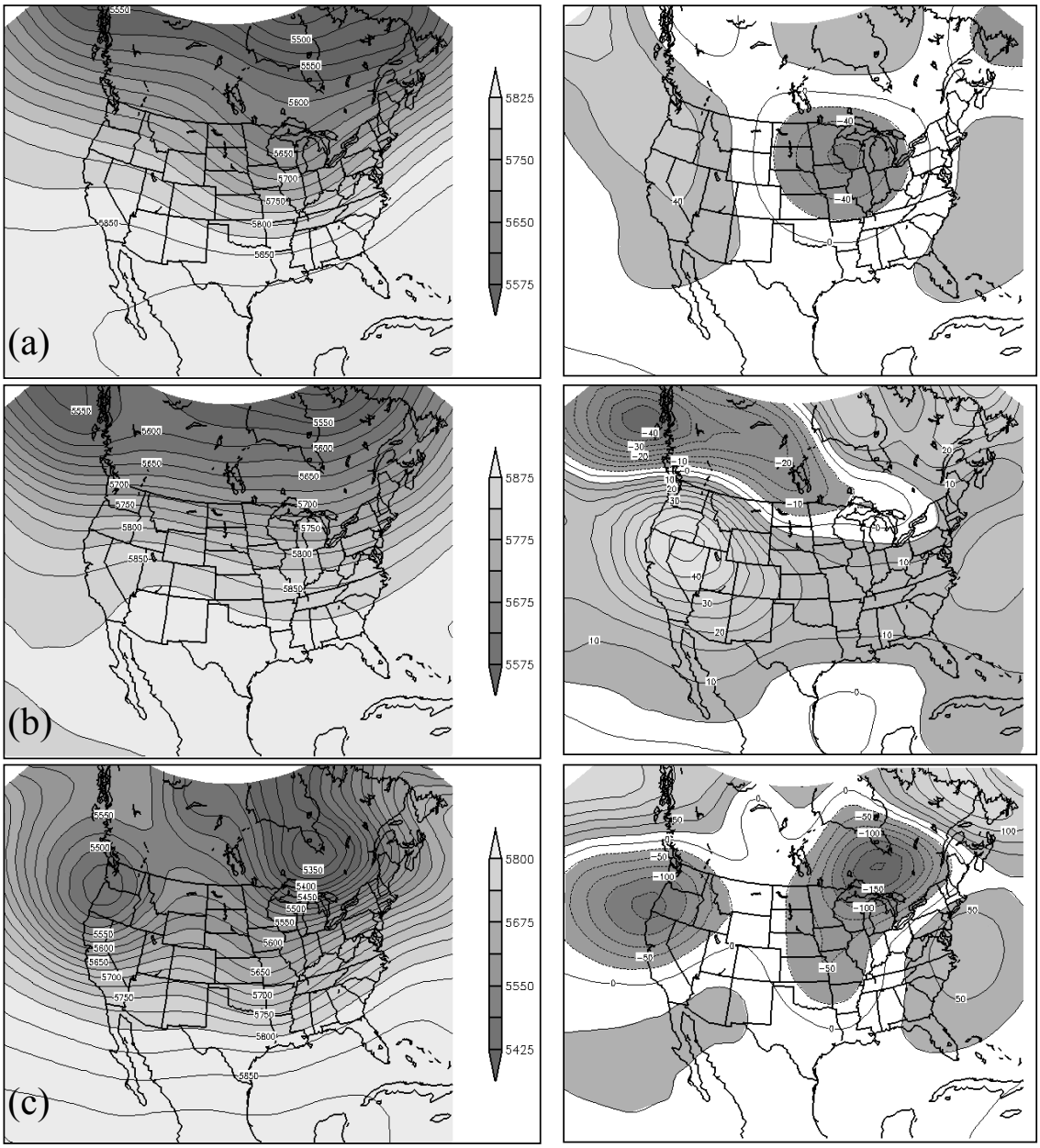

Figure 4.12. 500 hPa geopotential height (m) composites for warm season severe wind-producing (a) squall lines, (b) irregular storms, and (c) supercells across Georgia from 2000-2003. Right column includes the corresponding anomalies. Composites created from the NOAA-CIRES Climate Diagnostics Center website at http://www.cdc.noaa.gov/.

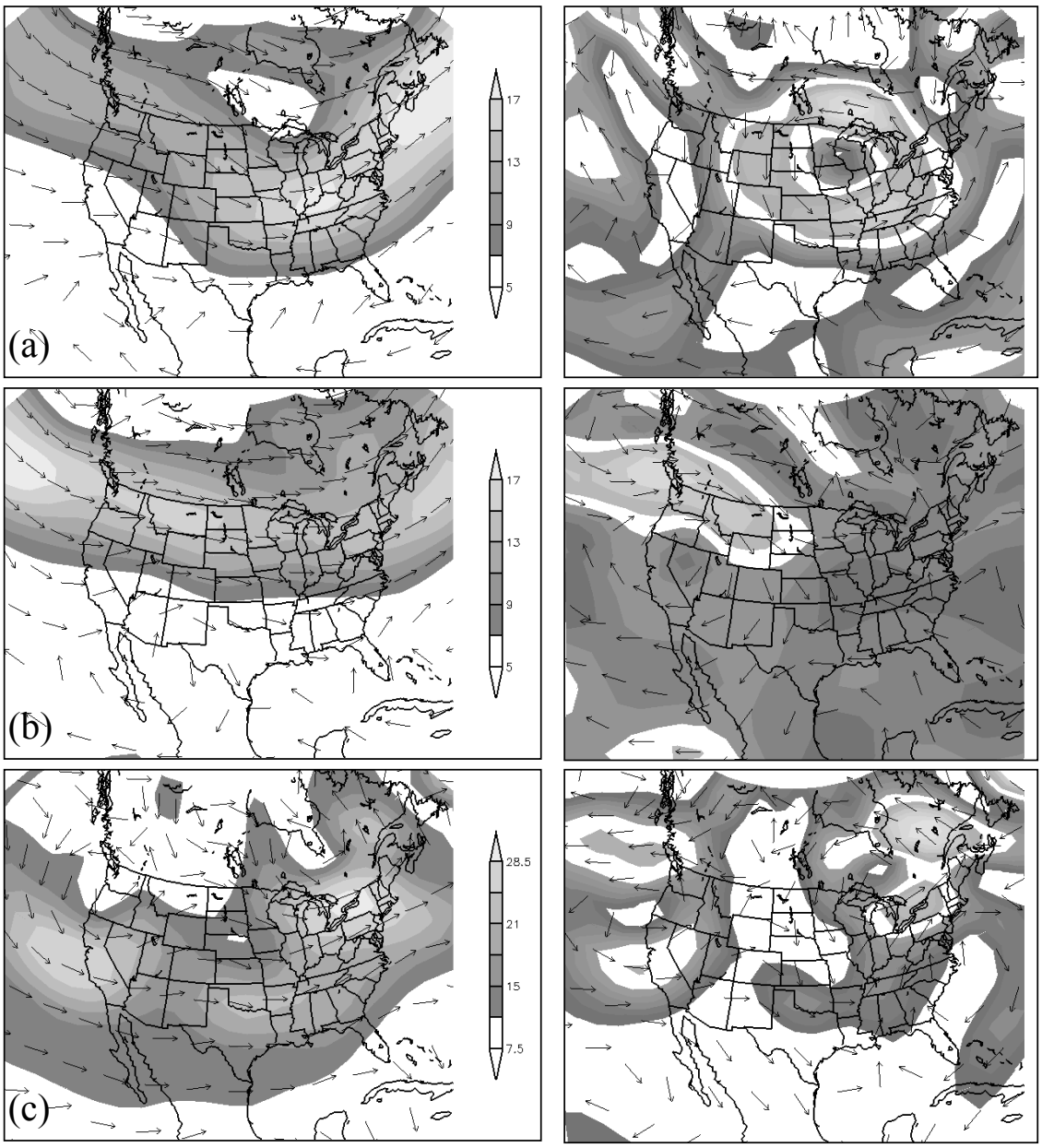

Figure 4.13. Same as Figure 4.12, but for mean vector winds at 500 hPa and anomalies. Wind speeds are shaded (m s^{-1}) and wind directions are indicated by arrows. Composites created from the NOAA-CIRES Climate Diagnostics Center website at http://www.cdc.noaa.gov/.

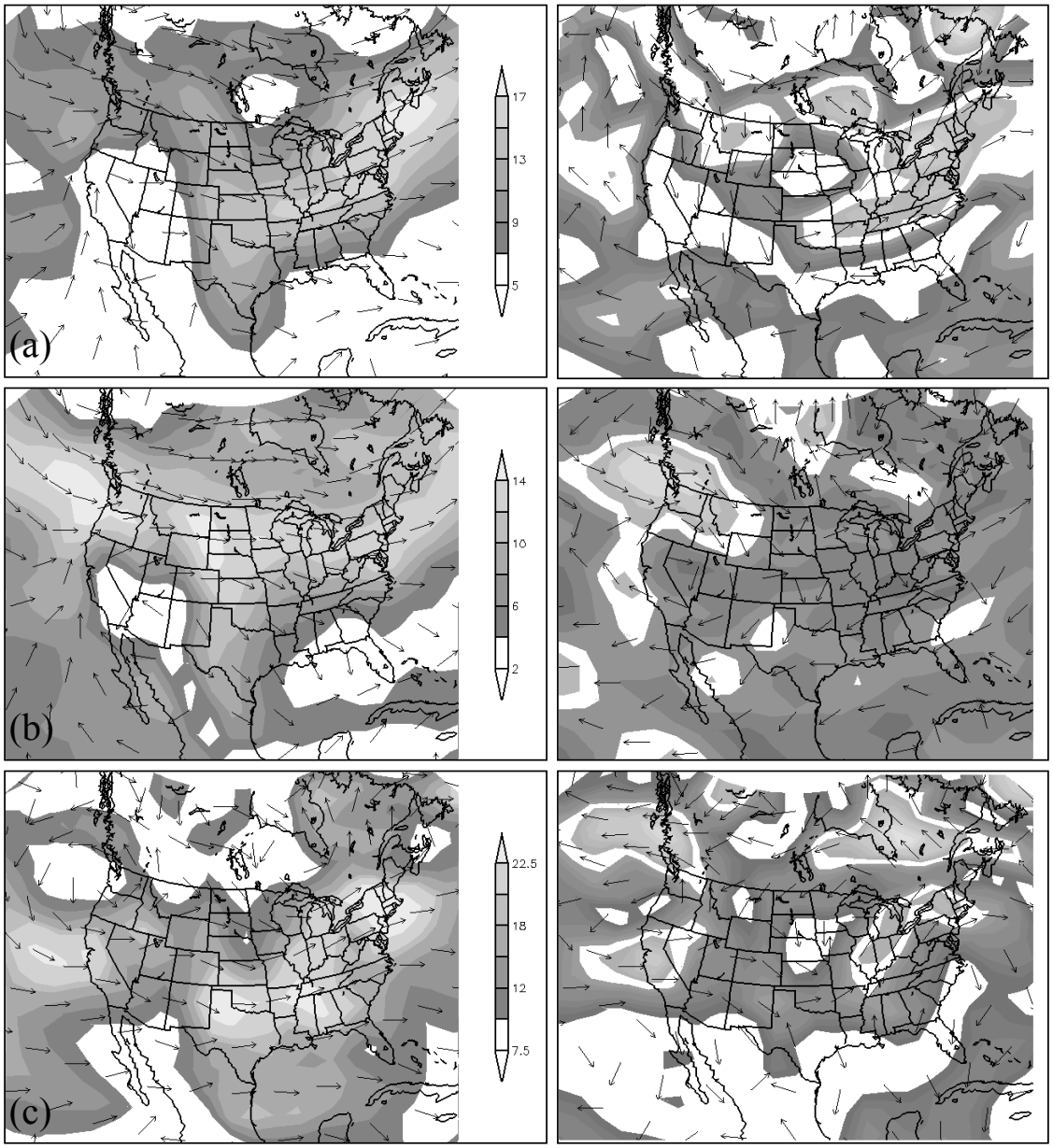

Figure 4.14. Same as Figure 4.12, but of mean wind shear calculated from the surface to 500 hPa and anomalies. Mean differences in wind speed are shaded (m s^{-1}) and wind directions are indicated by arrows. Composites created from the NOAA-CIRES Climate Diagnostics Center website at http://www.cdc.noaa.gov/.

are shown to develop upstream of a mid-level trough, the lower-troposphere is still rather moist with 925 hPa specific humidity above 0.01 kg kg^{-1} over the Southeast (Figure 4.15). Parker and Kuchera (forthcoming) demonstrate that entrainment of dry air at the low and mid-levels of the troposphere do not discriminate between a severe wind environment and non-severe environment in the Midwest as much as previously thought (see Fujita 1985). The same conclusion can be reached for severe wind environments over Georgia, as 700 hPa specific humidity values across the storm types are either equal to or slightly above the climatological mean (Figure 4.16). The amount of instability across the region during these events is rather modest compared to the climatology (Figure 4.17), indicating that the atmosphere does not have to be abnormally unstable to generate severe winds. Indeed, Fujita and Wakimoto (1981) determined that a distinguishing feature of a wet microburst environment compared to a dry microburst environment is a less unstable atmosphere.

4.2.2 Mesoscale Environment

Box plots illustrating the distribution of sounding parameters calculated at 00 UTC over Peachtree City, GA, (KFFC) and Jacksonville, FL, (KJAX) for convective windstorm days and non-severe convective days are given in Figure 4.18. A Student's t-test was used to assess the statistical significance of the differences in the mean values between the windstorm types and non-severe environments. Four of the nine sounding parameters indicate significant differences at the 95% confidence interval ($\alpha = 0.05$): convective available potential energy (CAPE) (Figure 4.18d), convective inhibition

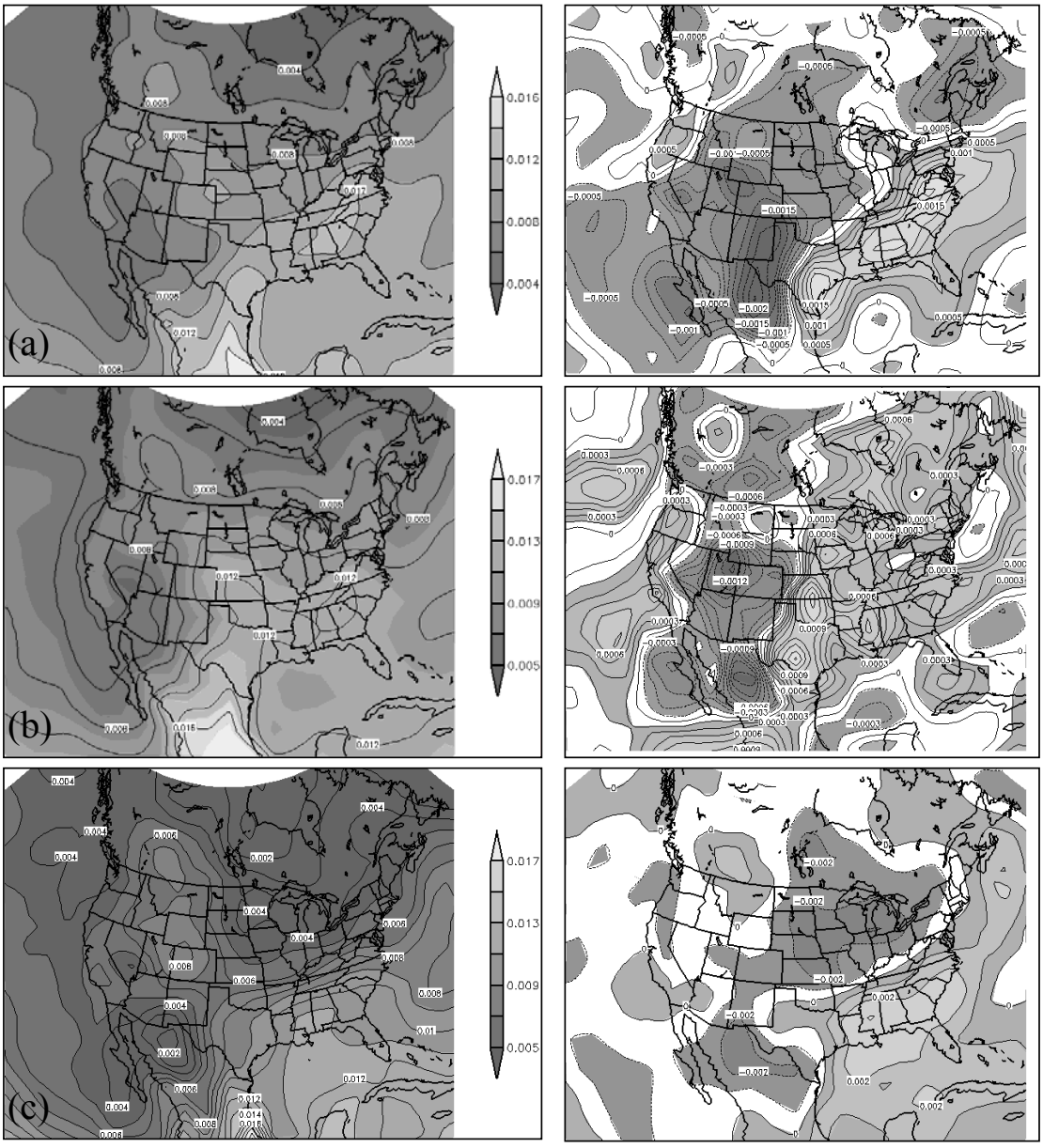

Figure 4.15. Same as Figure 4.12, but of mean 925 hPa specific humidity and anomalies (kg kg^{-1}). Composites created from the NOAA-CIRES Climate Diagnostics Center website at http://www.cdc.noaa.gov/.

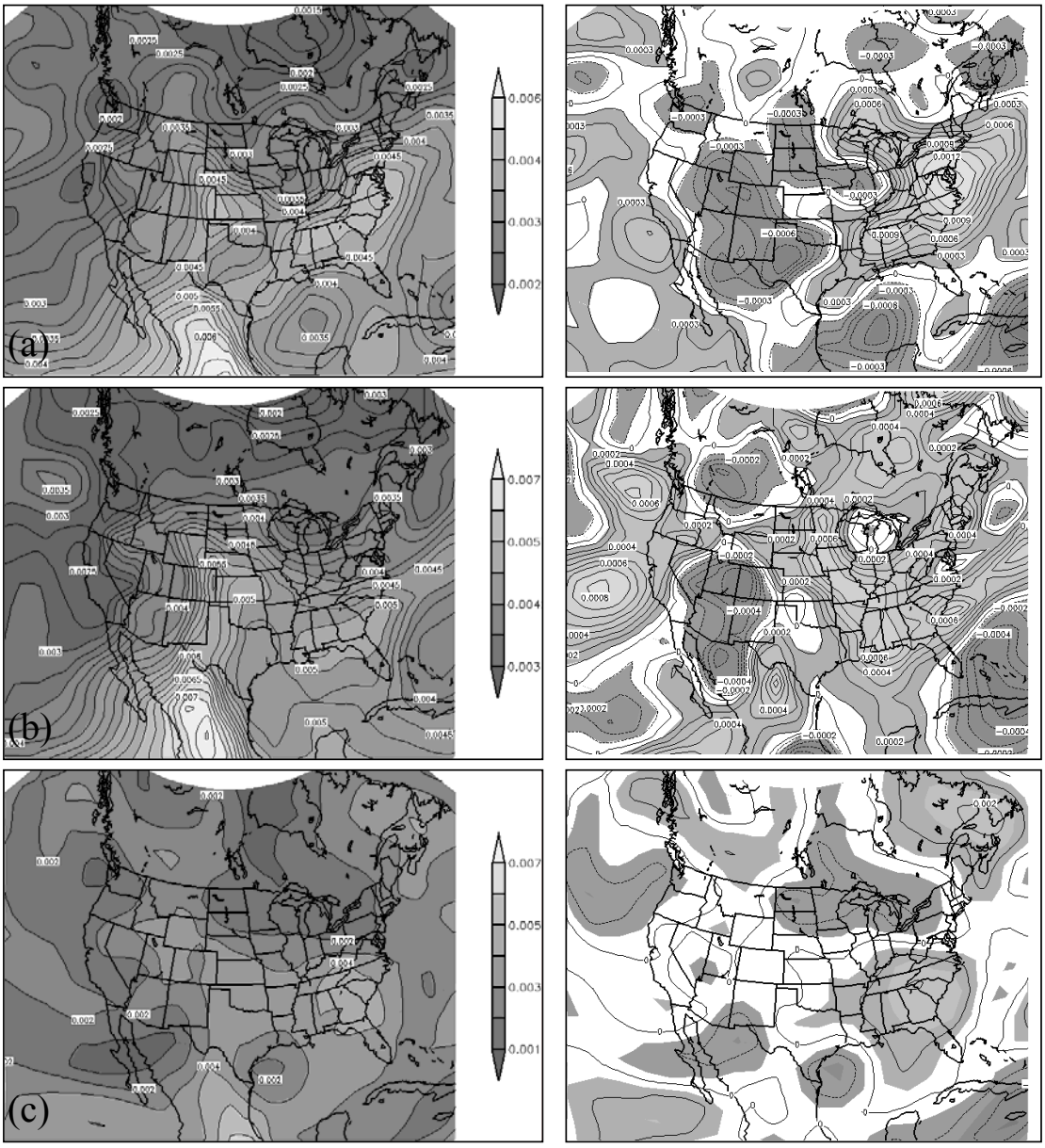

Figure 4.16. Same as Figure 4.12, but of mean 700 hPa specific humidity and anomalies (kg kg^{-1}). Composites created from the NOAA-CIRES Climate Diagnostics Center website at http://www.cdc.noaa.gov/.

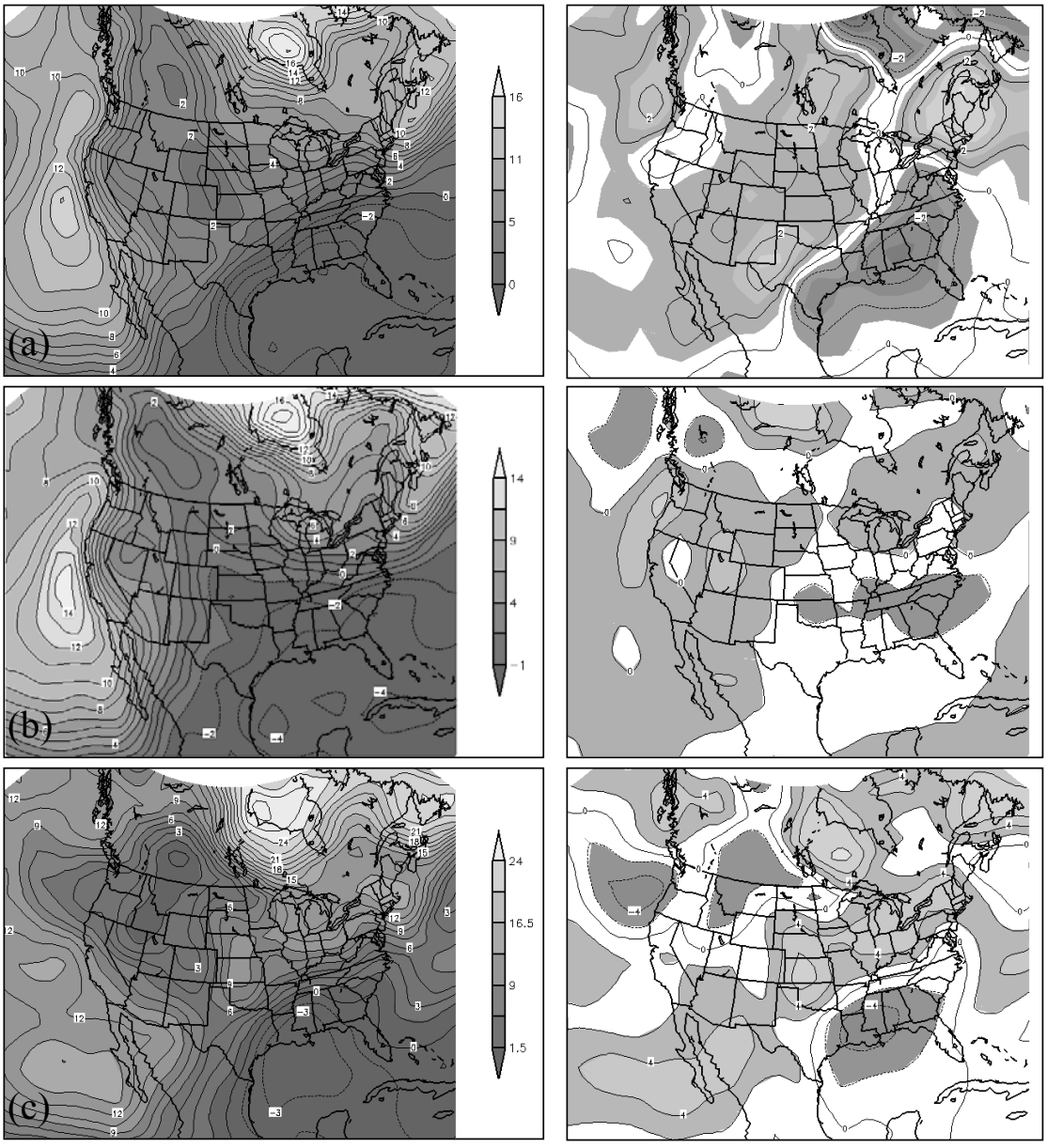

Figure 4.17. Same as Figure 4.12, but of mean lifted index values and anomalies (°C). Composites created from the NOAA-CIRES Climate Diagnostics Center website at http://www.cdc.noaa.gov/.

(Figure 4.18e), Bulk Richardson number (Figure 4.18f), and the lifting condensation level (LCL) (Figure 4.18g).

A significant amount of potential energy, as suggested by a strong capping inversion and high CAPE values, and horizontal wind shear exist in severe wind environments. Although the tropospheric shear profile suggests multi-cellular storm development, strong storms with damaging winds may develop along mesoscale surface boundaries. Koch and Ray (1997) identified a feature known as the Piedmont trough which forms in response to strong thermal and moisture gradients over scales generally less than 200 km. These gradients develop frequently across Georgia and the Carolinas during the warm season due to variations in soil type (i.e. predominantly clay soils in the Piedmont and sandy soils in the coastal plain) and soil moisture, which alter both sensible and latent heat fluxes. Ambient shear from these mesoscale circulations may interact with storm systems propagating through these regions, particularly if the synoptic-scale shear profile is weak (Markowski et al. 1998).

Severe convective windstorms also exhibit a higher LCL than non-severe convective events. A high LCL is suggestive of low surface-based relative humidity (i.e. a sub-saturated layer) which promotes more evaporative cooling and stronger outflows (Kuchera and Parker, forthcoming). Although an inflow of moisture is important in promoting deep convection, as indicated by high equivalent potential temperatures and total column precipitable water, it does not appear to be essential in producing a severe wind environment. Further, there is not a significant difference in the moisture content of the mixed layer between severe wind and non-severe convective environments. This layer is typically regarded as the origin of storm electrification, as three phases of water

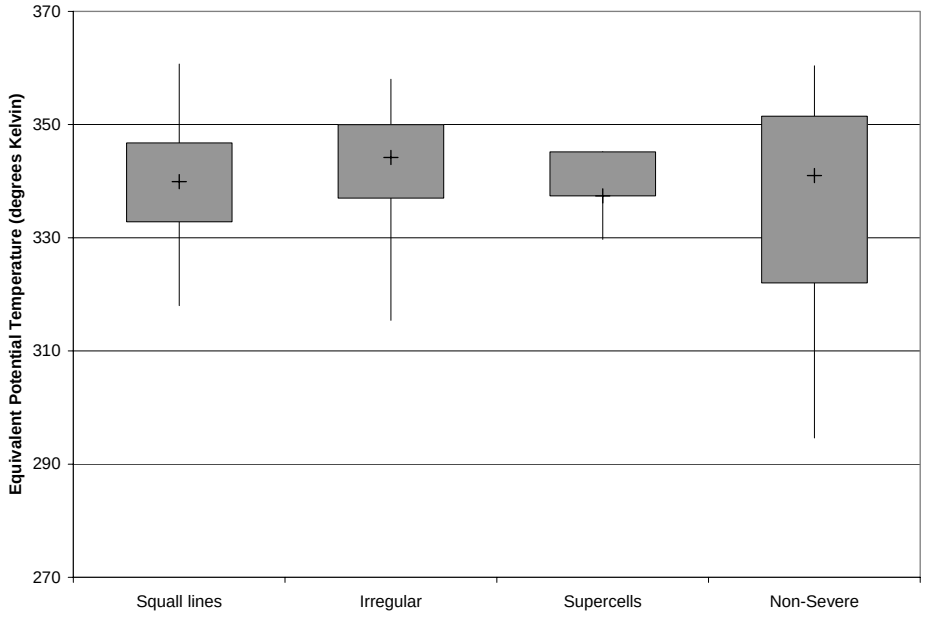

(a)

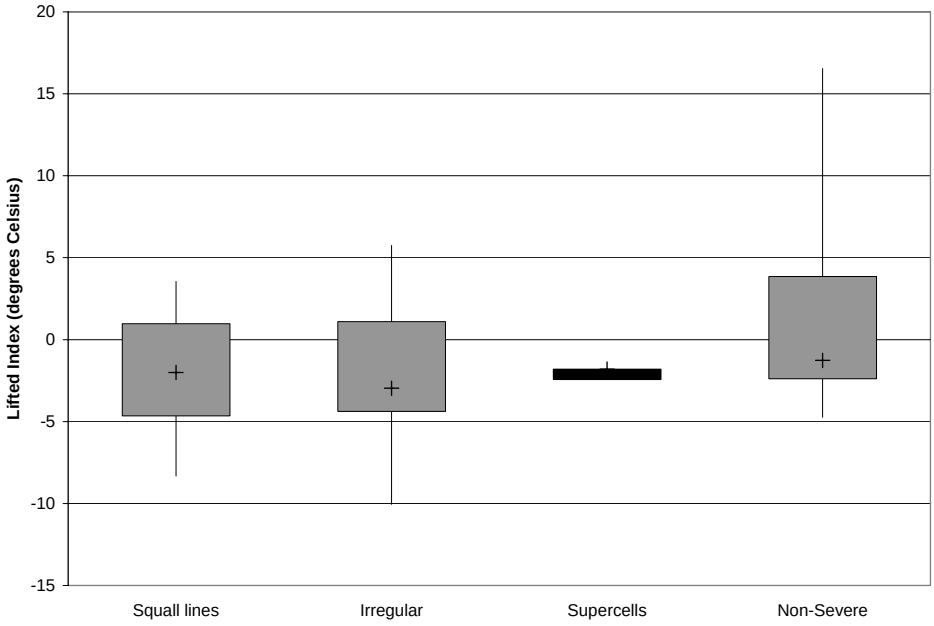

(b)

Figure 4.18. Box plot of (a) equivalent potential temperature, (b) lifted index, (c) K-index, (d) convective available potential energy, (e) convective inhibition, (f) Bulk Richardson Number, (g) lifting condensation level, (h) mean mixed-layer mixing ratio, and (i) total column precipitable water calculated at 00 UTC over Peachtree City, GA, (KFFC) and Jacksonville, FL, (KJAX) for 30 severe wind-producing squall lines, 37 irregular storms, 2 supercells, and 57 non-severe convective days. Each box plot shows the median (cross), 25th and 75th percentiles (box), and the minimum and maximum values (whiskers).

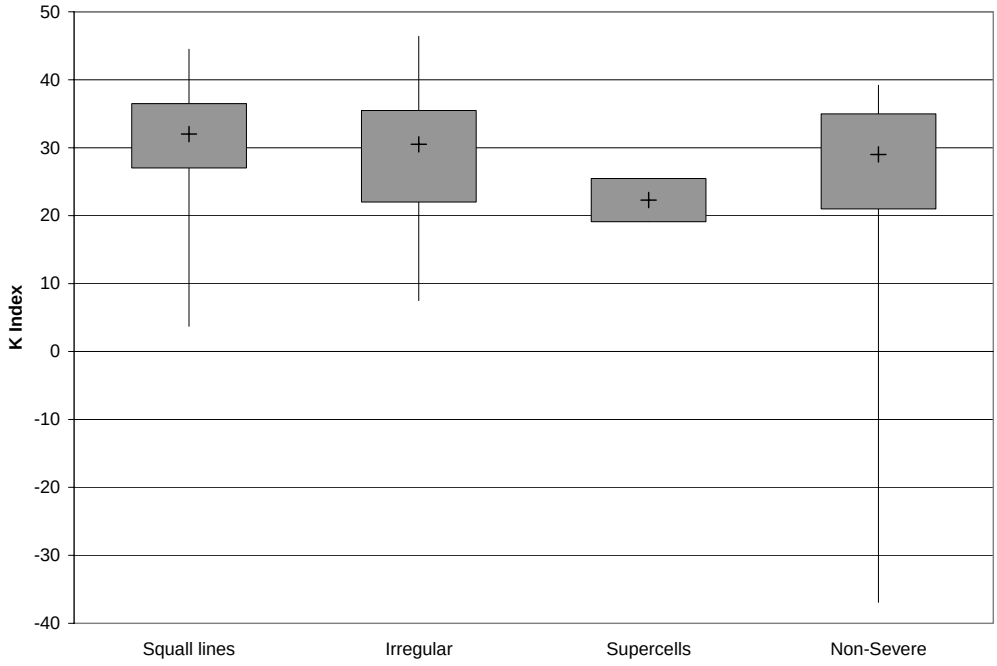

(c)

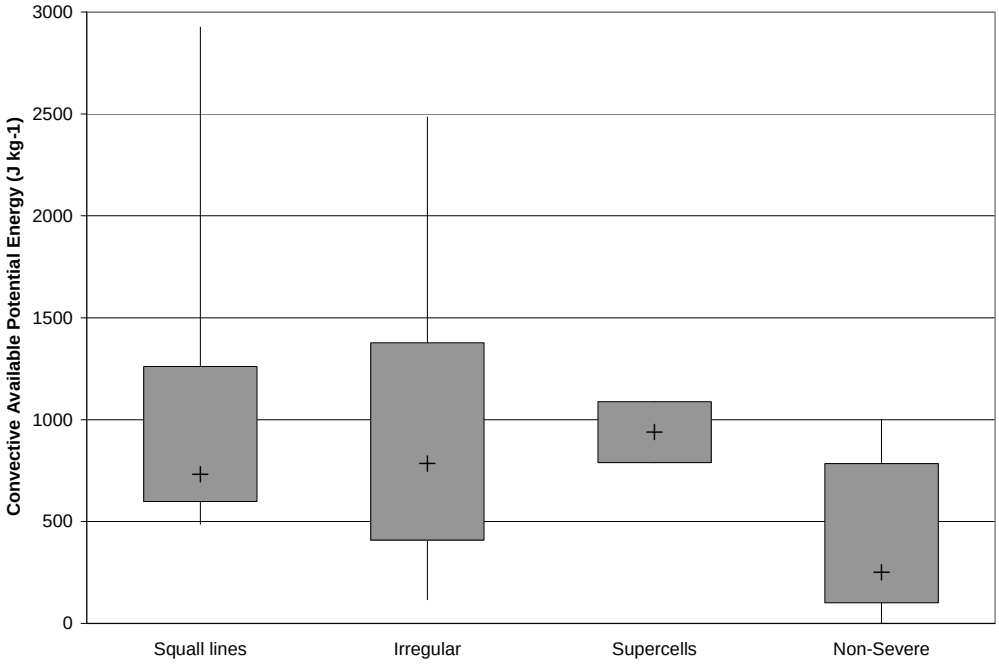

(d)

Figure 4.18. (continued)

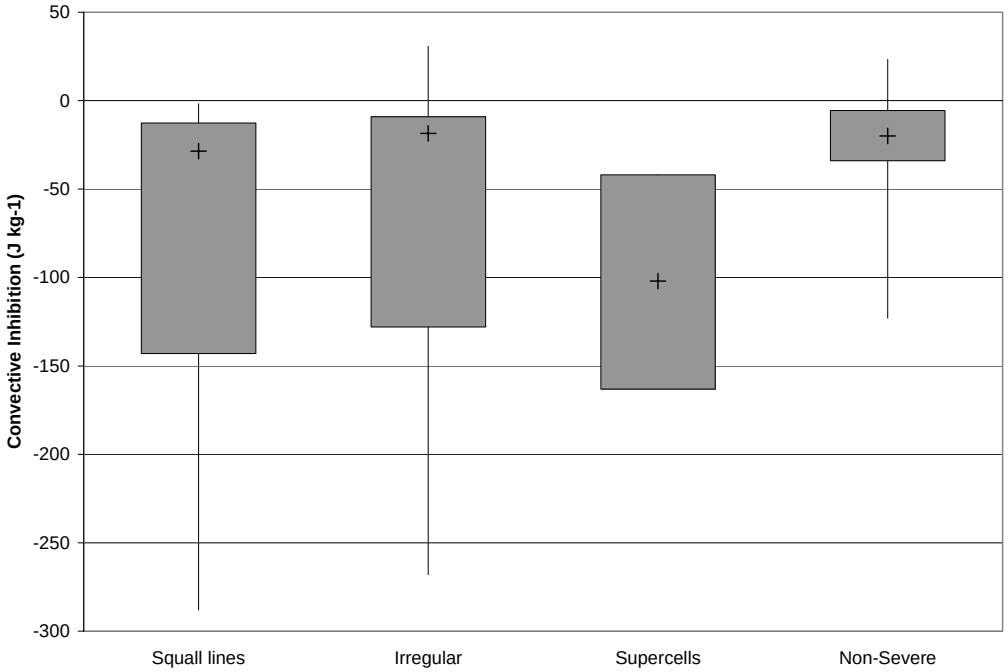

(e)

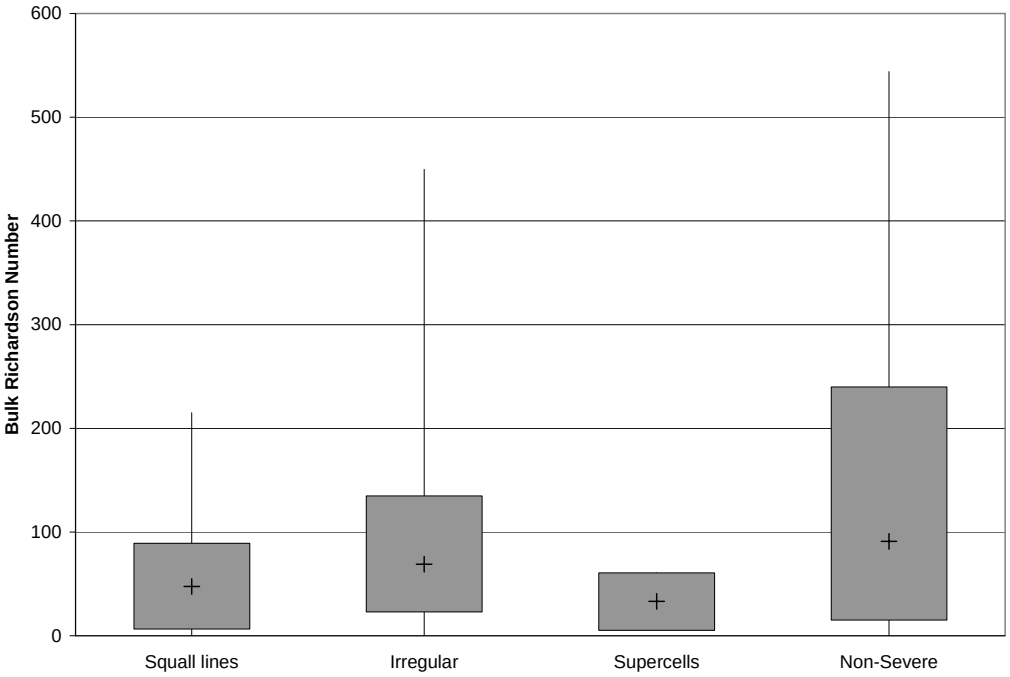

(f)

Figure 4.18. (continued)

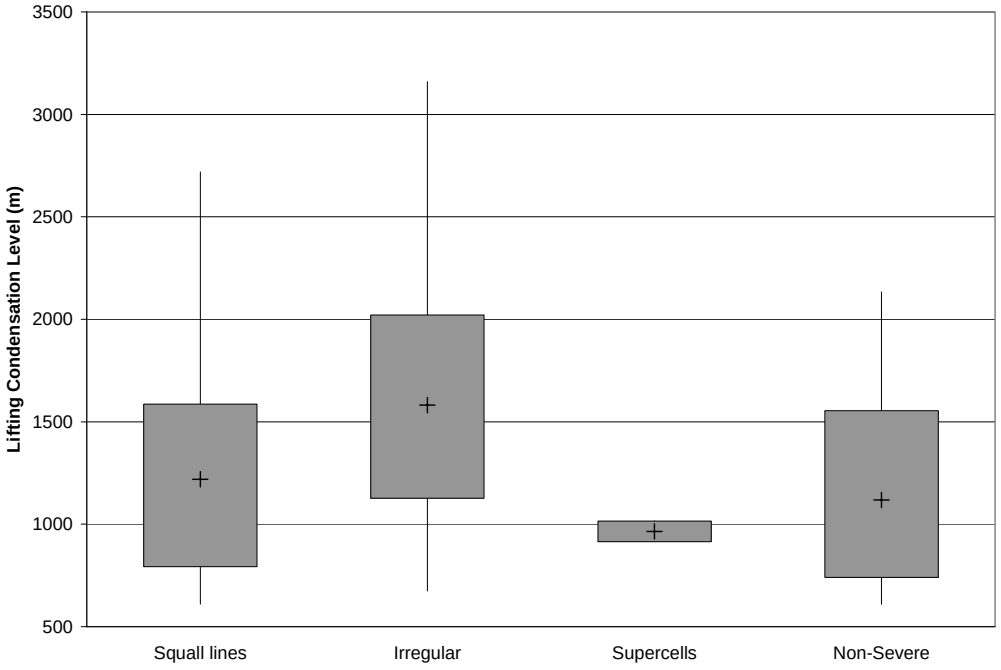

(g)

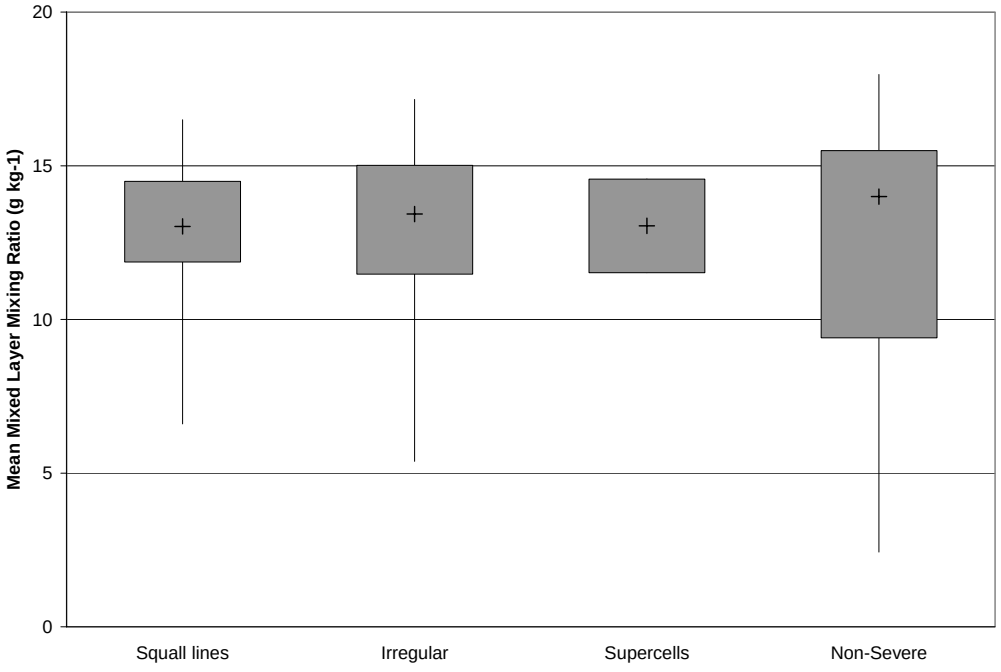

(h)

Figure 4.18. (continued)

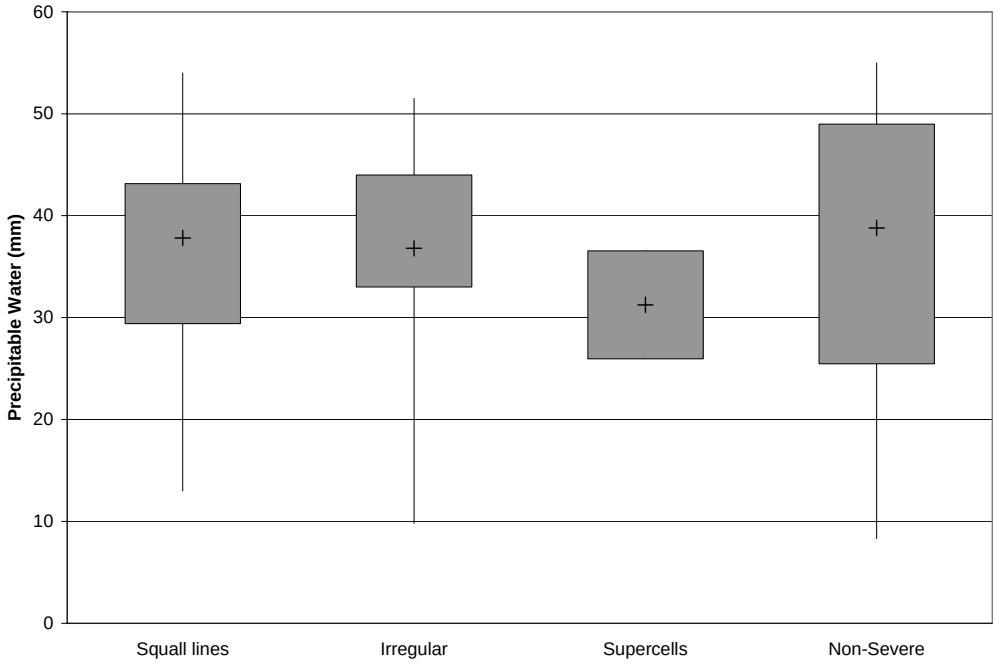

(i)

Figure 4.18. (continued)

necessary for charge separation (i.e. ice, graupel, super-cooled water) are present, and is bounded by the -10°C and -20°C environmental isotherms (Latham 1981; Bright et al. 2005). Particle-scale collisions in the turbulent mixed layer incite non-inductive, electrical charging, creating a vertical polarity dipole and pathway for charge separation (Lhermitte and Williams 1985). The characteristics of CG lightning associated with a severe windstorm is presented in the next section.

Similar to the results of Kuchera and Parker (forthcoming) for the Midwest, the entrainment of dry air through the mid-troposphere is not a good indicator of the potential for severe winds. Instead, strong ground-relative wind shear, low surface humidity, and a

high cloud base are features more unique to a severe wind environment. Since strong downdrafts are sustained by negative buoyancy, evaporative cooling is critical in keeping the descending air mass from warming dry adiabatically. The importance of low surface humidity is masked at the synoptic-scale, as 925 hPa specific humidity values over the Southeast were not lower than the climatological mean (see Figure 4.15). At the mesoscale, severe winds may occur in thunderstorms which form in response to strong moisture gradients and when the downdraft is located on the "dry" side of the boundary. The high frequency of wind reports associated with irregular convective modes through the Sandhills region of Georgia supports this theory.

4.3 Cloud-to-Ground Lightning Observations

The evolution of CG lightning associated with six severe wind-producing thunderstorms and five non-severe thunderstorms was analyzed. Pronounced differences were observed between the two groups, particularly in regards to the total CG lightning frequency and the percentage of positive CG (+CG) flashes. Since these differences were consistent among the events in each group, one event was chosen as an archetype for each group. Both the severe wind and non-severe cases selected for discussion occurred during the summer (June and August) on days when the influence of the sub-tropical high was strong. The severe wind case was classified as an irregular convective system and formed in response to an inland-propagating sea breeze. The non-severe case was associated with a cluster of moderate to strong convective cells that developed rapidly due to convergence along the fall line boundary.

Interestingly, the non-severe case, which encompassed three distinct convective cells, produced outflow boundaries that were visible on the base reflectivity scan. An examination of the corresponding hourly wind reports from the Automated Surface Observing station at Macon, GA, (KMCN) located approximately 20 km to the north of the event location, indicated sustained winds of 4-6 kt. and peak gusts of 16-19 kt. Indeed, non-severe thunderstorm outflow boundaries may reach as high as 2 km in depth and propagate at speeds approaching 20 kt. (Koch and Ray 1997). This provided an excellent case from which to compare the CG lightning observations of a thunderstorm producing severe wind with a thunderstorm producing non-severe downdrafts.

4.3.1 Severe Wind Case

Strong convective cells began to develop at 1838 UTC 3 June 2002 along the Georgia-South Carolina border approximately 10 km onshore. Shortly thereafter, new cells began to form along a line parallel to the coast resulting from low-level convergence associated with the inland-propagation of the sea breeze. The motion vector of these cells was generally west-northwest. Because these convective cells developed quickly, with maximum reflectivity factors >50 dBZ by 1908 UTC, small clusters of CG flashes were observed as early as 1858 UTC. By 1948 UTC, three distinct convective cells were visible on radar (Figure 4.19a), each with two plumes of enhanced convection (as indicated by the high reflectivity factors) collocated with CG flash clusters. Each cluster was almost entirely composed of –CG flashes and this remained consistent throughout the lifetime of each convective cell. At 2019 UTC, a severe wind gust was reported on the back side of the convective plume, which experienced a rapid decrease in CG flashes

from the previous image (Figure 4.19b). The decrease in CG flashes just prior to severe wind has been documented (Kane 1991; Elson 1993). Note in Figure 4.19b that the severe wind report occurred away from the strong convective plumes, where numerous CG flashes were observed.

A second severe wind report occurred approximately 20 min. after the first report (2040 UTC) and on the leading side of the same convective cell (Figure 4.19c). As with the first report, there was a near absence of CG flashes in the vicinity of the severe wind report. Four CG flashes, one of which was a +CG flash, were observed in the anvil of a nearby convective plume. The cluster of CG flashes associated with the convective plume increased substantially from the previous radar scan.

The third severe wind report associated with this event occurred 80 min. after the previous report (2200 UTC, Figure 4.19d). While the third report occurred beneath a region of the storm with a high reflectivity factor (>50 dBZ), only seven CG flashes were observed in its immediate vicinity. The strongest convective plumes were located to the south, where CG lightning activity was maximized. There is evidence of charge advection into the anvil region of the severe wind-producing cell (see Rutledge et al. 1990). It is important to note that the CG lightning patterns during the intervening scan time did not indicate charge advection. Similarly, the strong convective cell to the north, although producing a high frequency of CG flashes, does not suggest charge advection into the anvil region at this time. Fifteen minutes later, however, the convective cell began to merge with a decaying cell to the northeast and severe wind was reported (Figure 4.19e). It is possible that the decaying cell may have transferred its charged space to the severe convective cell before short circuiting. This could explain the

enhancement of +CG flashes in the core of the convective plume (from one +CG flash to seven +CG flashes), which was collocated with the severe wind report. Nevertheless, it is interesting that the severe wind reports occurred near convective cells undergoing observed changes in electrical behavior. Seven minutes later (2222 UTC), severe wind was reported to the northeast of the main convective cell near a small convective plume that was producing minimal CG lightning (Figure 4.19f).

The base reflectivity scan at 2245 UTC indicates the development of new convection downwind of the mature convective clusters (Figure 4.19g). Damaging wind was reported underneath the core of the convective plume where CG lightning activity was highest. The radar scan at 2339 UTC shows further development along an outflow boundary (i.e. gust front) extending in an arch-like pattern downstream of the convective cluster (Figure 4.19h). Two small, yet strong convective cells have developed along this boundary, with a 52-kt. wind gust reported beneath the smallest of the new cells. As this cell develops, it also experiences an increase in CG lightning activity, while continuing to produce severe wind along the leading edge of the gust front. Given that the electrical activity of a thunderstorm is strongly correlated with the amount of vertically integrated water (Elson and Margraf 1996), there is evidence that the severe wind reports associated with this cell are of microburst-origin. Specifically, when a sufficiently deep and dry sub-cloud layer is present, high precipitation rates can maximize evaporative cooling and water loading, allowing the descending air to remain negatively buoyant (Proctor 1989).

There were two reports of severe wind at 0015 UTC 4 June 2002, both of which occurred beneath convective cells with high CG lightning activity (Figure 4.19i). The northern-most severe cell continued to develop and eventually produced a damaging

wind gust. The collocation of the severe wind report and the clustering of –CG flashes is identifiable at the 0126 UTC radar scan (Figure 4.19j). As the cell beings to collapse, it experiences a rapid decrease in CG lightning activity (Figures 4.19k,l). While the timing and location of many of the severe wind reports suggest a relationship between cloud water content, lightning production, and strong downdrafts, there are likely other microphysical environments supportive of severe convective winds.

4.3.2 Non-Severe Case

A cluster of convective rain cells developed in the early afternoon of 22 August 2003 along the southern edge of the fall line boundary. A few of these cells became electrically active immediately prior to the 1903 UTC radar scan (Figure 4.20a). The first cell to develop only produced 10 CG flashes over a 5-min. period, yet three were +CG flashes. Recall that the frequency of +CG flashes in the severe wind case was maximized at only seven flashes. At the 2002 UTC scan time, the convective cell produced 14 CG flashes, five of which were +CG flashes (Figure 4.20b). Although unidentifiable on the smoothed radar scan, an outflow boundary has developed to the west of the convective cell. Two smaller cells are developing to the south and southwest of the initial cell, with the former producing a +CG flash. At the 2043 UTC scan time, the initial convective cell has begun to decay and the resulting outflow boundary is approaching the rapidly-developing cell to the southwest and the decaying cell to the south (Figure 4.20c). Although the cell to the southwest is producing much fewer CG flashes than the severe wind-producing cells from the previous case, there are three +CG flashes observed beneath the non-severe cell.

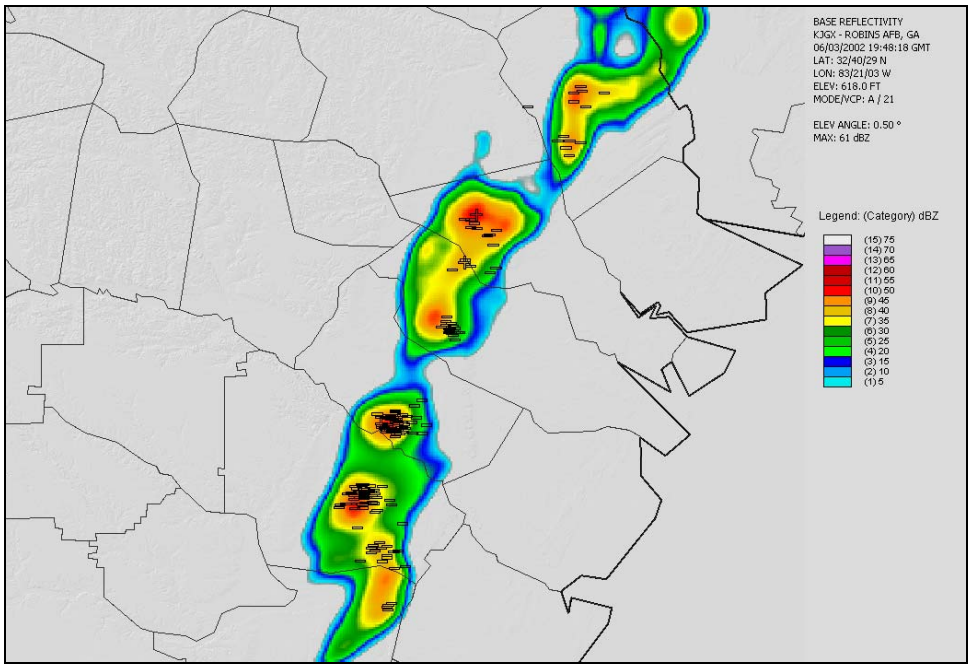

(a)

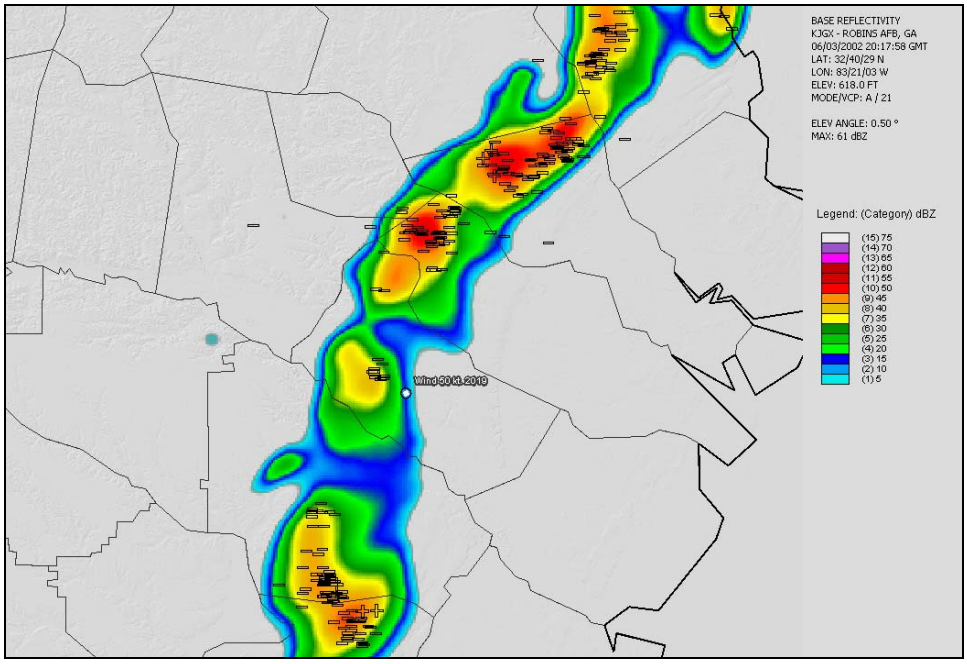

(b)

Figure 4.19. Base reflectivity scans (KJGX) and CG lightning distribution for a severe wind case on 3-4 June 2002. Subfigures (a) to (l) represent radar scan times indicated on the figures as well as CG flash distributions for the preceding 5-min. period. Negative flashes are indicated by "–" and positive flashes are indicated by "+". Severe wind report locations (estimated gust speed or damage-based) are provided for the corresponding scan times. The horizontal scale is not fixed among the subfigures.

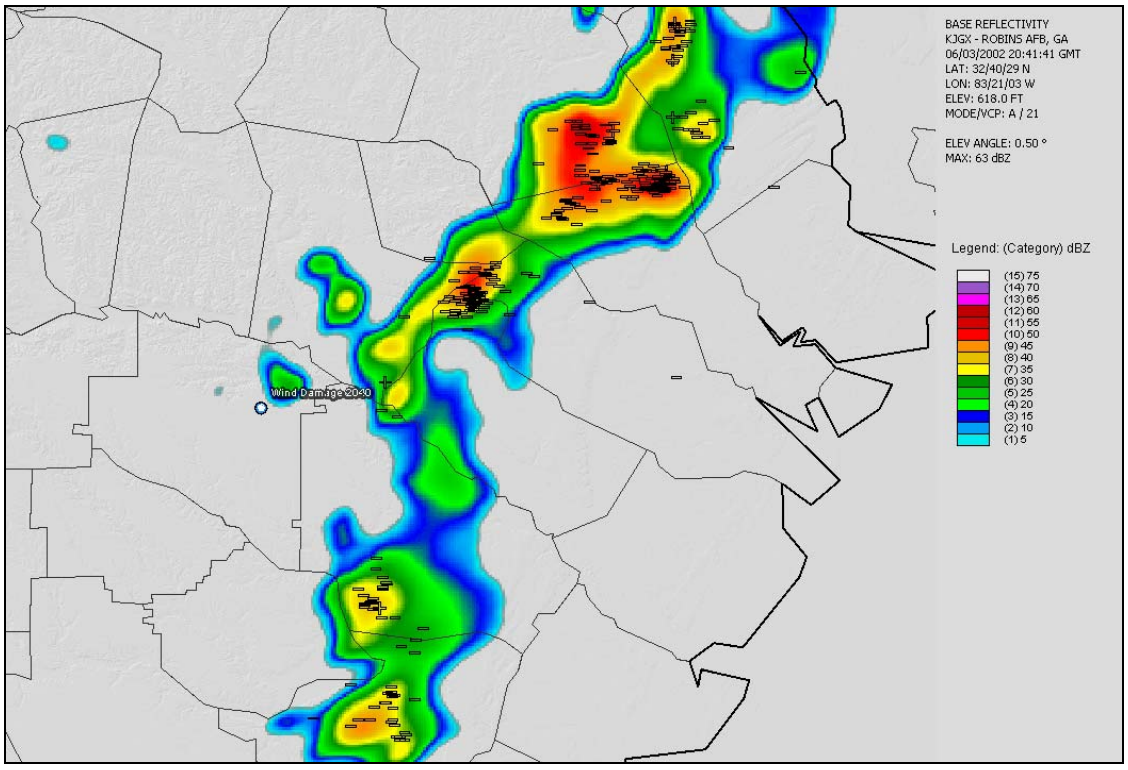

(c)

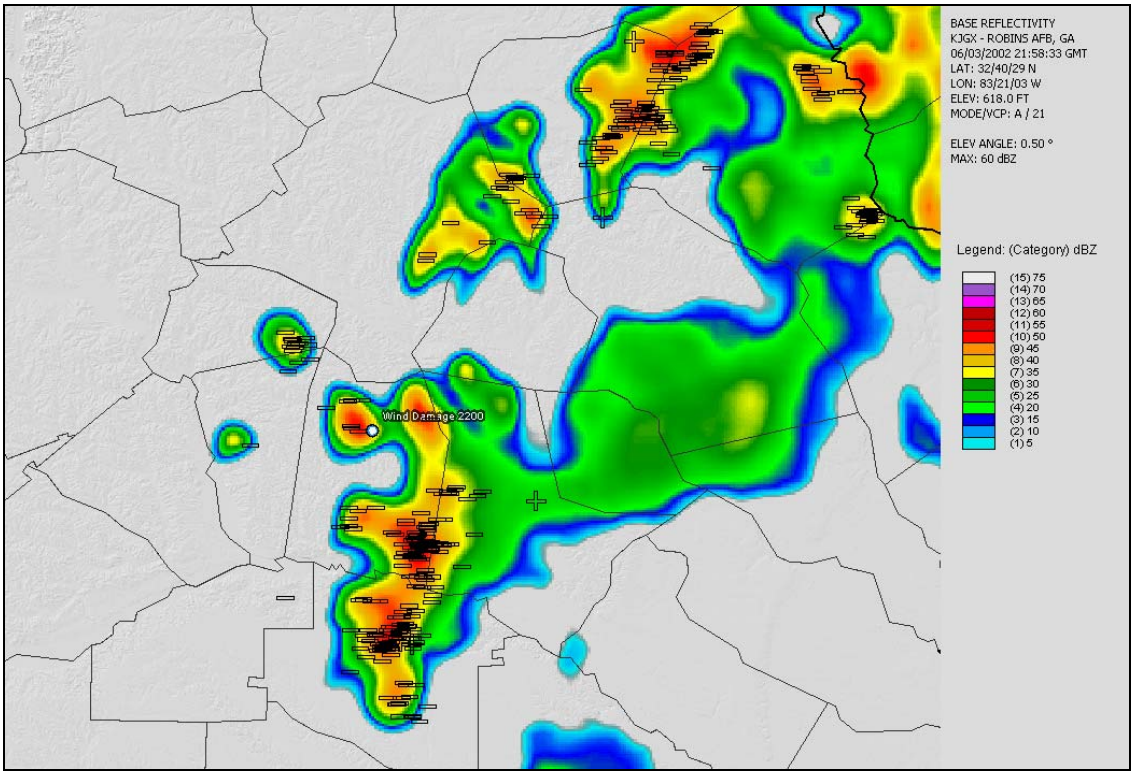

(d)

Figure 4.19. (continued)

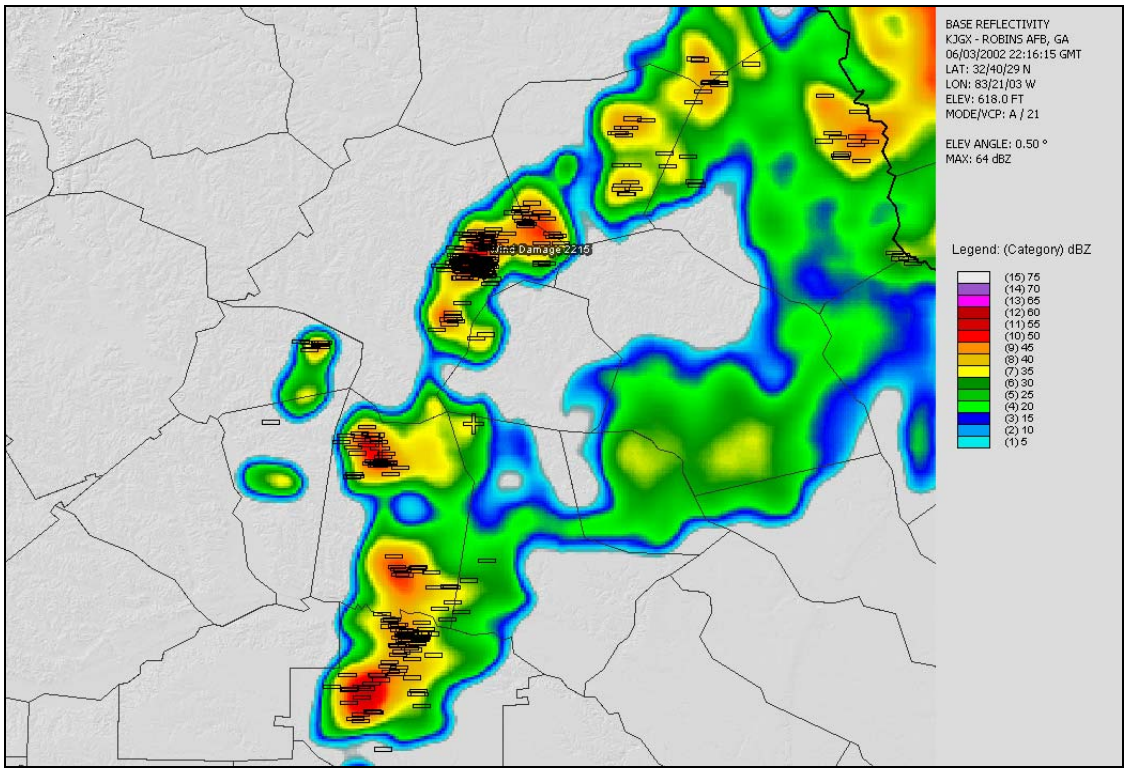

(e)

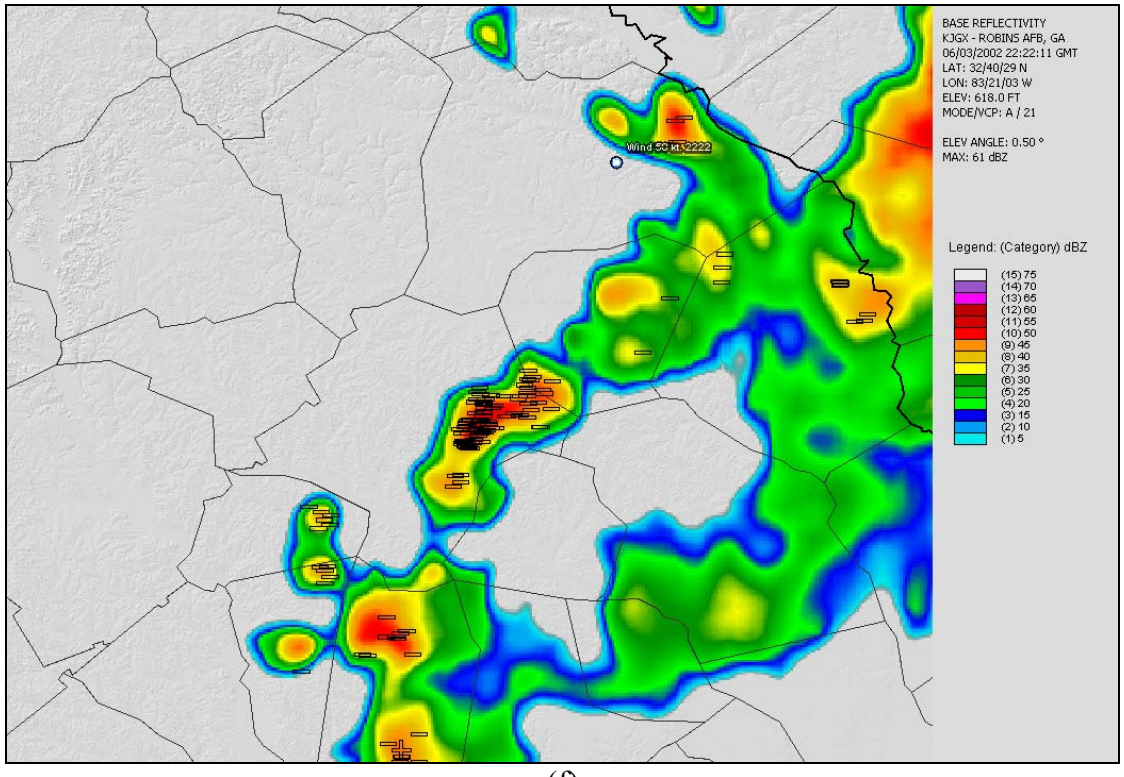

(f)

Figure 4.19. (continued)

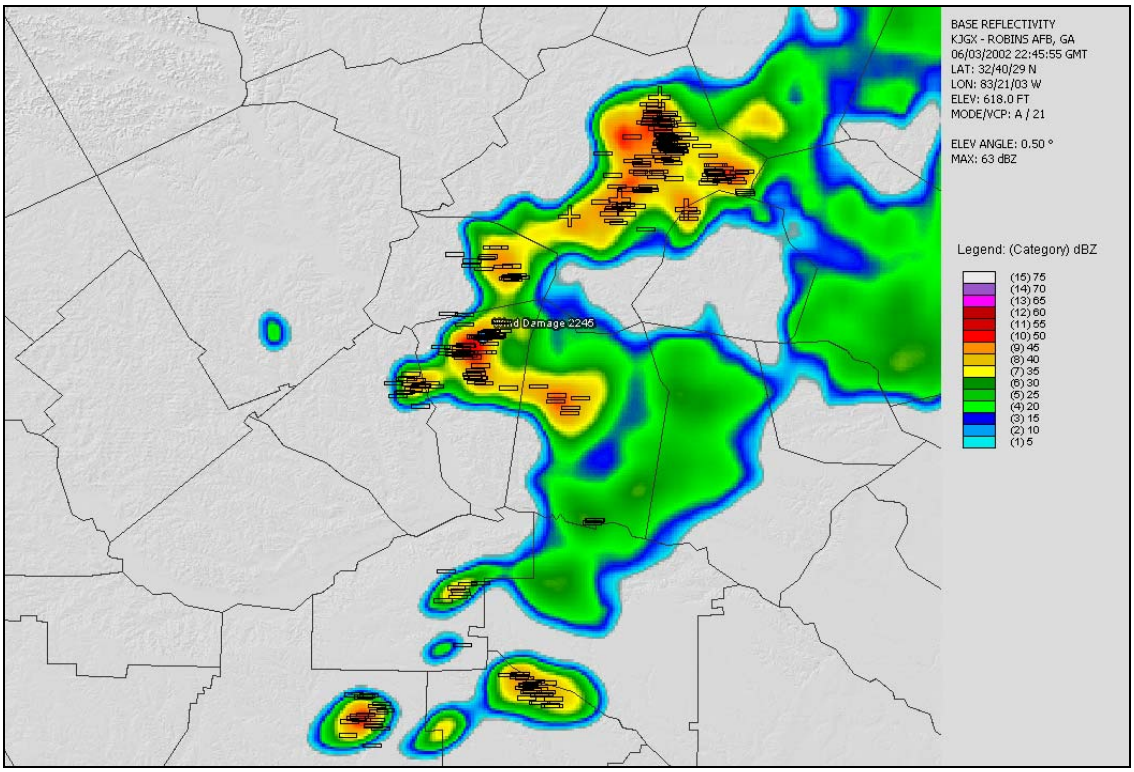

(g)

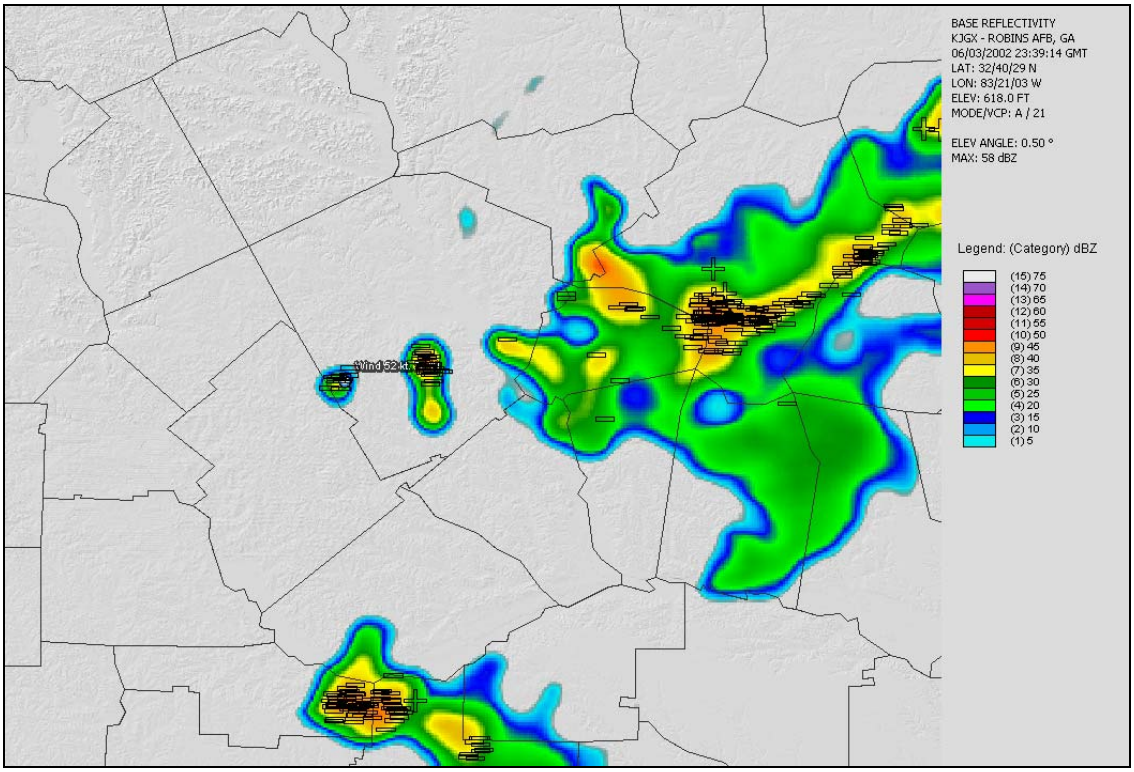

(h)

Figure 4.19. (continued)

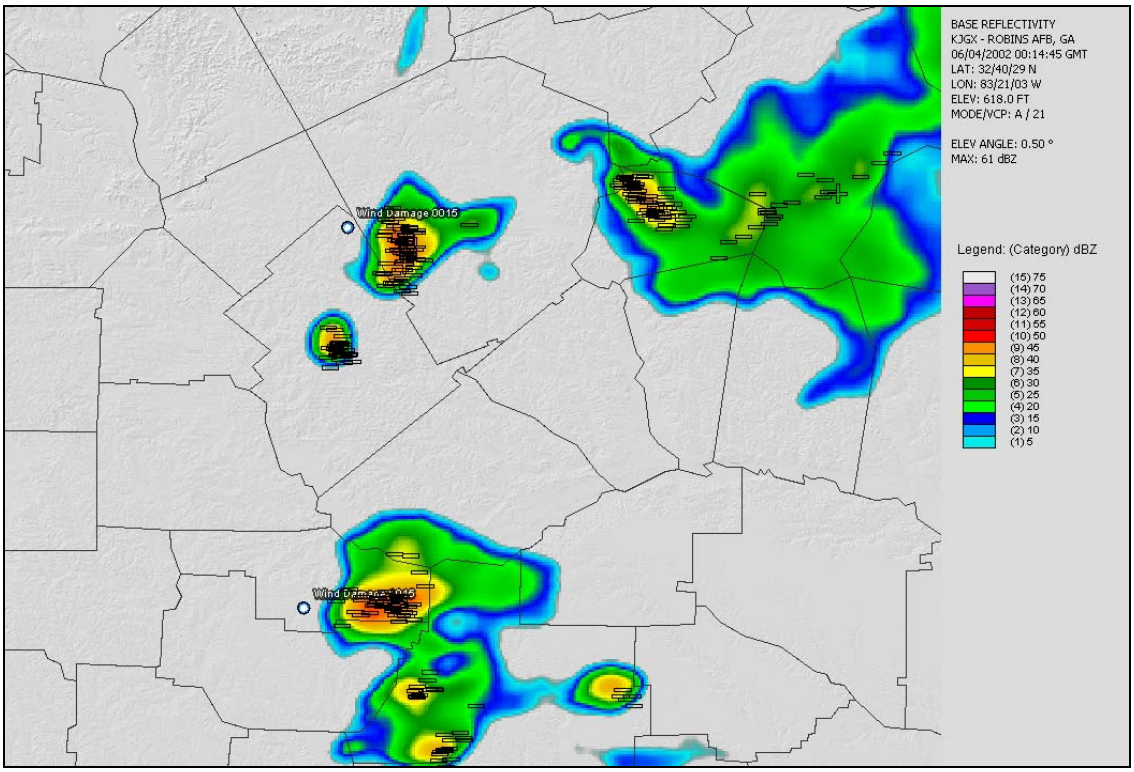

(i)

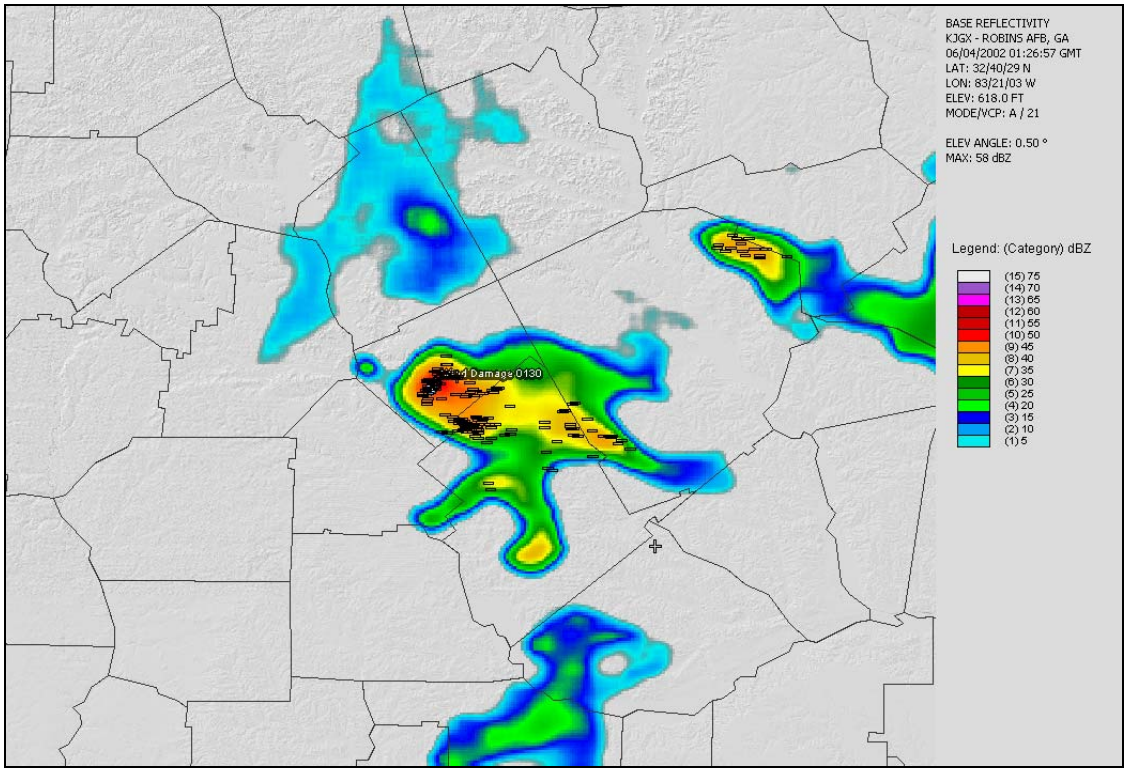

(j)

Figure 4.19. (continued)

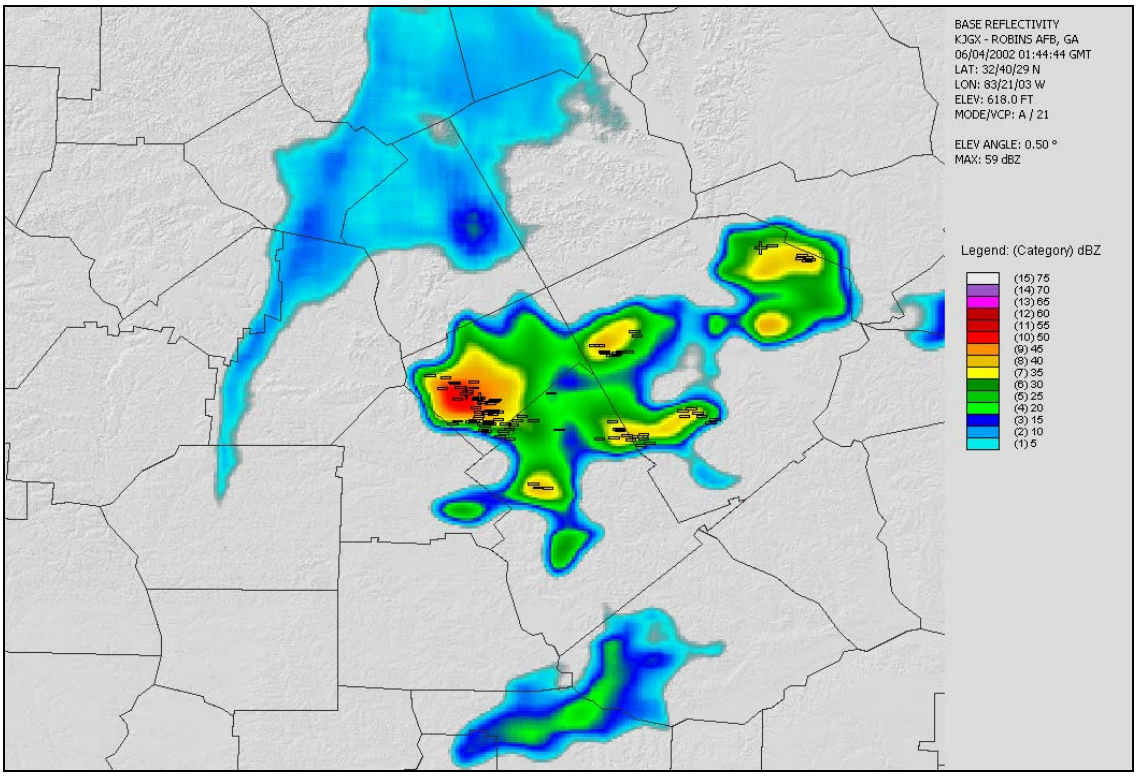

(k)

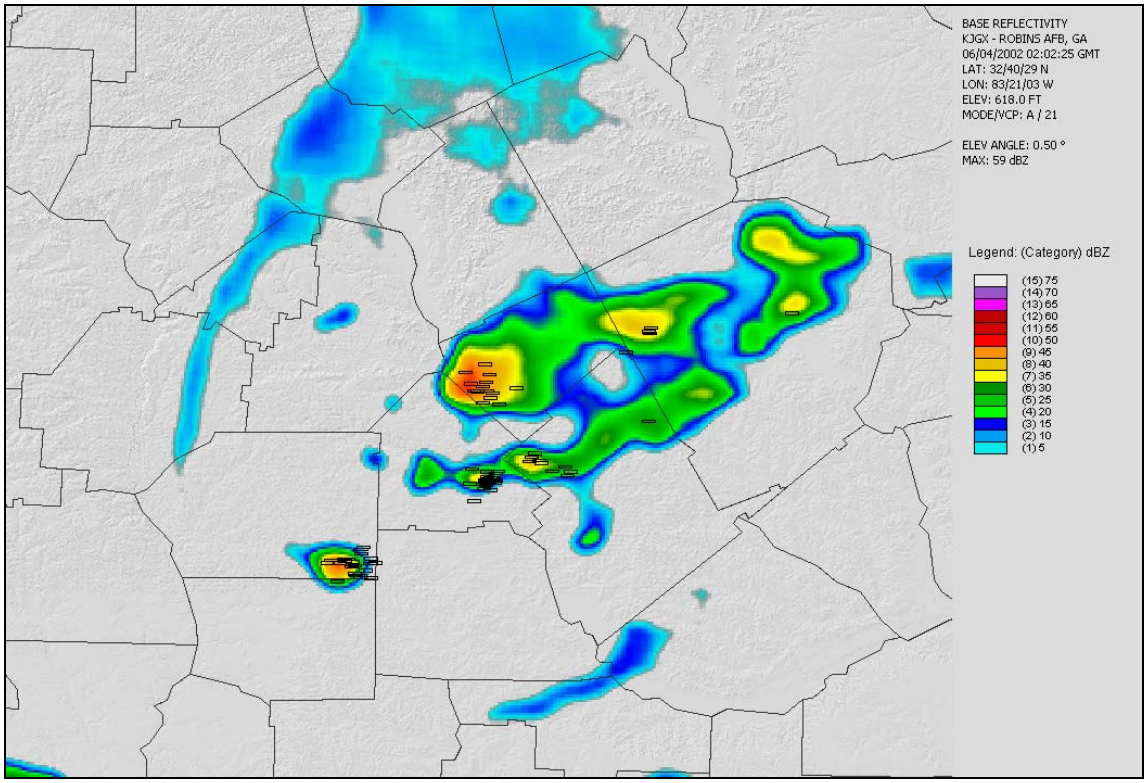

(l)

Figure 4.19. (continued)

The initial convective cell is identifiable in the 2118 UTC scan by its convective decay and disaggregated electrical activity (Figure 4.20d). The outflow boundary from this cell has merged with both the cell to the south and the cell to the southwest. An examination of the 2154 UTC (Figure 4.20e) and 2229 UTC (Figure 4.20f) scan times reveals that the CG lightning activity in the cell to the southwest has diminished, while CG lightning activity in the cell to the south has increased rapidly and is producing 32% +CG lightning. The resulting outflow from the rejuvenated cell is clearly visible in the 2229 UTC scan. It is suggested in the 2305 UTC scan (Figure 4.20g) that this outflow removed much of the buoyant energy from the cell's convective core and a lack of frozen hydrometeors rendered the cell incapable of producing frequent CG flashes, although numerous intra-cloud flashes may still have occurred as the main negatively charged center short circuited.

4.4 Summary

Severe convective windstorms occur rather frequently across the state of Georgia during the warm season months (April-September), on average every two to three days. While the majority of individual severe wind reports exhibit strong diurnal dependence, a few organized, severe wind-producing convective systems may initiate earlier in the day and dissipate in the predawn hours. Perhaps the most revealing aspect of this research is that more than two-thirds of severe wind-producing convective systems are associated with irregular radar-observed signatures. These storms may be characterized as clusters of strong, disorganized convective cells with no linear structure. These events initiate most often in localized areas along mesoscale surface boundaries and within the coastal

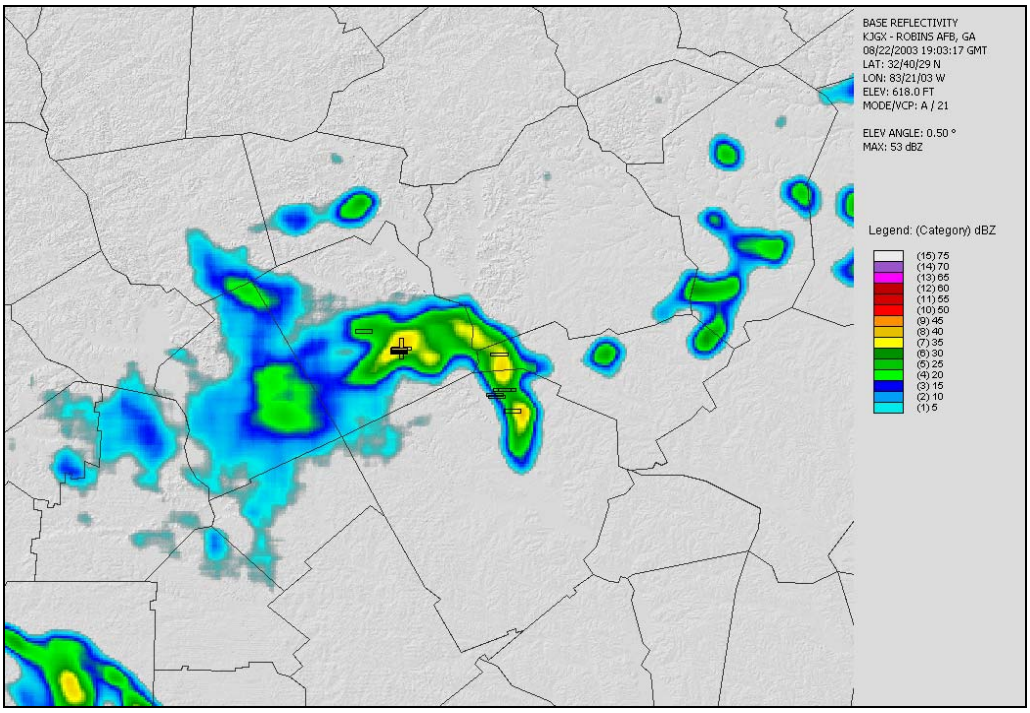

(a)

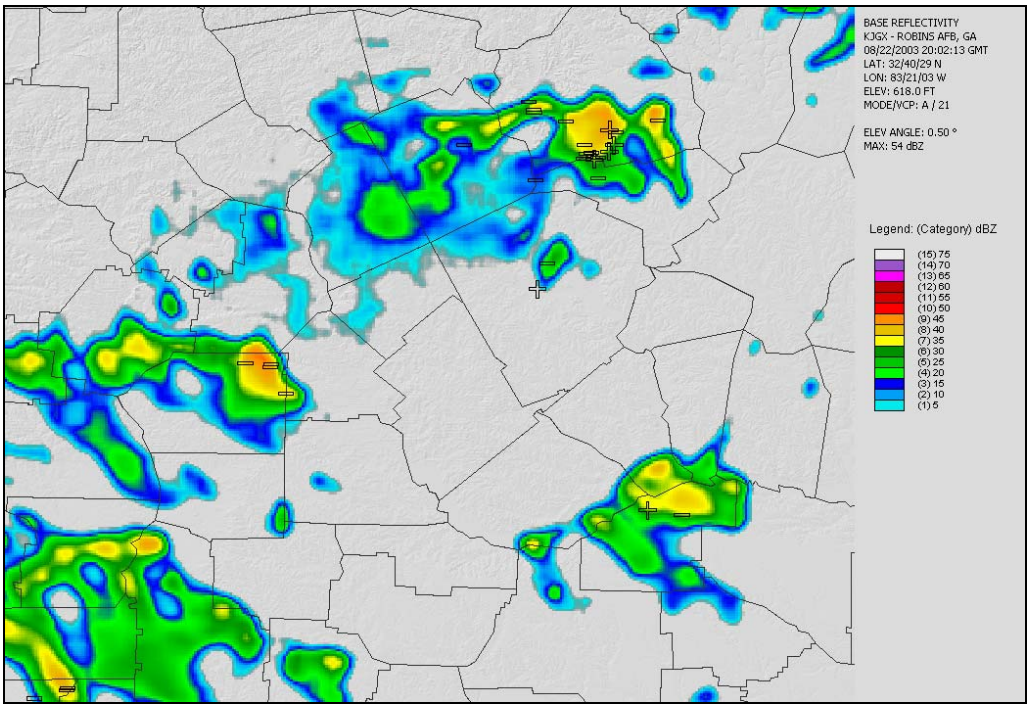

(b)

Figure 4.20. Same as Figure 4.19, but for a non-severe thunderstorm case on 22 August 2003. Subfigures (a) to (g) represent radar scan times indicated on the figures as well as CG flash distributions for the preceding 5-min. period.

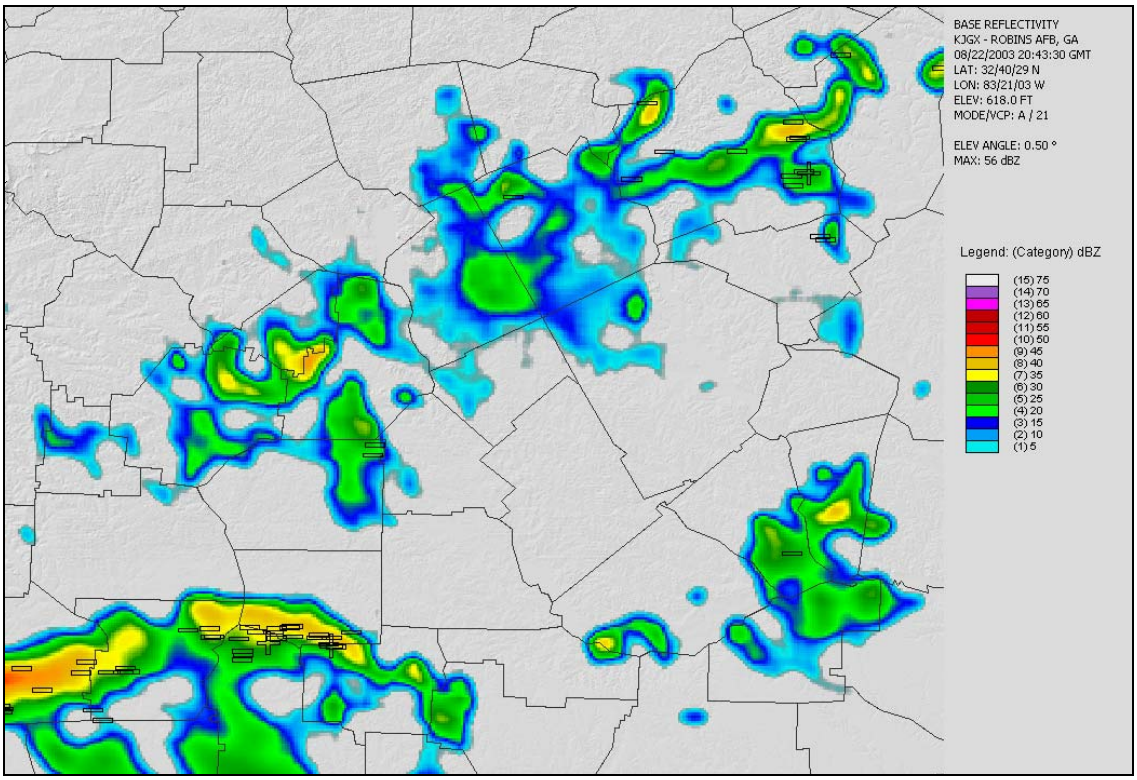

(c)

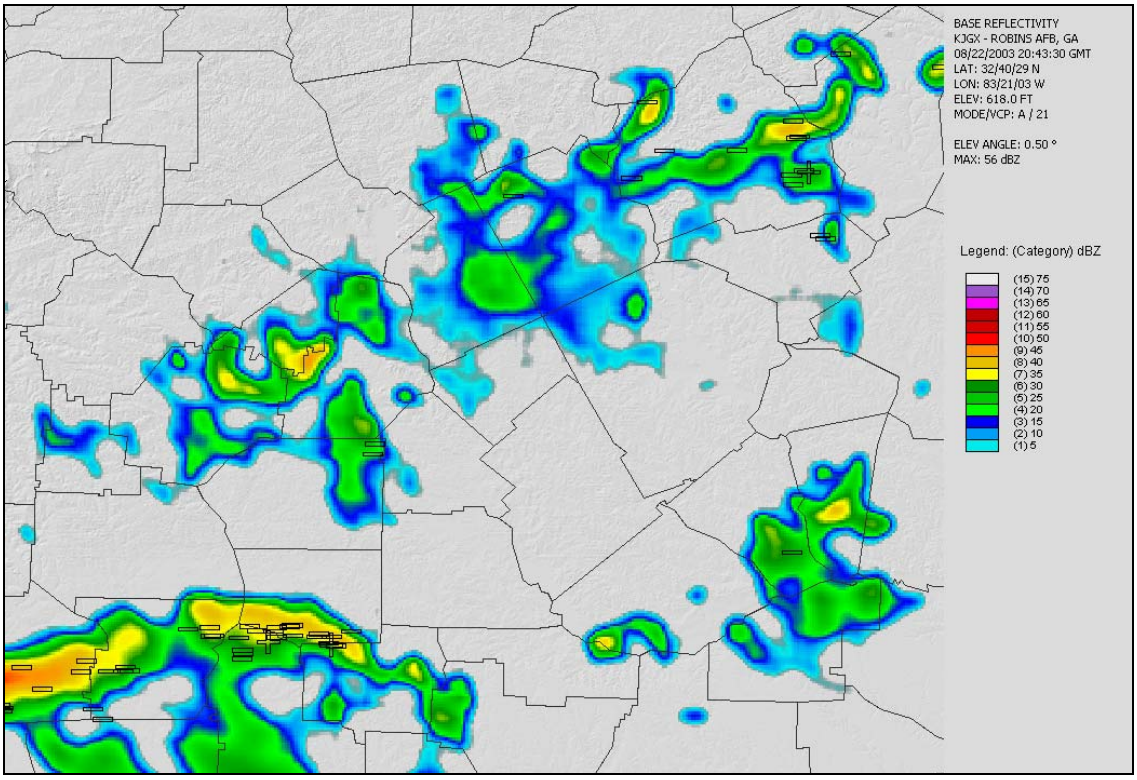

(d)

Figure 4.20. (continued)

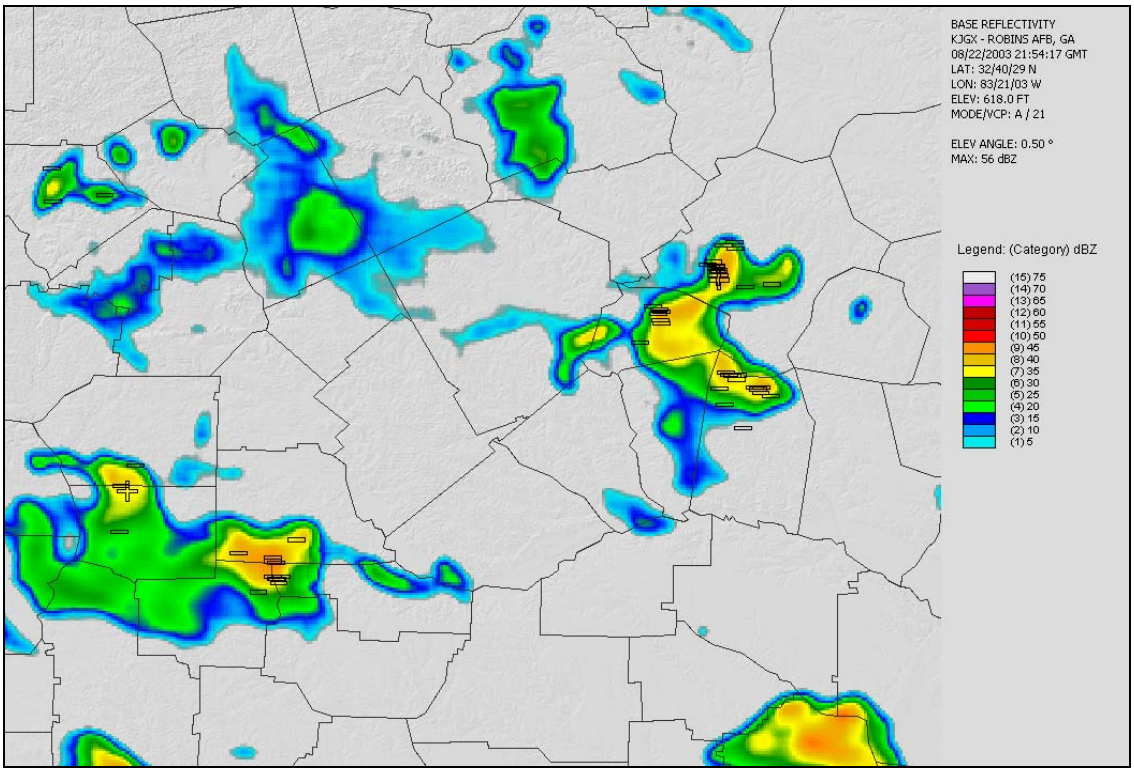

(e)

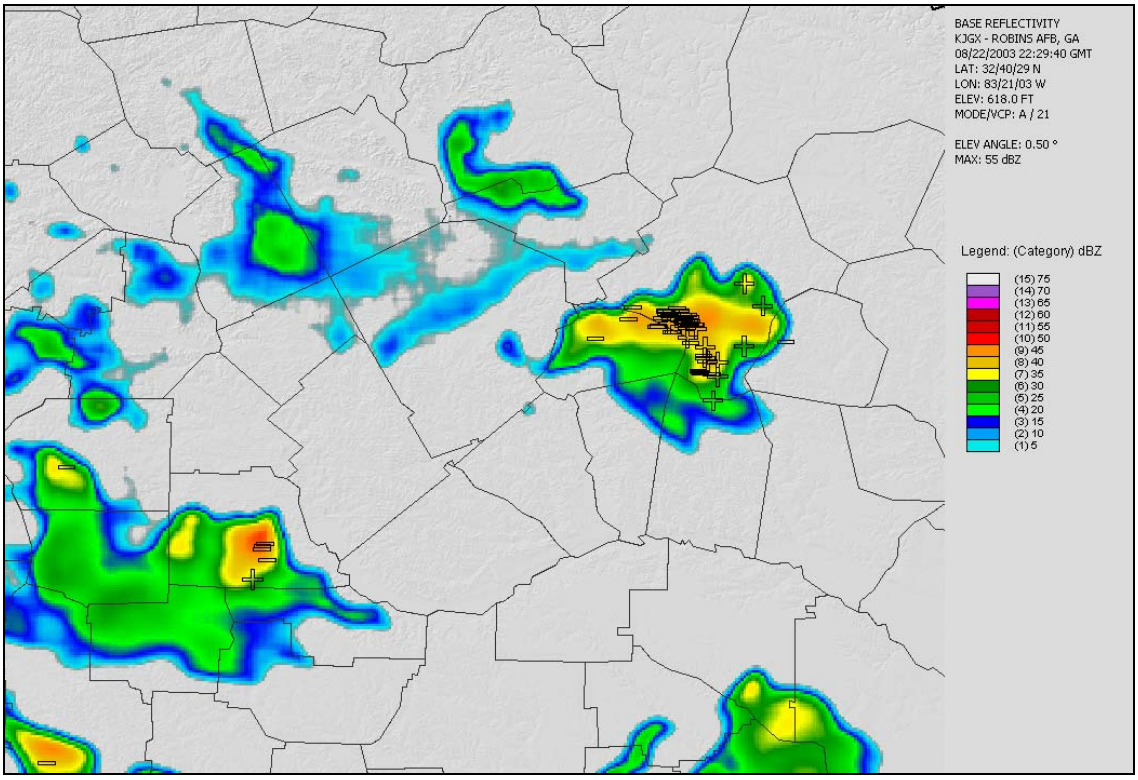

(f)

Figure 4.20. (continued)

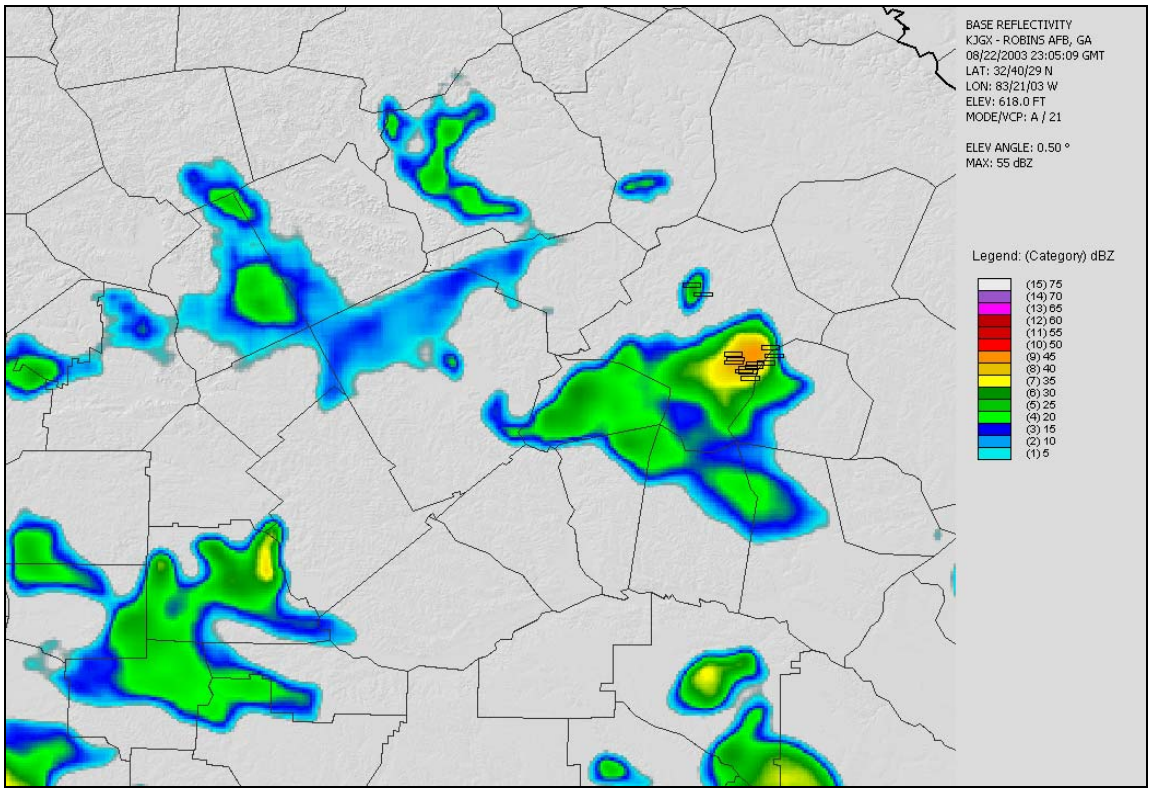

(g)

Figure 4.20. (continued)

plain. Since upper-level support and large-scale surface boundaries are generally absent during these events, they remain quasi-stationary or move generally to the southeast in response to the sea-breeze circulation. These results are contrary to what Klimowski et al. (2003) observed over the NHP, where more than 80% of severe wind-producing convective systems were found to be associated with linear and/or organized modes of convection, namely squall lines, bow echoes, and supercells.

An examination of sounding parameters reveals the importance of mid-tropospheric shear and convective energy in the production of severe winds. A mesoscale layer of dry air is also important in facilitating negative buoyancy, particularly

since the synoptic-scale moisture profile over the Southeast is likely too high to prevent sinking air parcels from warming dry adiabatically. The behavior of CG lightning associated with severe wind-producing thunderstorms varies considerably throughout the course of an event. Severe winds are observed during periods of enhanced and suppressed CG lightning activity and are also observed beneath and at considerable distances from the main convective plume. The most reliable signature in CG lightning behavior associated with the subset of six severe wind-producing thunderstorms is a decrease in the frequency of +CG flashes.

CHAPTER 5

SUMMARY AND CONCLUSIONS

Recent research has demonstrated that severe convective winds occur frequently across parts of the Southeast U.S. (Senn 2003; Doswell et al. 2005). Even so, there is a paucity of studies that summarize the environments favorable for severe winds across the region. The objective of this research was to improve the conceptual models of warm season severe wind environments in Georgia by examining the predominant modes of convection, the synoptic-to-mesoscale environments, and CG lightning patterns associated with these events. This study was limited to the state of Georgia due to the confines of the CG lightning dataset. It is suggested, however, that these results may be applied to other parts of the Southeast, particularly where the local topography influences convective processes. With an understanding of the range of environments conducive to severe thunderstorm winds, forecasters may better predict when and where these events will occur.

National composite radar summaries and base reflectivity scans from radar sites in the WSR-88D network were examined to determine the predominant convective modes associated with archived reports of severe or damaging thunderstorm wind. It was initially hypothesized that about an equal number of severe windstorms in Georgia are associated with organized and unorganized convective modes. Unlike what is typically seen across the NHP region and Midwest, where severe winds are primarily associated

with organized convective systems (e.g. bow echoes, Klimowski et al. 2003; Snook and Gallus 2004), nearly three-quarters of the severe wind-producing convective systems in Georgia were identified as irregular. This convective mode may be characterized as either a single convective cell or cluster of cells with high reflectivity factors and no linear organization. These events typically occurred on days when a synoptic-scale frontal boundary was absent across the Southeast. On these days, the Southeast region was usually under the influence of a sub-tropical ridge. Events classified as irregular that occurred on days when a synoptic-scale frontal boundary was located over the region typically exhibited linear organization during part of their lifetime (similar to the "broken squall line" morphology used by Snook and Gallus 2004), but in these cases the linear structure was not a persistent feature. Since the radar-observed characteristics of these systems were based on a subjective and rather rigid set of criteria developed by previous studies, some of the irregular storms could be classified as squall lines using a more flexible set of criteria. The same may be said for those squall lines with instantaneous bow echo characteristics that did not persist for the majority of the convective system's lifetime (e.g. a bow echo structure lasting for one radar scan).

The spatial distribution of severe wind reports in Georgia exhibits two main patterns. The clustering of reports around the Atlanta metropolitan area is likely the result of population density. Although somewhat far reaching, it is interesting to note the secondary cluster of reports associated with squall lines located to the south of downtown Atlanta. This is in close proximity to the Atlanta NWS forecast office located in Peachtree City. One may only speculate as to whether severe thunderstorm winds, and severe weather reports in general, are more likely to be reported in areas where damage

surveyors and storm spotters are more frequently located. In addition to population density, severe wind reports also tend to cluster along the coastal plain. Brown (2002) suggests that the sea breeze may be a trigger for severe weather in the Southeast and the present work supports this theory. It has also been demonstrated that strong synoptic support is not a necessary component to the development of severe wind-producing thunderstorms. This suggests that mesoscale circulations, under the proper conditions, may act as a primary triggering mechanism for severe convection. Indeed, Brown and Arnold (1998) have shown that deep, moist convection may initiate along mesoscale boundaries created by thermal and moisture gradients under weak synoptic flow across Illinois. It is unclear, however, whether these circulations on their own can initiate severe thunderstorms.

A recent study by McAvoy (2004) suggests that the development of a mesoscale surface boundary, which formed in response to a 5-7°C temperature gradient, enhanced the 0-3 km storm-relative helicity values on the northern edge of the boundary and provided a region favorable for mesocyclone formation in the Upstate of South Carolina. Since severe thunderstorms are typically driven by deep, moist convection, with the resulting outflows sustained through evaporative cooling, those storms producing severe winds are more likely to form in regions with strong thermal and moisture gradients. On the mesoscale, these boundaries may initially form in a pre-convective environment characterized by intermittent cloud cover or fog. When the synoptic-scale support is weak, mesoscale surface boundaries may provide the trigger for deep convection to overcome the capping inversion. Future research should combine both observational (in situ) and modeling approaches to address this issue.

The characteristics and evolution of CG lightning associated with subsets of severe wind-producing thunderstorms and non-severe thunderstorms were analyzed using graphical overlays of local radar imagery, severe wind reports, and CG flashes. These thunderstorms were classified as irregular and developed under the influence of the sub-tropical high pressure cell. Within these subsets, a number of revealing characteristics in CG lightning behavior and storm structure were observed. To illustrate these findings, an archetypical case from the severe wind-producing thunderstorm subset and non-severe thunderstorm subset was presented.

Generally speaking, severe wind-producing thunderstorms exhibit as much as 120% more CG lightning throughout their lifetime than non-severe thunderstorms, yet exhibit as much as 28% fewer +CG flashes. These patterns were consistent among the thunderstorms examined in this study and suggest that a +CG lightning signature (Branick and Doswell 1992) may be more prevalent in non-severe thunderstorms in Georgia. A review of the cloud scale mechanisms for the production of +CG (e.g. tilted dipole, precipitation unshielding) does not provide a physical explanation for this pattern in severe wind-producing thunderstorms (Williams 2001). However, severe downdrafts driven by water loading would likely create a cloud environment favorable for +CG flashes since the negatively-charged water droplets being expelled from the cloud base would expose the positively-charged region of the cloud to the ground. Since very few +CG flashes occurred in the subset of severe wind-producing thunderstorms, the negatively-charged region must not have collapsed. It is possible that severe downdrafts driven by the diabatic effects of evaporation and sublimation create a negatively-charged space near the base of the cloud, preventing the positively-charged region from being

exposed to the ground. Ordinary, or non-severe, thunderstorms have been characterized as having a tripole charging structure whereby a thin layer of positively-charged space is found near the cloud base (Williams 2001). The severe wind-producing thunderstorms examined in this study may instead be characterized by a more vertically-extensive negative charge layer whereby the evaporation and sublimation of hydrometeors dispels the thin layer of positive charge. Future research should utilize polarimetric radar data to determine the cloud scale charging structure of thunderstorms as they develop. Only a few experimental radar networks are currently capable of polarimetric time-height analysis (e.g. CHILL radar from Colorado State University), although additional radar sites in the WSR-88D network are expected to attain polarimetric capability in the near future[8].

Only 7% of the 36 severe wind reports occurring in the subset of thunderstorms exhibited decreases in CG lightning in the 5-min. interval immediately prior. Interestingly, more than 50% of these severe wind reports occurred away from the main center of CG lightning activity. Changnon (1992) found a similar pattern associated with CG lightning centers and hail shafts over Illinois. Initially, the lack of CG lightning flashes near severe wind reports was discouraging. However, there may be microphysical processes manifested at the cloud scale that can predict whether an impending severe wind gust will occur near or away from the main convective plume, or region of highest CG flash density. One possibility is the transfer of charge from decaying convective cells to re-generating convective cells. Further, the occurrence of +CG and –CG flashes beneath the anvil shield was routinely observed for each of these cases and may indicate the potential for severe winds.

[8] http://cimms.ou.edu/~schuur/jpole/

This research has identified the predominant convective modes associated with warm season severe windstorms in Georgia, the synoptic-to-mesoscale environments which favor their development, and the CG lightning characteristics which may distinguish them from non-severe thunderstorms. With this information, forecasters can develop predictive models as well as perform discriminant analysis techniques to better determine the sequence of atmospheric conditions and microphysical processes associated with severe wind-producing thunderstorms.

REFERENCES

Altino, K.M., Knupp, K.R. and S.J. Goodman, forthcoming: Correlation of lightning flash rates with a microburst event. *Wea. Forecasting*.

Anderson, C.J. and R.W. Arritt, 2001: Mesoscale convective systems over the United States during the 1997-98 El Nino. *Mon. Wea. Rev.*, **129**, 2443-2457.

Ashley, W.S., 2005: Derecho-producing convective systems in the United States: An assessment of hazards and family formation. Ph.D. dissertation, Dept. of Geography, The University of Georgia, 157 pp.

Ashley, W.S., and T.L. Mote, 2005: Derecho hazards in the United States. *Bull. Amer. Meteor. Soc.*, **86**, 1577-1592.

Ashley, W.S., Mote, T.L., and M.L. Bentley, 2005: On the episodic nature of derecho producing convective systems in the United States. *Intl. J. Clim.*, **25**, 1915-1932.

Atkins, N.T., and R.M. Wakimoto, 1991: Wet microburst activity over the southeastern United States. *Wea. Forecasting*, **6**, 470-482.

Bentley, M.L and T.L. Mote, 1998: A climatology of derecho-producing mesoscale convective systems in the central and eastern United States, 1986-95. Part I: Temporal and spatial distribution. *Bull. Amer. Meteor. Soc.*, **79**, 2527-2540.

Bentley, M.L. and T.L. Mote, 2000: A synoptic climatology of cool-season derechos events. *Phys. Geogr.*, **21**, 21-37.

Bentley, M.L., Mote, T.L., and P. Thebpanya, 2002: Using LANDSAT to identify thunderstorm damage in agricultural regions. *Bull. Amer. Meteor. Soc.*, **83**, 363-376.

Bentley, M.L., and J.A. Sparks, 2003: A 15 yr climatology of derecho-producing mesoscale convective systems over the central and eastern United States. *Clim. Res.*, **24**, 129-139.

Bentley, M.L., and J.A. Stallins, 2005: Descriptive climatology of cloud-to-ground lightning activity in the state of Georgia, 1992-2003. *Intl. J. Clim.*, **25**, 1979-1996.

Biagi, C.J., Jerauld, J., Cramer, J.A., Cummins, K.L., Krider, E.P., Kehoe, K.E., Rakov, V.A., and M.A. Uman, 2004: Performance validation of the 2002-2003 upgrade of the U.S. National Lightning Detection Network. *EOS Trans.*, AGU, 85(47).

Bornstein, R., and Q. Lin, 2000: Urban heat islands and summertime convective thunderstorms in Atlanta: Three case studies. *Atmos. Environ.*, **34**, 507-516.

Businger, S.B., Bauman, B.H., and G.F. Watson, 1991: The development of the Piedmont Front and associated outbreak of severe weather on 13 March 1986. *Mon. Wea. Rev.*, **119**, 2224-2251.

Branick, M.L., and C.A. Doswell, III, 1992: An observation of the relationship between supercell structure and lightning ground-strike polarity. *Wea. Forecasting*, **7**, 143-149.

Bright, D.R., Jewell, R.E., Wandishin, M.S., and S.J. Weiss, 2005: A physically-based parameter for lightning prediction and its calibration in ensemble forecasts. Preprints, *Conf. on Meteorological Applications of Lightning Data*, San Diego, CA, Amer. Meteor. Soc.

Brown, M.E., 2002: The spatial, temporal, and thermodynamic characteristics of Southern-Atlantic United States tornado events. *Phys. Geog.*, **23**, 401-417.

Brown, M.E., and D.L. Arnold, 1998: Land-surface-atmosphere interactions associated with deep convection in Illinois. *Intl. J. Clim.*, **18**, 1637-1653.

Brooks, H.E., Doswell, C.A. III, and J. Cooper, 1994: On the environments of tornadic and nontornadic mesocyclones. *Wea. Forecasting*, **10**, 606-618

Browning, K.A., 1977: The structure and mechanism of hailstorms. *Hail: A review of hail science and hail suppression, Meteor. Monogr.*, No. 38, Amer. Meteor. Soc., 1-43.

Bunkers, M.J., Klimowski, B.A., Zietler, J.W., Thompson, R.L., and M.L. Weisman, 2000: Predicting supercell motion using a new hodograph technique. *Wea. Forecasting*, **15**, 61-79.

Byers, H.R., and R.R. Braham Jr., 1949: *The Thunderstorm*. U.S. Government Printing Office, 287 pp.

Carey, L.D., and S.A. Rutledge, 1996: A multiparameter radar case study of the microphysical and kinematic evolution of a lightning producing storm. *Meteor. Atmo. Phys.*, **59**, 33-64.

Carey, L.D., Rutledge, S.A., and W.A. Petersen, 2003: The relationship between severe storm reports and cloud-to-ground lightning polarity in the contiguous United States from 1989 to 1998. *Mon. Wea. Rev.*, **131**, 1211-1228.

Changnon, S.A. 2001: Damaging thunderstorm activity in the United States. *Bull. Amer. Meteor. Soc.*, **82**(4), 597-608.

Coniglio, M.C., and D.J. Stensrud, 2004: Interpreting the climatology of derechos. *Wea. Forecasting*, **19**, 595-605.

Coniglio, M.C., Stensrud, D.J., and M.B. Richman, 2004: An observational study of derecho-producing convective systems. *Wea. Forecasting*, **19**, 320-337.

Cummins, K.L., M.J. Murphy, E.A. Bardo, W.L. Hiscox, R.B. Pyle, and A.E. Pifer, 1998: A combined TOA/MDF technology upgrade of the U.S. National Lightning Detection Network. *J. Geophys. Res.*, **103**, 9035-9044.

Dixon, P.G., and T.L. Mote, 2003: Patterns and causes of Atlanta's urban heat island-initiated precipitation. *J. Appl. Meteor.*, **42**, 1273-1284.

Djuric, D., 1994: Analysis of vertical soundings. In D. Djuric, ed., *Weather Analysis*. Englewood Cliffs, NJ: Prentice Hall, 69-87.

Dodge, J., Arnold, J., Wilson, G., Evans, J., and T.T. Fujita, 1986: The Cooperative Huntsville Meteorological Experiment (COHMEX). *Bull. Amer. Meteor. Soc.*, **67**, 417-419.

Doswell, C.A. III, Schaefer, J.T., McCann, D.W., Schlatter, T.W., and H.B. Wobus, 1982: Thermodynamic analysis procedures at the National Severe Storms Forecast Center, *Preprints, Ninth Conf. on Weather Forecasting and Analysis*, Seattle, Amer. Meteor. Soc., 304-309.

Doswell, C.A. III, 1982: The operational meteorology of convective weather. Volume I: Operational mesoanalysis. NOAA Technical Memorandum, NWS NSSFC-5. [Available online at http://www.weathergraphics.com/dl/nssfc5sm.pdf]

Doswell, C.A. III, 1987: The distinction between large-scale and mesoscale contribution to severe convection: A case study example. *Wea. Forecasting*, **2**, 3-16.

Doswell, C.A. III, and D.W. Burgess, 1988: On some issues of United States tornado climatology. *Mon. Wea. Rev.*, **116**, 495-501.

Doswell, C.A., III, and E.N. Rasmussen, 1994: The effect of neglecting the virtual temperature correction on CAPE calculations. *Wea. Forecasting*, **9**, 625-629.

Doswell, C.A., III, and L.F. Bosart, 2002: Extra-tropical synoptic-scale processes and severe convection. *Severe Convective Storms, Meteor. Monogr.*, No. 50, Amer. Meteor. Soc., 27-69.

Doswell, C.A., III, Brooks, H.E., and M.P. Kay, 2005: Climatological estimates of daily local nontornadic severe thunderstorm probability for the United States. *Wea. Forecasting*, **20**, 577-595.

Elson, D.B., 1993: Relating cloud-to-ground lightning to severe weather in Indiana on 2 June 1990. *Nat. Wea. Digest*, 18, 15-21.

Elson, D.B., and J. Margraf, 1996: A comparison of lightning strikes to radar observations of thunderstorms on July 9-10, 1993. NOAA-NWS Central Region Applied Research Paper 16-01. [Available online at http://www.crh.noaa.gov/crh/?n=arp16-01]

Emanuel, K.A., 1994: *Atmospheric Convection*. Oxford University Press, 580 pp.

Evans, J.S., and C.A. Doswell, 2001: Examination of derecho environments using proximity soundings. *Wea. Forecasting*, **16**, 329-342.

Fujita, T.T., 1978: Manual of downburst identification for project NIMROD. SMRP Research Paper 156, University of Chicago, 104 pp. [NTIS PB-2860481.]

Fujita, T.T., 1981: Tornadoes and downbursts in the context of generalized planetary scales. *J. Atmos. Sci*., **38**, 1511-1534.

Fujita, T.T., 1985: The downburst. SMRP Research Paper 210, University of Chicago, 122 pp.

Fujita, T.T., and F. Caracena, 1977: An analysis of three weather-related aircraft accidents. *Bull. Amer. Meteor. Soc.*, **58**, 1164-1181.

Fujita, T.T., and R.M. Wakimoto, 1981: Five scales of airflow associated with a series of downbursts on 16 July 1980. *Mon. Wea. Rev.*, **109**, 1438-1456.

Galway, J.G., 1956: The lifted index as a predictor of latent instability. *Bull. Amer. Meteor. Soc.*, **37**, 528-529.

Geerts, B., 1998: Mesoscale convective systems in the Southeast United States during 1994-95: A survey. *Wea. Forecasting*, **13**, 860-869.

Goodman, S.J., D.E. Buecheler, P.D. Wright, and W.D. Rust, 1988: Lightning and precipitation history of a micro-burst producing storm. *Geophys. Res. Lett*., **15**, 1185-1188.

Hamilton, R.E., 1970: Use of detailed intensity radar data in mesoscale surface analysis of the 4 July 1969 storm in Ohio. Preprints, *14th Conf. on Radar Meteor.*, Tucson, AZ, Amer. Meteor. Soc., 339-342.

Hart, J.A., and P.R. Janish, 1999: SeverePlot: Historical Severe Weather Report Database Version 2.0. Storm Prediction Center, Norman, OK. [Available online at http://www.spc.noaa.gov/software/svrplot2/index.html].

Hinrichs, G., 1888: Tornadoes and derechos. *Amer. Meteor. Journal*, **5**, 341-349.

Holton, J.R., 2004: *An Introduction to Dynamic Meteorology*, Elsevier Academic Press, 511 pp.

Houze, R.A., Smull, B.F., and P. Dodge, 1990: Mesoscale organization of springtime rainstorms in Oklahoma. *Mon. Wea. Rev*., **118**, 613-654.

Job, M., 1996: *Air disaster*. Aerospace Publications, Australia. 218 pp.

Johns, R.H., 1984: A synoptic climatology of northwest flow severe weather outbreaks. Part II: Meteorological parameters and synoptic patterns. *Mon. Wea. Rev.*, **112**, 449-464.

Johns, R.H., and C.A. Doswell III, 1992: Severe local storms forecasting. *Wea. Forecasting*, **7**, 588-612.

Johns, R.H., 1993: Meteorological conditions associated with bow echo development in convective storms. *Wea. Forecasting*, **8**, 294-299.

Johns, R.H., and W.D. Hirt, 1987: Derechos: Widespread convectively induced windstorms. *Wea. Forecasting*, **2**, 32-49.

Kalnay, E. and Co-authors, 1996: The NCEP/NCAR 40-year reanalysis project. *Bull. Amer. Meteor. Soc*., **77**, 437-471.

Kane, R.J., 1992: Correlating lightning to severe local storms in the northeastern United States. *Wea. Forecasting*, **6**, 3-12.

Kelly, D.L., Schaefer, J.T., McNulty, R.P., Doswell, C.A., and R.F. Abbey, 1978: An augmented tornado climatology. *Mon. Wea. Rev*., **106**, 1172-1183.

Kelly, D.L., Schaefer, J.T., and C.A. Doswell, 1985: Climatology of nontornadic severe thunderstorm events in the United States. *Mon. Wea. Rev*., **113**, 1997-2014.

Klemp, J.B., 1987: Dynamics of tornadic thunderstorms. *Ann. Rev. Fluid. Mech*., **19**, 369-402.

Klimowski, B.A., Bunkers, M.J., Hjelmfelt, M.R., and J.N. Covert, 2003: Severe convective windstorms over the Northern High Plains of the United States. *Wea. Forecasting*, **18**, 502-519.

Knupp, K.R., and W.R. Cotton, 1985: Convective cloud downdraft structure: An interpretative survey. *Rev. Geophys.*, **23**, 183-215.

Koch, S.E., and C.A. Ray, 1997: Mesoanalysis of summertime convergence zones in central and eastern North Carolina. *Wea. Forecasting*, **12**, 56-77.

Kuchera, E.L., and M.D. Parker, forthcoming: Severe convective wind environments. *Wea. Forecasting*.

Latham, J., 1981: The electrification of thunderstorms. *Quart. J. Roy. Meteor. Soc.*, **107**, 277-298.

Lhermitte, R.M., and E.R. Williams, 1985: Thunderstorm electrification: A case study. *J. Geophys. Res*., **90**, 6071-6078.

Lemon, L.R., 1976: The flanking line, a severe thunderstorm intensification source. *J. Atmos. Sci*., **33**, 686-694.

Lemon, L.R., and C.A. Doswell, 1979: Severe thunderstorm evolution and mesocyclone structure as related to tornadogenesis. *Mon. Wea. Rev.*, **107**, 1184-1197.

Livingston, E.S., Nielsen-Gammon, J.W., and R.E. Orville, 1996: A climatology, synoptic assessment, and thermodynamic evaluation for cloud-to-ground lightning in Georgia: A study for the 1996 Summer Olympics. *Bull. Amer. Meteor. Soc*., **77**, 1483-1495.

Locklear, B., Brennan, M., Hartfield, G., Palmer, T., Keeter, K., and J. Blaes, 2004: Event summary: March 07, 2004 high wind event. National Weather Service, Raleigh, NC, 11 pp.

Markowski, P.M., Rasmussen, E.N. and J.M. Straka, 1998: The occurrence of tornadoes in supercells interacting with boundaries during VORTEX-95. *Wea. Forecasting*, **13**, 852-859.

Martin, J., and C.E. Konrad II, forthcoming: Directional characteristics of potentially damaging wind gusts in the Southeast United States. *Phys. Geogr.*

McAvoy, B., 2004: The role of surface boundary and multiple cell-mergers in the development of the 21 April 2003 tornado in upstate South Carolina. Pre-prints, *22nd Conf. on Severe Local Storms*, Hyannis, MA, Amer. Meteor. Soc.

McCarthy, J., Wilson, J.W., and T.T. Fujita, 1982: The joint airport weather studies project. *Bull Amer. Meteor. Soc*., **63**, 15-22.

Moller, A.R., Doswell, C.A., Foster, M.P., and G.R. Woodall, 1994: The operational recognition of supercell thunderstorm environments and storm structures. *Wea. Forecasting*, **9**, 327-347.

Mueller, C.K., and R.E., Carbone, 1987: Dynamics of a thunderstorm outflow. *J. Atmos. Sci.*, **44**, 1879-1898.

Nolan, R.H., 1959: A radar pattern associated with tornadoes. *Bull. Amer. Meteor. Soc*., **40**, 277-279.

Nelson, S.P., 1987: The hybrid multicellular-supercellular storm an efficient hail producer. Part II: General characteristics and implications for hail growth. *J. Atmo. Sci.*, **44**, 2060-2073.

Newton, C.W., and J.C. Fankhauser, 1975: Movement and propagation of multicellular convective storms. *Pure Appl. Geophys*., **113**, 747-764.

Orf, L.G., and J.R. Anderson, 1999: A numerical study of traveling microbursts. *Mon. Wea. Rev*., **127**, 1244-1258.

Orlanski, I., 1975: A rational subdivision of scales for atmospheric processes. *Bull. Amer. Meteor. Soc*., **56**, 527-530.

Orville, R.E., and G.R. Huffines, 2001: Cloud-to-ground lightning in the United States: NLDN results in the first decade, 1989-1998. *Mon. Wea. Rev*., **129**, 1179-1193.

Orville, R.E., R.W. Henderson, and L.F. Bosart, 1983: An east coast lightning detection network. *Bull. Amer. Meteor. Soc*., **64**, 1029-1037.

Parker, M.D., and R.H. Johnson, 2000: Organizational modes of midlatitude mesoscale convective systems. *Mon. Wea. Rev.*, **128**, 3413-3436.

Parker, M.D., Rutledge, S.A., and R.H. Johnson, 2001: Cloud-to-ground lightning in linear mesoscale convective systems. *Mon. Wea. Rev.*, **129**, 1232-1242.

Pautz, M.E., 1969: Severe local storm occurrences 1955-1967. ESSA Tech. Memor. WBTM FCST 12, 77 pp. [Available from the Storm Prediction Center, Norman, OK].

Price, C.G., and B.P. Murphy,2002: Lightning activity during the 1999 Superior derecho. *Geophys. Res. Lett.*, **29**, 57-61.

Proctor, F.H., 1988: Numerical simulations of an isolated microburst. Part I: Dynamics and structure. *J. Atmos. Sci.*, **45**, 3137-3160.

Proctor, F.H., 1989: Numerical simulations of an isolated microburst. Part II: Sensitivity experiments. *J. Atmos. Sci.*, **46**, 2143-2165.

Pryzbylinski, R., 1995: The bow echo: Observations, numerical simulations, and severe weather detection methods. *Wea. Forecasting*, **10**, 203-218.

Purdom, J.F.W., and K. Marcus, 1982: Thunderstorm trigger mechanisms over the Southeast U.S. Pre-prints, *12th Conf. on Severe Local Storms*, San Antonio, TX, Amer. Meteor. Soc., 487-488.

Rinehart, R.E., Borho, A., and C. Curtiss, 1995: Microburst rotation: Simulations and observations. *J. Appl. Meteor.*, **34**, 1267-1285.

Roberts, R.D., and J.W. Wilson, 1989: A proposed microburst nowcasting procedure using single-Doppler radar. *J. Appl. Meteor.*, **28**, 285-303.

Rust, W.D., and D.R. MacGorman, 1998: *The electrical nature of storms*. Oxford Univ. Press, New York, 422 pp.

Rutledge, S.A., Lu, C., and D.R. MacGorman, 1990: Positive cloud-to-ground lightning in mesoscale convective systems. *J. Atmos. Sci.*, **47**, 2085-2100.

Saunders, C.P.R., 1995: Thunderstorm electrification. *Handbook of Atmospheric Electrodynamics*, H. Volland, Ed., CRC Press, 61-92.

Schaefer, J.T., and H.E. Brooks, 2000: Convective storms and their impact. Preprints, *2nd Symposium on Environmental Applications*, Long Beach, CA, Amer. Meteor. Soc., 152-157.

Senn, M.E., 2003: A severe weather synoptic climatology for the spring season in the southeast United States. M.A. thesis, Dept. of Geography, The University of North Carolina at Chapel Hill, 133 pp.

Smith, J.R., Fuelberg, H.E., and A.I. Watson, 2005: Warm season lightning distributions over the northern Gulf of Mexico coast and their relation to synoptic-scale and mesoscale environments. *Wea. Forecasting*, **20**, 415-438.

Snook, N., and W. Gallus, 2004: A climatology of severe weather reports as a function of convective system morphology. Pre-prints, *22nd Conf. on Severe Local Storms*, Hyannis, MA, Amer. Meteor. Soc.

Trapp, R.J., Wheatley, D.M., Atkins, N.T. and R.W. Przybylinski, 2005: A word of caution on the use of severe wind reports in post-event assessment and research. BAMEX Workshop.

van den Broeke, M.S., Schultz, D.M., Johns, R.H., Evans, J.S., and J.E. Hales, 2005: Cloud-to-ground lightning production in strongly forced, low-instability convective lines associated with damaging wind. *Wea. Forecasting*, **20**, 517-530.

Wacker, R.S., and R.E. Orville, 1999: Changes in measured lightning flash count and return stroke peak current after the 1994 U.S. National Lightning Detection Network upgrade. 1: Observations and 2: Theory. *J. Geophys. Res.*, **104**, 2151-2162.

Wakimoto, R.M., 1982: The life cycle of thunderstorm gust fronts as viewed with Doppler radar and rawinsonde data. *Mon. Wea. Rev.*, **110**, 1060-1082.

Wakimoto, R.M., 1985: Forecasting dry microburst activity over the high plains. *Mon. Wea. Rev.*, **113**, 1131-1143.

Wakimoto, R.M., and N.T. Atkins, 1994: Observations of the sea-breeze front during CaPE. Part I: Single-Doppler, satellite, and cloud photogrammetry analysis. *Mon. Wea. Rev.*, **122**, 1092-1114.

Wakimoto, R.M., 2001: Convectively driven high wind events. *Meteor. Monogr.*, 7, Amer. Meteor. Soc., 255-298.

Weisman, M.L., 2001: Bow echoes: A tribute to T.T. Fujita. *Bull. Amer. Meteor. Soc.*, **82**, 97-116.

Weisman, M.L., 1993: The genesis of severe, long-lived bow echoes. *J. Atmos. Sci.*, **50**, 645-670.

Weisman, M.L., and C.A. Davis, 1998: Mechanisms for the generation of mesoscale vortices within quasi-linear convective systems. *J. Atmos. Sci.*, **55**, 2603-2622.

Weisman, M.L., and J.B. Klemp, 1982: The dependence of numerically simulated convective storms on vertical wind shear and buoyancy. *Mon. Wea. Rev.*, **110**, 504-520.

Weisman, M.L., and J.B. Klemp, 1986: Characteristics of isolated convective storms. *Mesoscale Meteorology and Forecasting*, Ed. P.S. Ray, Amer. Meteor. Soc., Boston, 331-358.

Weiss, S.J., and M.D. Vescio, 1998: Severe local storm climatology 1955-1996: Analysis of reporting trends and implications for NWS operations. *Preprints*, 18th Conf. on Severe Local Storms, Minneapolis, MN, Amer. Meteor. Soc., 536-539.

Weiss, S.J., Hart, J.A. and P.R. Janish, 2002: An examination of severe thunderstorm wind climatology: 1970-1999. *Preprints*, 21st Conf. on Severe Local Storms, San Antonio, TX, Amer. Meteor. Soc., 446-449.

Wetzel, S.W. and J.E. Martin, 2001: An operational ingredients-based methodology for forecasting mid-latitude winter season precipitation. *Wea. Forecasting*, **16**, 156-167.

Wicker, L.J., and R.B. Wilhemson, 1995: Simulation and analysis of tornado development and decay within a three-dimensional supercell thunderstorm. *J. Atmos. Sci.*, **52**, 2675-2703.

Williams, E.R., M.E. Weber, and R.E. Orville, 1989: The relationship between lightning type and convective state of thunderclouds. *J. Geophys. Res*., **94**, 13213-13220.

Williams, E.R., 1995: Meteorological aspects of thunderstorms. *CRC Handbook on Atmospheric Electrodynamics*, Vol, I., H. Volland, Ed., CRC Press, 27-60.

Williams, E.R., 2001: The electrification of severe storms. *Meteor. Monogr.*, 7, Amer. Meteor. Soc., 527-561.

Wolfson, M.M., Distefano, J.T., and T.T. Fujita, 1985: Low-altitude wind shear in the Memphis, TN area based on mesonet and LLWAS data. Preprints, *14th Conf. on Severe Local Storms, Indianapolis*, IN, Amer. Meteor. Soc., 322-327.

Zajac, B.A. and S.A. Rutledge, 2001: Cloud-to-ground lightning activity in the contiguous United States from 1995-1999. *Mon. Wea. Rev*., **129**, 999-1019.

Zipser, E.J., 1969: The role of organized unsaturated convective downdrafts in the structure and rapid decay of an equatorial disturbance. *J. Appl. Meteor.*, **8**, 799-814.

APPENDIX A

SEVERE WINDSTORM EVENTS

This appendix provides a tabular summary of the 211 non-tornadic, severe windstorm events (including single reports and indeterminate systems) identified in Georgia during the warm season months (April-September) of 2000-2003. Individual reports of severe thunderstorm wind archived by the SPC were plotted using the SeverePlot software. A severe windstorm event was initially defined if two or more reports occurred in a pattern that suggested they may have originated from the same convective system. The events listed were confirmed through examination of available national radar composite summaries and local base reflectivity scans. Severe windstorm events were classified according to their radar signatures using criteria adopted from previous studies (see Section 3.5). The start and end times (UTC) provided for these events were defined using the severe wind reports, not the radar images. Event duration is defined as the number of hours with at least one severe wind report. If a single report was associated with a convective system occurring outside the study area, the event was classified as widespread. Otherwise, the event was classified as isolated.

Table A.1. Squall lines.

Event	Year	Month	Begin Day	Begin Time	End Day	End Time	Duration	Wind Reports
1	2000	4	3	2340	3	2345	1	2
2	2000	4	8	2004	8	2019	1	2
3	2000	7	11	1600	12	0100	7	18
4	2000	7	12	1700	12	2300	6	16
5	2000	7	13	2145	14	0025	3	3
6	2000	7	20	2312	21	0400	6	38
7	2000	7	24	1719	24	2100	2	2
8	2000	7	28	1716	29	0028	4	5
9	2000	8	10	2125	11	0530	8	16
10	2001	5	22	1349	23	0115	2	5
11	2001	5	25	2019	25	2249	2	2
12	2001	6	3	1855	4	0019	6	28
13	2001	6	4	2145	5	0445	5	15
14	2001	6	14	1825	14	2334	5	12
15	2001	6	22	1419	22	2115	5	9
16	2001	7	5	0047	5	0100	2	2
17	2001	7	5	2030	6	0016	4	12
18	2002	4	29	0001	29	0500	6	8
19	2002	5	3	2100	4	0015	3	11
20	2002	5	9	2104	9	2310	3	7
21	2002	5	13	1749	14	0208	9	36
22	2002	6	4	2101	5	0430	8	26
23	2002	6	14	2040	15	0130	3	6
24	2002	7	21	1843	21	2204	4	10
25	2003	5	1	1749	2	0643	5	7
26	2003	5	2	1900	3	0507	10	96
27	2003	5	6	1430	7	0145	8	30
28	2003	5	7	2019	8	0734	8	16
29	2003	5	11	1400	12	0101	6	12
30	2003	5	18	1915	18	2349	5	14
31	2003	6	3	1931	3	2130	3	6
32	2003	6	11	1800	12	0030	4	8
33	2003	7	10	2115	11	0134	5	6
34	2003	7	21	2100	22	0004	4	9
35	2003	7	22	1619	22	2134	6	44
36	2003	7	23	1740	24	0100	4	8
37	2003	9	27	2058	27	2345	2	3

Table A.2. Irregular Convective Systems.

Event	Year	Month	Begin Day	Begin Time	End Day	End Time	Duration	Wind Reports
1	2000	5	14	0034	14	0100	2	2
2	2000	5	14	2140	15	0130	2	3
3	2000	5	21	1900	22	0158	4	5
4	2000	5	22	1719	22	2130	2	2
5	2000	5	25	2100	25	2225	2	10
6	2000	5	28	2149	28	2245	2	4
7	2000	6	13	2240	13	2315	2	2
8	2000	6	14	2030	15	0100	5	8
9	2000	6	15	2200	15	2200	1	2
10	2000	6	17	2030	17	2215	3	4
11	2000	6	18	1800	18	2030	2	2
12	2000	6	21	1830	21	2330	3	4
13	2000	6	23	2025	23	2245	3	4
14	2000	6	25	1800	25	2255	5	9
15	2000	6	26	2125	27	0110	5	8
16	2000	6	29	2100	29	2100	1	2
17	2000	7	6	2300	6	2345	1	2
18	2000	7	14	1830	15	0134	3	4
19	2000	7	22	2030	22	2155	2	6
20	2000	7	29	1952	29	2100	2	3
21	2000	7	30	2119	31	0025	4	9
22	2000	8	2	2055	2	2110	2	2
23	2000	8	4	1725	4	2218	2	2
24	2000	8	9	1900	10	0830	7	16
25	2000	8	18	1855	19	0040	5	10
26	2000	8	19	2115	19	2245	2	3
27	2000	8	21	0238	21	0530	4	6
28	2000	8	24	2057	25	0115	5	10
29	2000	9	4	2215	5	0122	3	5
30	2001	5	27	1658	27	1719	2	3
31	2001	5	29	2225	29	2233	1	2
32	2001	6	1	0100	1	0119	1	4
33	2001	6	5	2219	6	0030	3	4
34	2001	6	6	1700	6	2130	2	2
35	2001	6	13	2034	14	0016	3	9
36	2001	6	19	2330	20	0030	2	2
37	2001	6	21	1530	22	0230	9	13
38	2001	6	27	1915	28	0045	4	5
39	2001	7	3	1945	3	2134	2	6
40	2001	7	9	1933	9	2330	4	9
41	2001	7	30	2213	30	2245	1	4
42	2001	8	24	1900	24	2334	6	16
43	2002	4	4	0101	4	0137	1	2
44	2002	5	11	2115	12	0034	2	3

Table A.2. (continued)

Event	Year	Month	Begin Day	Begin Time	End Day	End Time	Duration	Wind Reports
45	2002	5	30	2115	31	0210	2	3
46	2002	6	3	1930	4	0130	6	11
47	2002	6	5	2300	6	0130	3	6
48	2002	6	6	2200	6	2230	1	3
49	2002	6	18	2321	18	2340	1	2
50	2002	6	20	1900	20	2130	2	2
51	2002	6	27	2345	28	0040	2	4
52	2002	6	28	2100	28	2225	2	2
53	2002	6	30	2000	1	0049	5	11
54	2002	7	1	1840	1	2315	6	6
55	2002	7	2	1849	3	0130	7	21
56	2002	7	3	2015	3	2349	4	9
57	2002	7	4	2025	5	0030	4	6
58	2002	7	6	2130	7	0445	6	26
59	2002	7	7	1816	7	2300	5	8
60	2002	7	11	1845	11	2243	2	3
61	2002	7	19	2255	19	2319	2	2
62	2002	7	20	1919	20	2300	4	7
63	2002	7	26	2134	26	2315	2	3
64	2002	7	30	2030	31	0019	5	21
65	2002	8	1	2030	2	0049	4	7
66	2002	8	2	2215	2	2340	2	8
67	2002	8	18	1945	18	2334	3	4
68	2002	8	19	2146	19	2315	2	2
69	2002	8	20	2100	21	0110	4	14
70	2002	8	26	2019	26	2309	2	2
71	2002	9	18	1800	18	2045	2	2
72	2003	5	17	1845	17	2355	4	11
73	2003	5	25	2245	25	2258	1	2
74	2003	6	12	2100	13	0019	3	6
75	2003	6	13	2230	13	2248	1	2
76	2003	6	16	2055	17	0430	6	8
77	2003	6	28	1915	28	2225	3	3
78	2003	7	4	1900	4	2230	2	2
79	2003	7	7	2045	8	0119	2	2
80	2003	7	11	1930	11	1955	1	2
81	2003	7	12	2030	13	0849	4	4
82	2003	7	16	2100	16	2215	2	3
83	2003	7	17	1819	18	0340	6	10
84	2003	7	18	2200	19	0130	2	2
85	2003	7	19	2004	20	0030	3	4
86	2003	7	28	2019	28	2040	1	2
87	2003	7	29	1912	29	2245	4	8
88	2003	8	6	1910	6	2030	2	3

Table A.2. (continued)

Event	Year	Month	Begin Day	Begin Time	End Day	End Time	Duration	Wind Reports
89	2003	8	10	2225	11	0330	2	2
90	2003	8	11	1910	11	2004	6	11
91	2003	8	16	1849	16	2200	4	7
92	2003	8	19	1930	19	2200	2	4
93	2003	8	28	2019	28	2249	3	4
94	2003	9	4	2000	4	2040	1	2

Table A.3. Supercells

Event	Year	Month	Begin Day	Begin Time	End Day	End Time	Duration	Wind Reports
1	2002	5	10	2249	11	0004	3	3
2	2003	4	25	1407	25	2315	4	5

Table A.4. Single Reports

Event	Year	Month	Day	Time	Isolated or Widespread?
1	2000	5	20	2130	Isolated
2	2000	6	17	0055	Isolated
3	2000	6	27	2015	Isolated
4	2000	7	7	0240	Widespread
5	2000	7	16	2355	Isolated
6	2000	7	31	2345	Isolated
7	2000	8	1	1900	Isolated
8	2000	8	8	1830	Isolated
9	2000	8	11	2143	Widespread
10	2000	8	27	2030	Widespread
11	2000	8	29	0540	Isolated
12	2001	4	15	1351	Widespread
13	2001	5	11	2231	Isolated
14	2001	5	29	0255	Widespread
15	2001	6	8	0010	Isolated
16	2001	6	15	2000	Isolated
17	2001	6	16	2134	Isolated
18	2001	6	25	2345	Isolated
19	2001	6	26	2115	Isolated

Table A.4. (continued)

Event	Year	Month	Day	Time	Isolated or Widespread?
20	2001	7	1	2000	Isolated
21	2001	7	3	0015	Isolated
22	2001	7	10	2245	Widespread
23	2001	7	13	2310	Widespread
24	2001	7	20	2033	Widespread
25	2001	7	26	1800	Isolated
26	2001	8	11	0137	Isolated
27	2001	8	18	2230	Isolated
28	2001	8	28	2314	Isolated
29	2001	9	22	2130	Isolated
30	2002	4	1	0030	Isolated
31	2002	4	3	2149	Widespread
32	2002	5	3	1115	Widespread
33	2002	5	17	2030	Widespread
34	2002	5	29	2230	Isolated
35	2002	6	7	2045	Widespread
36	2002	6	14	0100	Isolated
37	2002	6	29	2334	Isolated
38	2002	7	10	2140	Widespread
39	2002	7	22	2300	Isolated
40	2002	7	27	2125	Isolated
41	2002	8	6	2330	Isolated
42	2002	8	25	0045	Widespread
43	2002	8	25	2319	Widespread
44	2002	8	27	2125	Isolated
45	2002	9	5	2143	Isolated
46	2003	4	8	0055	Widespread
47	2003	4	18	2149	Isolated
48	2003	4	26	0046	Widespread
49	2003	5	15	1909	Isolated
50	2003	5	16	2030	Isolated
51	2003	6	5	0049	Isolated
52	2003	6	14	2100	Widespread
53	2003	6	29	1900	Widespread
54	2003	7	2	2200	Widespread
55	2003	7	8	2019	Widespread
56	2003	7	21	0330	Isolated
57	2003	7	26	2200	Isolated
58	2003	7	30	1934	Isolated
59	2003	8	1	0219	Isolated
60	2003	8	1	2010	Widespread
61	2003	8	8	2310	Isolated
62	2003	8	17	2149	Isolated
63	2003	8	29	2134	Widespread

Table A.5. Indeterminate Convective Systems.

Event	Year	Month	Begin Day	Begin Time	End Day	End Time	Duration	Wind Reports
1	2000	7	10	1830	10	2207	2	2
2	2000	8	25	1815	25	1840	1	3
3	2000	9	21	0510	21	0725	3	3
4	2000	9	23	0255	23	0345	2	3
5	2001	5	2	2340	2	2340	1	1
6	2001	6	11	0704	11	704	1	1
7	2001	8	1	1937	1	1940	1	2
8	2001	8	5	0524	5	0524	1	1
9	2001	8	31	1946	31	1953	1	2
10	2002	7	23	2000	23	2315	4	5
11	2003	5	7	0630	7	0716	2	4
12	2003	7	17	0752	17	0830	2	2
13	2003	8	3	1800	3	1800	1	1
14	2003	8	4	2104	5	0234	4	6
15	2003	9	22	1854	22	2055	2	3

APPENDIX B

DESCRIPTION OF THERMODYNAMIC PARAMETERS

This appendix provides descriptions of the thermodynamic parameters used in this research as well as their computations where applicable. These parameters were calculated from radiosonde observations at Peachtree City, GA, (KFFC) and Jacksonville, FL, (KJAX). Only the soundings at 00 UTC were used, as very few events occurred during the early morning hours.

1. Convective Available Potential Energy (CAPE) (J kg^{-1}) represents the maximum amount of buoyant energy available to accelerate an air parcel vertically through an unstable column of the troposphere. It is defined as

$$CAPE = \int_{p_n}^{p_f} (\alpha_p - \alpha_e) dp$$

where α_e is the environmental specific volume profile, α_p is the specific volume of an air parcel moving upward moist-adiabatically from the level of free convection (LFC), ρ_f is the pressure at the LFC, and ρ_n is the pressure at the level of neutral buoyancy. On a thermodynamic diagram (i.e. Skew-T Log-P), CAPE is represented as the positive area between an air parcel's ascent along the moist adiabat and the environmental temperature

curve from the LFC to the equilibrium level. The positive area is where warm air parcels will rise moist adiabatically, assuming parcel theory. When this area appears "skinny" on a Skew-T diagram it implies a relatively slower updraft, but may also imply a tall cloud height, which enhances evaporative cooling and water loading. Conversely, when the positive area appears "fat" it implies a strong updraft and possible updraft rotation. A large temperature difference between an air parcel and the environment suggests high CAPE and updraft acceleration to produce strong convection. A CAPE value exceeding 1000 J kg^{-1} is indicative of a moderately unstable environment, while a value exceeding 2500 J kg^{-1} suggests a very unstable environment (Weisman and Klemp 1982). For this research, the surface-based air parcel was used to calculate CAPE because elevated convection is typically not associated with downburst winds reaching the surface.

2. Convective Inhibition (CIN) (J kg^{-1}) is the amount of negatively buoyant energy available to suppress vertical motion. It may also be interpreted as the amount of energy the environment must expend to raise an air parcel to the LFC. It is defined as

$$CIN = -\int_{\rho_i}^{\rho_f} R_d (T_{vp} - T_{ve}) d \ln \rho$$

where ρ_i is the pressure at the level at which the air parcel originates, ρ_f is the pressure at the LFC, R_d is the specific gas constant for dry air, T_{vp} is the virtual temperature of the lifted air parcel, and T_{ve} is the virtual temperature of the environment. On a Skew-T diagram, CIN is represented as the negative area enclosed by the dry and moist adiabats

and the environmental temperature curve from the surface to the LFC. The negative area develops in response to a capping inversion, which represents the region of negative buoyancy below the LFC. Capping inversions typically inhibit deep convection, although some convective cells may overcome the inversion in the presence of a strong lifting mechanism. These cells are able to access large amounts of buoyant energy stored in the boundary layer and provide the best chance for severe weather.

3. K-Index (KI) provides a measure of convective development that is based on the vertical temperature lapse rate and the extent of lower-tropospheric moisture (Djuric 1994). It is defined as

$$KI = T_{850} + Td_{850} - (T_{700} - Td_{700}) - T_{500}$$

where T is the temperature and Td is the dewpoint at the indicated pressure levels. This index is useful for predicting convection in an environment absent of a large-scale forcing mechanism, such as a surface boundary or progressive trough. It is also useful in diagnosing the entrainment of dry air at 700 hPa, which reduces an air parcel's buoyancy. A high K-index suggests greater potential for convective development.

4. Lifted Index (LI) provides a measure of stability by calculating the temperature difference between the environment at 500 hPa and an air parcel originating in the bottom 500 m of the troposphere that has been lifted dry-adiabatically to its LCL and then lifted wet-adiabatically to 500 hPa (L) (Galway 1956). It is defined as

$$LI = T_L - T_{500}$$

and is sensitive to diurnal variations in surface temperature (i.e. 12 UTC sounding will generally underestimate convection taking place in the afternoon). As such, it is also a poor measure of elevated convection. A negative LI implies that the air parcel temperature exceeds the environmental temperature at 500 hPa. Values of -6°C or less suggest deep convection.

5. Bulk-Richardson Number (BRN) incorporates the amount of buoyant energy (CAPE) and the vertical shear of the horizontal wind in the bottom 6,000 m (U_{6000}) and in the bottom 500 m (U_{500}) to determine the type of convective storm that is likely to form. It is defined as

$$BRN = \frac{CAPE}{\frac{1}{2}(U_{6000} - U_{500})^2}$$

where BRN values greater than 45 suggest that ordinary, multi-cellular thunderstorms (i.e. non-severe) are likely to form due to relatively high CAPE values (Weisman and Klemp 1986). BRN values less than 45 support supercell convection since a strongly sheared environment is favorable for the development of a rotating updraft. A large BRN, however, does not imply that severe thunderstorms cannot form. The ambient

shear produced by the horizontal convergence of outflow boundaries and other mesoscale circulations can promote an environment favorable for isolated downbursts.

6. Equivalent Potential Temperature (Θ_e) (K) is the temperature that would result if all the water vapor in an atmospheric column were condensed (i.e. conversion of latent heat to sensible heat) and the resulting air parcel was expanded or compressed to 1000 hPa. High values of Θ_e imply a moisture-laden air mass and are often associated with deep convection (i.e. increased CAPE).